

Interactive comment on “Decennial time trends and diurnal patterns of particle number concentrations in a Central European city between 2008 and 2018” by Santtu Mikkonen et al.

Anonymous Referee #1

Received and published: 7 July 2020

I found the manuscript well written and scientifically sound. I only found one error/inconsistency in Figure 7: In the text it says that Figure 7 illustrates the GLMM model predicts the observations in all size fractions within a randomly selected period of one week in March 2015, but in reality the time period is from 2013-2019

We thank the reviewer on the positive comment.

Thank you for noticing that the Figure 7 was incorrect, the correct figure is now changed to the manuscript.

Anonymous Referee #2

We thank the reviewer for the review and constructive comments. Below we address each comment point by point. Reviewer comments are marked as **black**, our response as blue and corrections to the changes to the manuscript as **red**.

General comments

The paper presents convincing arguments with statistical methods as why it is likely that decreased traffic emissions have led to decreased particle pollution in Budapest. Hence, these results are extremely important from a policy making point of view. In other words, it is necessary that there are no doubts as to why concentrations have gone down. For this reason, the paper must undergo additional analysis to prove the point that car emissions have indeed led to the decrease of particle concentrations in Budapest. If this analysis can not conclusively prove the reason for the decrease, then I must stress the need to be more careful about the conclusion in the abstract and conclusion section as to the reason for the decrease. And provide a sentence that other reasons for the decrease can not be ruled out.

A: As the reviewer pointed out, we cannot be certain that the decreasing particle numbers are due to traffic emissions. Improvements in heavy-duty vehicle fleet has been done, as stated in the conclusion and that certainly affects. Total number of passenger cars has increased, though the fraction of diesel cars from the total number of passenger cars has been increasing. Diesel engines have smaller particle emissions than gasoline engines as shown e.g. in Wihersaari et al. (2020) which can be assumed to lead smaller total particulate emissions of passenger car fleet. The sentence in the abstract is reformulated as:

This was interpreted as a consequence of the decreased anthropogenic emissions at least partly from road traffic alongside to household heating and industry.

Hence, I suggest to accept the paper subject to major revision of data analysis as suggested below. In addition there are a few minor remarks that need to be addressed.

Major remarks

Table 2 seems to indicate that there are increasing number of cars and car age as function of time in Budapest. How this can lead to decrease in emissions from traffic in chapter 3.1 is not quite convincing despite that Euro regulations are imposing restrictions to emissions from new cars. The total emissions are likely dominated by the ageing cars, and the average age of cars is increasing with time. Is there still a likelihood that the statistical analysis could be wrong for some unknown reason, and the reason for decreasing concentrations is arising as function of varying meteorological conditions between different years as expressed by the MCP parameter and not due to decreased car emissions? After all, the gas concentrations are not decreasing with time as the authors admit. I want the authors to quantify how often MCP weather patterns of type 3, 7, and 12 occur during April, May and August during the earlier years compared to the later years, and see if this can explain why the N6-1000 is higher in the earlier years than the later years (and also for the MCP that do not favor NPF, type6).

A: Our present interpretation of the reduced traffic emissions cannot be completely conclusive in all aspects and further investigations and collection of new data are planned on the basis of the present results. As the GLMM model accounts for the meteorological patterns on daily level, it is highly unlikely that the changes in occurrence of certain MCP patterns could cause the decreasing trend in particle numbers. To ensure this, we studied the occurrence of the MCP patterns in detail and we saw no significant change in frequencies of any of the patterns, specifically in the NPF favouring or disfavouring ones pointed out by the reviewer. In addition, MCP types 3 and 7 are rather rare (Table 1), and thus cannot have significant effect on trends in total. The following sentences are added to the manuscript section 3.2.2

In order to see if the decreasing concentrations are due to changes in meteorological patterns, we investigated separately the occurrence of the MCP patterns during the measurement period. We found no significant changes in the occurrence of the patterns and thus the decreasing particle concentrations are due to something else than the meteorological patterns.

The statistical method of DLM and GLMM are not enough for interpreting the results. A manual analysis of the MCP as described above must be done as well to provide further evidence for decreasing particle trend as being caused by decreasing traffic emissions. I stress also to use an educated guess/calculation of how you expect to see reductions in emissions of particles based on the values of car age and number of vehicles and diesel car share as function of year, and see if your expectations in-deed would indicate a decrease in emissions. Just because there is a tendency for decreasing car emissions in Germany, doesn't prove that the same thing is happening for Budapest if the traffic fleet composition is different in Budapest. Also, I want the authors to look more carefully on meteorological parameters manually as well. Even though for example the average temperature is the same for the different years, doesn't mean that it is not varying between different days that lead to the particle concentration trends between different years.

A: We do not state that the decrease is only from traffic emissions, and with the text modifications above we try to clarify that. However, even though there might be certain differences between the composition of passenger car fleet between Germany and Budapest, the traffic emissions can still be assumed to be decreased also in Hungary even though the renewal rate of the fleet might be slower. We do not have exact details on the car fleet composition, and we do not have the expertise to make such educated guesses suggested by the reviewer. Thus, we can only speculate the magnitude of the effect of traffic emission reduction but, as stated above, the direction is clear.

Minor remarks

Please denote that the station is an "urban background" station in the abstract, introduction and methodology sections. This is needed for other readers to relate to the expected pollution level, and to know if this is the most polluted place in Budapest, or as you have in this case, a medium population exposure location in the city center, so called urban background. Alternatively, if it is not a typical urban background site, but slightly more polluted (I don't know this), please explain in the introduction and methodology section that the site has a

pollution level between a typical heavy trafficked street level site and an urban background site, but closer to typical urban background levels.

A: The requested information was added to the Abstract (1) (lines 11-13) and this point was also further emphasized in the body text (lines 115-117) where the measurement site is described (2).

(1) Multiple atmospheric properties were measured semi-continuously in the Budapest platform for Aerosol Research and Training Laboratory, which represents the urban background for a time interval of 2008-2018.

(2) This location represents a well-mixed, average atmospheric environment for the city centre of Budapest due to its geographical and meteorological conditions (Salma et al., 2016a), thus it can be regarded as an urban background site.

Lines 133-134. "the most extensive inter-comparison was realised in summer 2015(Salma et al., 2016a) and autumn 2019". Please denote which kind of intercomparisons were made.

A: The explanation was extended as requested. The following text was inserted to Page 4 lines 136-142.

First, the measured data by the CPC deployed in the DMPS system were compared to that of an identical stand-alone CPC operated in parallel. The agreement between the instruments was in accordance with the nominal specification of CPCs. In the next step, the integrated concentrations obtained from the size-resolved DMPS data were compared to the concentrations measured directly by the stand-alone CPC. The two instruments were again operated in parallel. The median CPC/DMPS ratio was utilised as correction factor for particle diffusion losses in the DMPS system (Salma et al., 2016a).

Chapter 2.1: SO₂, CO, NO, NO_x, O₃, and PM₁₀ measurements: What is the pollution level of the site measuring these parameters: urban background or street level pollution, or something in between, or cleaner than an urban background site? Please describe this station as well. Otherwise, we cannot compare the time trends for this site as compared to the BpArt site. For example, the BpArt site might be closer to traffic than the gas measurement site explaining why the BpArt concentrations are decreasing with decreasing traffic emission trends, but not at the gaseous concentration site, which is then relatively more influenced by background long range sources.

A: Further details on the character of the monitoring station for criteria pollutants was added as requested on page 5, lines 157-160.

This station ordinarily measures the smallest levels of the criteria air pollutants among the four monitoring stations located in the city centre. It can, therefore, be considered to represent the air pollution in between the urban background and street level/kerbside site.

Chapter 2.2: The MCP codes are developed for 00:00 UTC time. When you have a time of your particle or gas concentration data or meteorological data, which is the MCP type that you use? For example, if the measurement time is August 1, 14:00 local time, what is the MCP coding for that time? Is it the MCP coding from August 1, 00:00UTC, or MCP coding from August 2, 00:00? Or is it denoted as a combination of both MCP codes? It should be clearly stated in the manuscript. The MCP coding from one day to the other might change completely, meaning MCP codes for a measurement time in between two MCP coding times can be ambiguous.

A: The MCP codes represent the macro-circulation conditions in the whole Carpathian Basin as a geographical unit, and are determined on a daily bases in a discrete manner. They were assigned to the concentration and meteorological data of the whole given day. This is now clarified in page 6 line 191 in the revised manuscript:

Thus defined MCP was assigned to the following day in the data.

Chapter 2.3.1. Would you please explain the autoregressive component?

A: Autoregressive component is a parameter taking account the autocorrelation in the data which means that subsequent (here daily) measurements of variables are correlated. We added the following description to section 2.3.1, page 8, lines 232-234 in the revised manuscript (1) and added a new equation 4, describing the autoregressive component with description (2) on lines 242-245:

(1) The autoregressive component is added to the model in order to take account the autocorrelation in the data, i.e. the correlation between subsequent observations. Here it refers to first order autoregressive model (AR(1)).

$$(2) \eta_t = \rho\eta_{t-1} + \varepsilon_{AR}, \varepsilon_{AR} \sim N(0, \sigma_{AR}^2), \quad (4)$$

where y_t is the investigated concentration at time t , μ_t is the mean level and α_t is the change in the level from time $t-1$ to time t , γ_t is the seasonal component, η_t is an autoregressive error component and ρ is the coefficient for autoregressive component, here fixed to $\rho = 0.6$.

Equation (4): The MCP is not a continuous variable, but it is discrete. How can you construct a linear output factor from Beta-6 multiplied with MCP-i? Would you mind explaining how Beta-6 and MCP-i and their product are constructed?

A: All levels of the MCP coding will get their own characteristic level for typical conditions calculated with the GLMM and thus β_6 is a (13×1) vector of coefficients. The levels of these coefficients are shown in Figure 5. To clarify this, we modified the description of β_6 in Eq. 5 (note changed numbering due to changes above) to following form (page 9, lines 282-284):

..., β_6 is the (13×1) vector of coefficients for different macro-circular patterns (MCP) indicating the characteristic level of number concentration during each MCP type, which are treated here as categorical variable...

Line 274: Q (GRad) calculation is incorrect. The equation is correct only if you have 100 % data coverage. You have between 90 and 100 % data coverage as indicated in the method section. Hence, the calculated value will be systematically underestimated unless you interpolate data for the missing hours of GRad data. This could potentially be the reason why Table 2 Q values are different for different years, and not due to varying total insolation during one year to the other.

A: The calculation method of the annual insolation was revised and improved taking into account the reviewer comment. As there were no big gaps in radiation measurements the missing data were interpolated and the calculation schema was also modified. The corresponding text (page 10, lines 289-293) and values in Table 2 were amended accordingly.

Annual insolation (Q), which expresses the total energy density at the receptor site, was derived from the individual hourly mean $GRad_{i,j}$ data, where index i represents the hour of day (from 0 to 23), index j stands for the day of year (from 1 to 365) as $Q = 3.6 \times 10^{-6} \times \sum_{i,j} GRad_{i,j}$. The dimensions of the $GRad_{i,j}$ data and Q are $W m^{-2}$ and $GJ m^{-2} y^{-1}$, respectively. The few randomly missing datapoints were interpolated linearly.

Lines 317-318. It is a strong statement to say that "this decoupling confirms that the causes of the decrease in particle number concentrations are not primarily related to meteorological conditions because they would jointly affect the gas concentrations as well". That gas concentrations don't go down and particle number concentrations go down could by accident also be related to a difference in availability of different MCP days during different years and seasons. NPF events could be favored in earlier years due to for example quite high number of certain MCP days with lower particle surface area, which favours NPF, which don't appear as frequent in the later years. This could happen even if the median particle surface area is decreasing every year (as indicated by decreasing N100-N1000). But, this difference in MCP does not automatically mean that the gas concentrations should change in the same way as N6-1000. Hence, I would rephrase the wording from "confirms" to "suggests".

A: Wording rephrased as suggested.

Conclusion: You mention that the accumulation mode particles don't show a decreasing annual trend. But, according to Table 3 they do.

A: The sentence is rephrased as (page 21, lines 579-580):

The decennial statistical trends showed decreasing character in all applied size fractions of particle concentrations.

New references

Wihersaari H., et al. (2020) Particulate emissions of a modern diesel passenger car under laboratory and real-world transient driving conditions, *Environmental Pollution*, 265, 114948, <https://doi.org/10.1016/j.envpol.2020.114948>.

Platt, S. M., El Haddad, I., Pieber, S. M., Zardini, A. A., Suarez-Bertoa, R., Clairotte, M., Daellenbach, K. R., Huang, R.-J., Slowik, J. G., Hellebust, S., Temime-Roussel, B., Marchand, N., de Gouw, J., Jimenez, J. L., Hayes, P. L., Robinson, A. L., Baltensperger, U., Astorga, C., and Prévôt, A. S. H.: Gasoline cars produce more carbonaceous particulate matter than modern filter-equipped diesel cars, *Sci. Rep.*, 7, 4926, 2017, <https://doi.org/10.1038/s41598-017-03714-9>.

Decennial time trends and diurnal patterns of particle number concentrations in a Central European city between 2008 and 2018

Santtu Mikkonen^{1,2}, Zoltán Németh³, Veronika Varga³, Tamás Weidinger⁴, Ville Leinonen¹,
Taina Yli-Juuti¹, and Imre Salma³

¹ Department of Applied Physics, University of Eastern Finland, P.O. Box 1627, 70211 Kuopio, Finland

² Department of Environmental and Biological Sciences, University of Eastern Finland, P.O. Box 1627,
70211 Kuopio, Finland

³ Institute of Chemistry, Eötvös University, H-1518 Budapest, P.O. Box 32, Hungary

⁴ Department of Meteorology, Eötvös University, H-1518 Budapest, P.O. Box 32, Hungary

Correspondence to: Imre Salma (salma@chem.elte.hu) and Santtu Mikkonen (santtu.mikkonen@uef.fi)

Abstract. Multiple atmospheric properties were measured semi-continuously in the Budapest platform for Aerosol Research and Training Laboratory which represents the urban background for a time interval of 2008-2018. Dataset of 6 full measurement years during a decennial time interval were subjected to statistical time trend analyses by an advanced dynamic linear model and a generalized linear mixed model. The main interest in the analysed data set was on particle number concentrations in the diameter ranges from 6 to 1000 nm (N_{6-1000}), from 6 to 100 nm (N_{6-100} , ultrafine particles), from 25 to 100 nm (N_{25-100}) and from 100 to 1000 nm ($N_{100-1000}$). These data were supported by concentrations of SO₂, CO, NO, NO_x, O₃, PM₁₀ mass, air temperature, relative humidity, wind speed, atmospheric pressure, global solar radiation, condensation sink, gas-phase H₂SO₄ proxy, classes of new aerosol particle formation (NPF) and growth events and meteorological macro-circulation patterns. The trend of the particle number concentrations derived as a change in the statistical properties of background state of the data set decreased in all size fractions over the years. Most particle number concentrations showed decreasing decennial statistical trends. The estimated annual mean decline of N_{6-1000} was (4–5)% during the 10-year measurement interval, which corresponds to a mean absolute change of -590 cm^{-3} in a year. This was interpreted as a consequence of the decreased anthropogenic emissions mainly at least partly from road traffic alongside to household heating and industry. Similar trends were not observed for the air pollutant gases. Diurnal statistical patterns of particle number concentrations showed tendentious variations, which were associated with typical diurnal activity–time pattern of inhabitants in cities, particularly of vehicular road traffic. The trend patterns for NPF event days contained a huge peak from late morning to late afternoon, which is unambiguously caused by NPF and growth processes. These peaks were rather similar to each other in the position, shape and area on workdays and holidays, which implies that the dynamic and timing properties of NPF events are not substantially influenced by anthropogenic activities in central Budapest. Diurnal pattern for N_{25-100} exhibited the largest relative changes, which were related to particle emissions from high-temperature sources. The diurnal pattern for $N_{100-1000}$ – which represents chemically and physically aged particles of larger spatial scale – were different from the diurnal patterns for the other size fractions.

37 **1 Introduction**

38 Atmospheric aerosol can be characterised by various properties. There are several important phenomena
39 and processes in which individual particles play a role. In these cases, particle number concentrations
40 or particle number size distributions are the relevant metrics. Number concentrations of (insoluble)
41 particles produce adverse effects on human health (Oberdörster et al., 2005; Rich et al., 2012; Cassee et
42 al., 2013; Braakhuis et al., 2014; Ostro et al., 2015; Schmid and Stoeger, 2016; Ohlwein et al., 2019).
43 Individual particles and their properties are also important in cloud formation processes and, therefore,
44 in indirect aerosol climate forcing (Makkonen et al., 2009; Merikanto et al., 2009; Sihto et al., 2011;
45 Kerminen et al., 2012; Carslaw et al., 2013; Gordon et al., 2016). Particle numbers and associated size
46 distributions are relevant properties in several optical interactions in the atmosphere (e.g. Moosmüller
47 et al., 2009) and in various surface-controlled chemical reactions (e.g. Pöschl et al., 2007).

48 In the global troposphere, it is the new aerosol particle formation (NPF) and consecutive growth process
49 that is the dominant source of particle numbers (Spracklen et al., 2006; Yu et al., 2010; Kulmala et al.,
50 2013; Dunne et al., 2016). This source type occurs in various atmospheric environments around the
51 world and produces secondary particles (Kerminen et al., 2018 and references therein). The major
52 anthropogenic source of (primary) particles is combustion. It includes traffic exhaust mainly from diesel
53 engines, fuel or waste burning in industrial and domestic installations, residential heating and cooking
54 (Paasonen et al., 2016; Masiol et al., 2018). Nanotechnology and its products can have importance in
55 some limited or occupational environments. In large cities and in longer time intervals, primary particles
56 often prevail over secondary particles (Brines et al., 2015; Salma et al., 2017; Saha et al., 2018).

57 Ultrafine (UF) particles (with a diameter $d < 100$ nm) account for most of the particle number
58 concentrations but have usually negligible contribution to particulate matter (PM) mass. This implies
59 that particle numbers are not covered by legislative regulations on the ambient air quality, which are
60 ordinary based on the PM mass. Particle number concentrations have not been promulgated among the
61 air quality standards yet. There are, however, mitigation policies and control regulations, which intend
62 to reduce their ambient levels as part of an overall air-quality improvement strategy since 1990s. The
63 legislations, for instance in the EU including Hungary, focus on the particle emissions from diesel
64 engines (Giechaskiel et al., 2018). There were some important changes in the car emissions during the
65 time interval under the investigation in this study. These included the introduction of Euro 5 and 6
66 regulations for light-duty vehicles in January 2011 and Euro VI regulations for heavy-duty vehicles in
67 September 2015 (the number of emitted particles with diameters > 23 nm should be $< 6 \times 10^{11}$ km⁻¹ for
68 type approval). A prerequisite for the efficient operation of exhaust after treatment devices is having
69 fuel with low sulfur content. The reduction of sulfur in diesel fuel for on-road transport was decreased
70 after several previous phases to < 10 ppm in January 2009 (Directive 2009/30/EC). Sulfur content in
71 fuels for mobile non-road diesel vehicles – including mobile machinery, agricultural and forestry

72 tractors, inland waterway vessels and recreational crafts – was limited at a level of 1000 ppm from 2008
73 and at 10 ppm from 2011. The unsuitable/dangerous fuel types for domestic heating are also listed, their
74 emission factors are determined, and the accumulated information is disseminated among potential
75 users. As far as secondary particles are concerned, it is not straightforward to reduce their concentration
76 levels because the effects of gaseous and aerosol species on the NPF are complex and uncertain due to
77 nonlinear relationship and feedbacks in their related processes.

78 It is relevant to investigate the potential changes, namely overall and diurnal tendencies of particle
79 number concentrations from different sources on longer run because of their role in both health-risk and
80 climate-change issues. The major source types of particle numbers can be separated by measuring their
81 size distributions. Atmospheric NPF events produce particles of the nucleation mode, which occurs
82 intermittently, and which gradually merges into the larger Aitken mode. High temperature emission
83 sources ordinarily produce Aitken-mode particles, while transformation processes (physical and
84 chemical aging) of existing particles in the atmosphere give rise to the accumulation mode. An important
85 property of the nucleation- and Aitken-mode particles is that their residence time is limited to several
86 hours (Raes et al., 2000; Salma et al., 2011). This is different from accumulation-mode particles, which
87 reside in the air up to 7 days. This means that the particles of the former two modes are present in the
88 air until their sources are active, and that their concentrations can change substantially and rapidly over
89 a day (e.g. Mikkonen et al., 2011a, Salma et al., 2014, 2017; Paasonen et al., 2016). This is advantageous
90 when source types are to be identified or quantified. At the same time, the relatively short residence time
91 is not beneficial when time trends are to be studied and derived. The limited residence time can cause
92 additional, substantial and sudden variability in time with or without time patterns, which can complicate
93 the evaluation.

94 Particle number concentrations or particle number size distributions in the relevant diameter range (i.e.
95 from few nanometers to ca. 1 μm) are measured for various purposes. They include fundamental studies
96 on atmospheric nucleation and particle growth phenomena, which usually require semi-continuous long-
97 term measurements. The related experimental data sets have been accumulating gradually (Wehner and
98 Wiedensohler, 2003; Asmi et al., 2013; Kerminen et al., 2018; Nieminen et al., 2018). They can also be
99 exploited for time trend analysis by using appropriate statistical models. At present, however, knowledge
100 on time trends particularly in various size fractions and over several years is largely lacking with few
101 recent exceptions (Masiol et al., 2018; Saha et al., 2018; Sun et al., ~~2019~~2020).

102 Research activities dedicated to NPF and growth events in Budapest have been going on since November
103 2008. Measurements for 6 full years were realised in the city centre at a single fixed location. Semi-
104 continuous and critically evaluated data sets consisting of particle number size distributions,
105 concentrations of criteria air pollutants and meteorological data were available for the study. They were
106 combined in a coherent set, which was utilised in two statistical models developed specifically to

107 determine the time trends for particle number concentrations in several important size fractions from
108 2008 to 2018. The main objectives of this study are to present and discuss the statistical models, to
109 interpret their results on time trends and diurnal variability, to quantify the change rates, and to relate
110 the temporal tendencies to different atmospheric sources, processes and environmental circumstances.

111 **2 Methods**

112 **2.1 Measurements**

113 Most experimental data dealt with in the present study were obtained at a single urban site, namely at
114 the Budapest platform for Aerosol Research and Training (BpART) research laboratory (N 47° 28' 29.9",
115 E 19° 3' 44.6", 115 m above mean sea level). This location represents a well-mixed, average atmospheric
116 environment for the city centre of Budapest due to its geographical and meteorological conditions
117 (Salma et al., 2016a), thus it can be regarded as an urban background site. The local emissions include
118 diffuse urban traffic exhaust, household/residential emissions and limited industrial sources together
119 with some off-road transport (diesel rail, shipping and airplane emissions). Experimental data for 6 full-
120 year-long time intervals, i.e. from 3 November 2008 to 2 November 2009, from 13 November 2013 to
121 12 November 2014, from 13 November 2014 to 12 November 2015, from 13 November 2015 to 12
122 November 2016, from 28 January 2017 to 27 January 2018 and from 28 January 2018 to 27 January
123 2019 were available for this single site. A decennial time interval from 03 November 2008 to 02
124 November 2018 was considered in the statistical analysis. Local time (LT=UTC+1 or daylight-saving
125 time, UTC+2) was chosen as the time base of the data processing because the ordinary daily activities
126 of inhabitants substantially influence the atmospheric concentrations and several processes in cities
127 (Salma et al., 2014).

128 The major aerosol measuring system was a flow-switching type differential mobility particle sizer
129 (DMPS, Alto et al., 2001). It records particle number concentrations in an electrical mobility diameter
130 range from 6 to 1000 nm in the dry state of particles (with a relative humidity of RH<30%) in 30
131 channels (Salma et al., 2011). The measuring system was updated twice; in spring 2013 and winter 2016.
132 Its major parts including a differential mobility analyser (DMA, Hauke-type with a length of 28 cm) and
133 a condensation particle counter (CPC, TSI model 3775) remained, however, unchanged. They were
134 cleaned and serviced. The diameter resolution of the DMA was also calibrated during the updates.
135 Several data validation or comparative exercises were realised over the years; the most extensive inter-
136 comparison was realised in summer 2015 (~~Salma et al., 2016a~~) and autumn 2019. First, the measured
137 data by the CPC deployed in the DMPS system were compared to that of an identical stand-alone CPC
138 operated in parallel. The agreement between the instruments was in accordance with the nominal
139 specification of CPCs. As the next step, the integrated concentrations obtained from the size-resolved
140 DMPS data were compared to the concentrations measured directly by the stand-alone CPC. The two

141 instruments were again operated in parallel. The median CPC/DMPS ratio was utilised as correction
142 factor for particle diffusion losses in the DMPS system (Salma et al., 2016a). The time resolution of the
143 DMPS measurements was approximately 10 min in the year 2008–2009 and it was 8 min from 13
144 November 2013 on. The sampling inlet was installed at a height of 12.5 m above the street level. There
145 was no upper-size cut-off inlet applied to the sampling line, and a rain shield and insect net were only
146 adopted. The measurements were performed according to the international technical standard
147 (Wiedensohler et al., 2012).

148 Meteorological data for air temperature (T), relative humidity (RH), wind speed (WS), wind direction
149 and atmospheric pressure (p) were obtained from a measurement station of the Hungarian
150 Meteorological Service (HMS) operated in a distance of ca. 70 m from the BpART laboratory by
151 standardised methods (Vaisala HMP45D humidity and temperature probe, Vaisala WAV15A
152 anemometer, Vaisala pressure, all Finland) with a time resolution of 10 min. Global solar radiation
153 (GRad) data were measured by a CMP11 pyranometer (Kipp and Zonnen, The Netherlands) at another
154 station of the HMS situated in 10 km in Eastern direction with a time resolution of 1 h. Concentrations
155 of pollutants SO₂, CO, NO, NO_x, O₃, and PM₁₀ mass were acquired from a measurement station of the
156 National Air Quality Network in Budapest in Széna Square, which is located in the upwind prevailing
157 wind direction in a distance of 4.5 km from the BpART laboratory. This station ordinarily measures the
158 smallest levels of the criteria air pollutants among the four monitoring stations located in the city centre.
159 It can, therefore, be considered to represent the air pollution in between the urban background and street
160 level/kerbside site. They are measured by UV fluorescence (Ysselbach 43C), IR absorption (Ysselbach
161 48C), chemiluminescence (Thermo 42C), UV absorption (Ysselbach 49C) and beta-ray attenuation
162 (Thermo 5014I) methods, respectively with a time resolution of 1 h.

163 The availability of the DMPS data over the six one-year-long time intervals were 95, 99, 95, 73, 99 and
164 90%, respectively. The meteorological data were accessible in >90% of time in each year, while the
165 concentration data for key pollutants were available in >85% of the yearly time intervals.

166 **2.2 Data treatment**

167 Particle number concentrations in the diameter ranges 1) from 6 to 1000 nm (N_{6-1000}), 2) from 6 to 100
168 nm (N_{6-100}), 3) from 25 to 100 nm (N_{25-100}) and 4) from 100 to 1000 nm ($N_{100-1000}$) were calculated from
169 the measured and inverted DMPS data. The size ranges were selected to represent 1) the total particles,
170 2) UF particles, 3) UF particles emitted mainly from incomplete combustion (and partially grown by
171 condensation; this size ranges is dominated by primary particles in cities in most of the time) and 4)
172 physically and chemically aged particles which usually represent larger spatial extent, respectively
173 (Salma et al., 2014, 2017).

174 Condensation sink (CS) for vapour molecules onto the surface of existing aerosol particles was
 175 calculated for discrete size distributions (Kulmala et al., 2001, 2012; Dal Maso et al., 2002, 2005). Dry
 176 particle diameters were considered in the calculations and condensing vapour was assumed to have
 177 sulphuric acid properties.

178 One of the key components for NPF events is the gas-phase H_2SO_4 (Sipilä et al., 2010; Sihto et al.,
 179 2011). It is challenging to measure its atmospheric concentration and, therefore, the experimental data
 180 for long time intervals are rare. The relative effects of gas-phase H_2SO_4 are, however, often estimated
 181 by deriving its proxy value. In this study, the H_2SO_4 proxy was calculated according to Mikkonen et al.
 182 (2011b), where the best proxy was based on GRad, SO_2 concentration, RH and CS. The proxy is defined
 183 for $\text{GRad} > 10 \text{ W m}^{-2}$. Other widely used proxy was introduced by Petäjä et al. (2009), but that was
 184 created for clean boreal forest environment. The most recent proxy from Dada et al. (2020) is currently
 185 under review and has not been tested against the proxy used here. All experimental data were used with
 186 their maximum time resolution.

187 The influence of large-scale weather types was considered on a daily basis by including codes for macro-
 188 circulation patterns (MCPs) invented specifically for the Carpathian Basin (Péczely, 1957; Károssy,
 189 2016). The classification is based on the extension and development of cyclones and anticyclones
 190 relative to the Carpathian Basin via the daily sea-level pressure maps constructed for 00:00 UTC in the
 191 North-Atlantic–European region. Thus defined MCP was assigned to the following day in the data.
 192 Basic information on the MCPs are summarised in Table 1.

193 **Table 1.** Macro-circulation patterns (Péczely codes) and their seasonal and annual occurrences in the Carpathian
 194 Basin for years 1958–2010 (Maheras et al., 2018).

No.	Code	Description	Occurrence (%)				
			Winter	Spring	Summer	Autumn	Annual
1	mCc	Cyclone with a cold front over NE Europe, N wind	7.3	11.3	12.1	8.0	9.7
2	AB	Anticyclone over the British Isles, N wind	5.6	7.1	8.6	6.4	6.9
3	CMc	Mediterranean cyclone with a cold front over S Europe, N wind	2.5	3.5	1.8	1.9	2.4
4	mCw	Mediterranean cyclone with a warm front over NE Europe, S wind	9.2	9.7	5.7	7.2	7.9
5	Ae	Anticyclone over E Europe, S wind	14.2	11.3	7.3	17.6	12.6
6	CMw	Mediterranean cyclone with a warm front over S Europe, S wind	8.9	8.7	3.7	8.3	7.4
7	zC	Highly developed cyclone over N Europe, W wind	5.0	3.2	2.7	2.9	3.5
8	Aw	Anticyclone over W Europe, W wind	13.1	11.2	20.8	12.8	14.6

9	As	Anticyclone over S Europe, W wind	7.0	4.4	2.9	5.6	4.9
10	An	Anticyclone over N Europe, E wind	10.9	12.8	11.3	10.1	11.3
11	AF	Anticyclone over Fennoscandia, E wind	2.8	5.2	5.9	3.7	4.4
12	A	Anticyclone over the Carpathian Basin, changing wind direction	11.8	7.3	13.3	13.3	11.4
13	C	Cyclone over the Carpathian Basin, changing wind direction	1.7	4.3	3.9	2.2	3.0

195
196 Each data line containing the date and time, concentrations, CS, H₂SO₄ proxy, meteorological data and
197 MCP codes was further labelled by several indices on a daily basis. These labels served to differentiate
198 between various environmental conditions, which can lead to substantial changes in some variables
199 (Salma et al., 2014). The workdays were marked by label WD, while the holidays were denoted by label
200 HD. Varying classes of NPF event days were also labelled differently. The classification was
201 accomplished via the particle number size distribution surface plots (Dal Maso et al., 2005; refined in
202 Németh et al., 2018 for urban sites) on a daily basis. The main classes were: NPF event days (marked
203 by label NPF), non-event days (label NE), days with undefined character and days with missing data.
204 The earliest estimated time of the beginning of a nucleation (t_1) was also derived (Németh and Salma,
205 2014) and was added to the data record as a parameter. Finally, the data lines were labelled according
206 to the actual technical status of the DMPS system. The data obtained from the beginning of the
207 measurements to the 1st update was labelled as S1, the data derived between the 1st and 2nd updates were
208 label as S2, and label S3 was given to the data obtained after the 2nd update.

209 2.3 Statistical modelling

210 Atmospheric data are usually not normally distributed, and, therefore, non-parametric methods are often
211 used to detect their long-term trends (Asmi et al., 2013; Masiol et al., 2018). The coherent data set
212 prepared as described in Sect. 2.2 was analysed in two ways. First, time trends for concentrations of
213 particles and air pollutants were estimated by using a dynamic linear model (DLM) method. Secondly,
214 the factors affecting the changes in particle concentrations were detected with a generalized linear mixed
215 model (GLMM).

216 2.3.1 Dynamic linear model

217 Dynamic linear models (Durbin and Koopman, 2012; Petris et al., 2009; Laine, 2020) are state-of-the-
218 art tools for time trend detection. The trend is seen as a statistical change in the properties of the
219 background state of the system. Although changes in aerosol concentrations have previously been
220 approximated with linear trends (e.g. Sun et al., ~~2019~~2020), this is not always the most suitable method
221 since the processes affecting the concentrations are continuously evolving over time. Additionally, time
222 series of atmospheric measurements can include multiple time-dependent cycles (e.g. seasonal and
223 diurnal cycles) which are typically non-stationary – meaning that their distributional properties change

224 over time. The DLM approach effectively decomposes the data series into basic components such as
 225 level, trend, seasonality and effect of external forcing by describing statistically the underlying structure
 226 of the process that generated the measured data. All these components are defined by Gaussian
 227 distributions, and they are allowed to vary in time, and the significance and magnitude of this variation
 228 can also be modelled and estimated. In the basic setup of DLM, the sign or the magnitude of the trend
 229 is not defined in advance by the model formulation but estimated from the data. The method can detect
 230 and quantify trends, but the explanations for the observed changes is provided by the user. Nevertheless,
 231 it determines if the observations are consistent with the selected model. We used the DLM to explain
 232 variability in the particle concentration time series using following components: locally linear mean
 233 level, trend, seasonal effect, autoregressive component and noise. The autoregressive component is
 234 added to the model in order to take account the autocorrelation in the data, i.e. the correlation between
 235 subsequent observations. Here it refers to first order autoregressive model (AR(1)). The evolution of the
 236 investigated concentrations – after the seasonal and noise components were filtered out – is modelled
 237 by using the smoothed mean level. Here, the change in the mean level is the trend of the variable. The
 238 statistical model can be described by the following equations (Mikkonen et al., 2015):

$$239 \quad y_t = \mu_t + \gamma_t + \eta_t + \varepsilon_{obs}, \varepsilon_{obs} \sim N(0, \sigma_t^2), \quad (1)$$

$$240 \quad \mu_t = \mu_{t-1} + \alpha_t + \varepsilon_{level}, \varepsilon_{level} \sim N(0, \sigma_{level}^2), \quad (2)$$

$$241 \quad \alpha_t = \alpha_{t-1} + \varepsilon_{trend}, \varepsilon_{trend} \sim N(0, \sigma_{trend}^2), \quad (3)$$

$$242 \quad \eta_t = \rho\eta_{t-1} + \varepsilon_{AR}, \varepsilon_{AR} \sim N(0, \sigma_{AR}^2), \quad (4)$$

243 where y_t is the investigated concentration at time t , μ_t is the mean level and α_t is the change in the level
 244 from time $t-1$ to time t , γ_t is the seasonal component, ~~and~~ η_t is an autoregressive error component and
 245 ρ is the coefficient for autoregressive component, here fixed to $\rho = 0.6$. Here, this latter level is fixed.
 246 The Gaussian stochastic ε terms are used for the observation uncertainty and for random dynamics of
 247 the level and the trend. The seasonal component γ_t contains dummy variables for each month, so it has
 248 a different value for each month with a condition that 12 consecutive months sum to zero. More detailed
 249 description on how the model is written through state space equation can be found in Mikkonen et al.
 250 (2015).

251 2.3.2 Generalized linear mixed model

252 Linear mixed models (McCulloch et al., 2008) belong to the family of models that combine several
 253 different kinds of models used in multivariate analysis when the data do not fulfil the standard
 254 independency and homogeneity assumptions. This is the normal case with atmospheric and
 255 climatological measured variables (e.g. Mikkonen et al., 2011a). The main goal of the mixed models is
 256 to estimate not only the mean of the measured response variable but also the variance-covariance

257 structure of the data, which makes the model more valid for complex atmospheric data. In addition,
 258 modelling the (co)variances of the variables reduces the bias of the estimates, and prevents
 259 autocorrelation of the residuals. The model is constructed from general linear model, written in matrix
 260 format as $y = \mathbf{X}\boldsymbol{\beta} + \boldsymbol{\varepsilon}$, by adding a so-called random component (denoted $\mathbf{Z}\mathbf{u}$) to the model, thus the model
 261 is given by $y = \mathbf{X}\boldsymbol{\beta} + \mathbf{Z}\mathbf{u} + \boldsymbol{\varepsilon}$. Here, if we let n equal to number of observations, p equal to number of fixed
 262 parameters and q equal to number of random parameters in the model, \mathbf{y} is the $(n \times 1)$ vector of
 263 measurements of the variable of interest, $\boldsymbol{\beta}$ denotes the unknown $(p \times 1)$ vector of intercept and slope
 264 estimates of the model, \mathbf{X} is the $(n \times p)$ matrix of observations from predictor variables and $\boldsymbol{\varepsilon}$ contains
 265 the residuals of the model. In the random part, \mathbf{Z} is the $(n \times q)$ design matrix for the $(q \times 1)$ vector of
 266 random covariates \mathbf{u} with a q -dimensional normal distribution. With adequate choices of the matrix \mathbf{Z} ,
 267 different covariance structures $\text{Cov}(\mathbf{u}) = \mathbf{G}$ and $\text{Cov}(\boldsymbol{\varepsilon}) = \mathbf{R}$ can be defined and fitted. Successful modelling
 268 of variances and covariances of the observations provides valid statistical inference for the fixed effects
 269 $\boldsymbol{\beta}$ of the mixed model. In contrast to general linear models, the error terms $\boldsymbol{\varepsilon}$ can be correlated, which
 270 makes the modelling more robust. It follows from this that the distribution of observations can be
 271 described by a normal distribution with the expectation of $\bar{\mathbf{X}}$ and covariance matrix \mathbf{V} , which is given
 272 by $\mathbf{V} = \mathbf{Z}\mathbf{G}\mathbf{Z}' + \mathbf{R}$. With GLMM, it is possible to reliably detect the factors which affect particle number
 273 concentrations or which act as indicators for their different sources. The model can be expressed in a
 274 mathematical form as (Mikkonen et al., 2011a):

$$275 \quad N_{Di} = (\beta_0 + \beta_{setup} + u_m) + \alpha_d + (\beta_{wd} \cdot \beta_E) \cdot X_{Ti} + (\beta_1 + v_{1m}) \cdot SO_{2,i} + (\beta_2 + v_{2m}) \cdot NO_{2,i} + \\
 276 \quad (\beta_3 + v_{3m}) \cdot O_{3,i} + \beta_4 \cdot GRad_i + \beta_5 \cdot RH_i + \beta_6 \cdot MCP_i, \quad (45)$$

277 where N_{Di} is the number concentration in selected size range in time i , β_0 is a model intercept, β_{setup} is
 278 a correction term for changes in the measurement system due to two major upgrades, u_m is vector of
 279 random intercepts different for each month, α_d is average change of N_{Di} per day (i.e. slope of trend),
 280 β_{wd} and β_E are coefficients for workday and NPF event day, respectively, and X_{Ti} is the corresponding
 281 vector showing the type of the day (in both means: WD/HD and E/NE) in time i , $\beta_1 - \beta_5$ are fixed
 282 coefficients for SO_2 , NO_2 , O_3 , $GRad$ and RH , respectively, β_6 is the (13×1) vector of coefficients for
 283 different macro-circular patterns (MCP) [indicating the characteristic level of number concentration](#)
 284 [during each MCP type, which are treated here as categorical variable](#), and v_m are the random, month
 285 specific slopes for SO_2 , NO_2 , O_3 and $GRad$. The coefficients of the model can be interpreted in a similar
 286 manner as multivariate regression or general linear models, just with an addition of month-specific
 287 effects for given variables.

288 3 Results and discussion

289 Annual insolation (Q), which expresses the total energy density at a receptor site, was derived from the
 290 individual hourly mean $\text{GRad}_{i,j}$ data, where index i represents the hour of day (from 0 to 23) and index
 291 j stands for the day of year (from 1 to 365) as $Q = 3.6 \times 10^{-6} \times \sum_{i,j} \text{GRad}_{i,j}$. The dimensions of the
 292 individual $\text{GRad}_{i,j}$ data and Q are W m^{-2} and $\text{GJ m}^{-2} \text{y}^{-1}$, respectively. The few randomly missing
 293 datapoints were interpolated linearly. An overview on annual averages of the data analysed in this study
 294 is given in Table 2. Annual insolation, which expresses the total energy density at the receptor site, was
 295 derived from the individual GRad_i data as $Q = n_d \times 24 \times 3600 \times \sum_i \text{GRad}_i$ over the year of interest (n_d is
 296 the number of day in the year). Since the major sources of particles in cities include road vehicles and
 297 atmospheric nucleation, we added some indicative data on these specific sources as well. The median
 298 particle number concentrations are basically in line with many other comparable cities in the world (e.g.
 299 Kerminen et al., 2018; Masiol et al., 2018). They indicate a decreasing change (except for $N_{100-1000}$) over
 300 the years 2008–2018. At the same time, the annual averages of the other concentrations, meteorological
 301 data and auxiliary variables did not change substantially. Annual mean relative occurrence frequency of
 302 NPF events stayed almost constant with a mean and SD of $(20 \pm 4)\%$, except for the measurement year
 303 2015–2016 when it was unusually small. It is worth adding that the NPF increases the existing particle
 304 number concentrations in Budapest by a factor of approximately 2 on event days (Salma et al., 2017).
 305 The annual medians for the particle formation rate and particle growth rate also stayed constant and
 306 seemingly varied only as fluctuations within ca. $\pm 20\%$ and $\pm 8\%$, respectively. The number of passenger
 307 cars was registered in Budapest remained constant within $\pm 5\%$, while the share of the diesel-powered
 308 passenger cars increased modestly by a rate of approximately 12% from 2008 to 2018 (KSH, 2019). The
 309 number (ca. 4000) of buses registered in Budapest and the share (98%) of the diesel-power buses on the
 310 national bus fleet remained constant.

311 **Table 2.** Annual medians of particle number concentrations in the diameter ranges from 6 to 1000 nm (N_{6-1000}),
 312 from 6 to 100 nm (N_{6-100}), from 25 to 100 nm (N_{25-100}) and from 100 to 1000 nm ($N_{100-1000}$), concentrations of SO_2 ,
 313 CO , NO , NO_x , O_3 , PM_{10} mass, annual means of air temperature (T), relative humidity (RH), wind speed (WS),
 314 atmospheric pressure (P) and annual insolation (Q), annual mean relative occurrence frequency of nucleation
 315 (f_{NPF}), annual median formation rate of particles with a diameter of 6 nm (J_6), annual median growth rate of
 316 particles with a diameter of 10 nm (GR_{10} ; for the rates, see Salma and Németh, 2019), number of passenger cars
 317 registered in Budapest (Cars), the mean age and the share of diesel-powered vehicles (Diesel) separately for the 1-
 318 year-long measurement time intervals.

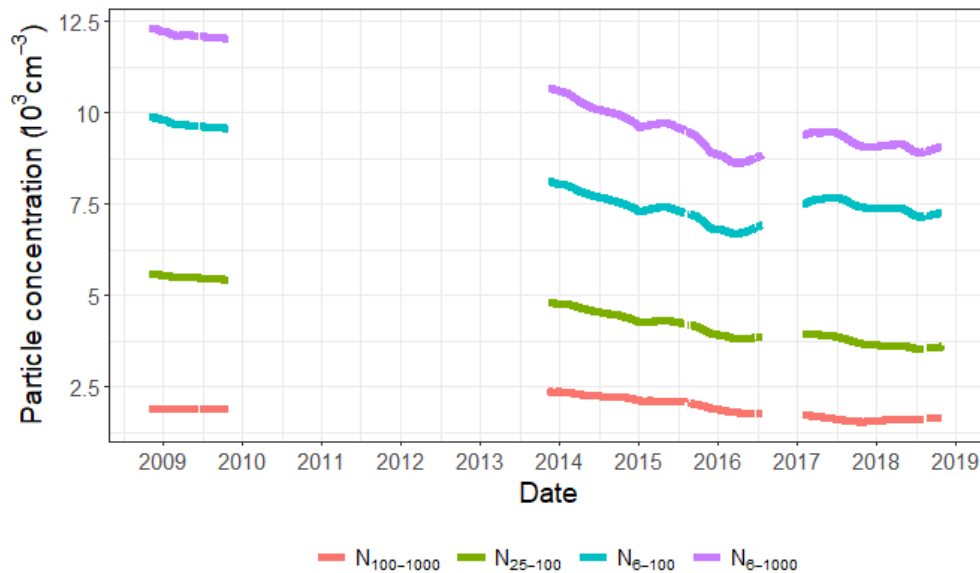
Variable	Unit	2008–2009	2013–2014	2014–2015	2015–2016	2017–2018	2018–2019
N_{6-1000}	10^3 cm^{-3}	11.5	9.7	9.3	7.5	8.6	8.3
N_{6-100}	10^3 cm^{-3}	9.1	7.2	6.9	5.7	6.8	6.5
N_{25-100}	10^3 cm^{-3}	5.1	4.3	4.1	3.3	3.6	3.2
$N_{100-1000}$	10^3 cm^{-3}	1.79	2.2	2.0	1.56	1.49	1.53
SO_2	$\mu\text{g m}^{-3}$	5.0	4.8	4.6	4.8	4.5	5.2

CO	$\mu\text{g m}^{-3}$	547	488	577	513	534	624
NO	$\mu\text{g m}^{-3}$	13.3	19.2	23	17.6	20	17.0
NO _x	$\mu\text{g m}^{-3}$	58	80	89	72	79	73
O ₃	$\mu\text{g m}^{-3}$	23	14.8	19.6	25	20	21
PM ₁₀	$\mu\text{g m}^{-3}$	33	31	39	29	28	36
<i>T</i>	°C	12.0	13.2	13.2	12.9	13.2	13.3
RH	%	64	69	64	69	63	67
WS	m s^{-1}	2.5	2.6	2.8	2.7	2.9	2.5
<i>P</i>	hPa	1001	1003	1005	1004	1004	1004
<i>Q</i>	$\text{GJ m}^{-2} \text{y}^{-1}$	4.45	4.39	4.58	4.52	4.77	4.66
<i>f</i> _{NPF}	%	24	20	23	13.0	23	20
<i>J</i> ₆	$\text{cm}^{-3} \text{s}^{-1}$	4.2	3.5	4.4	4.6	6.3	4.6
GR ₁₀	nm h^{-1}	7.6	6.6	6.5	8.0	7.5	7.0
Cars*	10 ³ pcs	582	573	584	597	634	659
Age*	y	10.8	13.0	13.4	13.7	14.1	14.2
Diesel*	%	20	24	26	28	29	n.a.

319 * Status at the end of years 2009, 2013, 2014, 2015, 2017 and 2018, respectively.
 320 n.a.: not yet available.

321 3.1 Decennial time scale

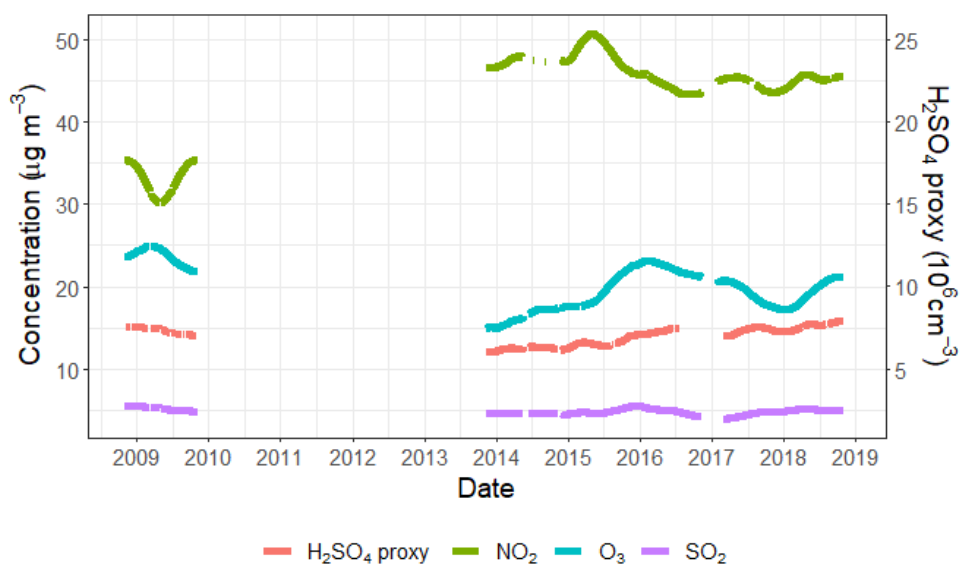
322 Overall statistical time trends for particle number concentrations in various size fractions obtained by
 323 the DLM are displayed in Figure 1. The curves confirm that the N_{6-1000} , N_{6-100} and N_{25-100} indeed
 324 decreased in Budapest between 2008 and 2018, while the change in $N_{100-1000}$ was not significant. The
 325 decline mostly took place in a monotonical manner except for perhaps the interval of summer 2016–
 326 spring 2017, when some partial/local increase could be realised for N_{6-1000} and N_{6-100} .



327 **Figure 1.** Statistical time trends of particle number concentrations in the diameter ranges from 6 to 1000 nm (N_{6-1000}),
 328 from 6 to 100 nm (N_{6-100}), from 25 to 100 nm (N_{25-100}) and from 100 to 1000 nm ($N_{100-1000}$) derived by DLM
 329 over a decennial interval.

330 There are several important sources, sinks and atmospheric transformation processes including
 331 environmental conditions which can influence the atmospheric concentrations. The major sources

332 include both high-temperature emissions and NPF events as discussed in Sect. 1. The latter source is
 333 affected by concentrations of precursor and other trace gases, meteorological properties for
 334 photochemical reactions, and the interactions among gas-phase chemical species of different origin/type
 335 with respect the formation yield of condensing vapours (Kulmala et al., 2014; McFiggans et al., 2019).
 336 The air pollutants listed in Table 2 and gas-phase H_2SO_4 proxy – which are known or expected to affect
 337 particle number concentrations – did not exhibit decreasing statistical trend between 2008 and 2018
 338 (Fig. 2). On one hand, this decoupling ~~confirms~~ suggests that the causes of the decrease in particle
 339 number concentrations are not primarily related to meteorological conditions because they would jointly
 340 affect the gas concentrations as well (if their sources are more-or-less constant over a certain time
 341 interval). On the other hand, the constant gas concentrations suggest that the decreasing trend in particles
 342 does not seem to be related to the major precursors or interacting gaseous chemical species (such as
 343 SO_2 , H_2SO_4 or NO_2).



344 **Figure 2.** Statistical time trends of gas-phase H_2SO_4 proxy, SO_2 , O_3 and NO_2 derived by DLM over the decennial
 345 interval.

346 As far as the meteorological conditions are concerned, some of them such as WS, atmospheric boundary
 347 mixing layer height and T have previously been shown to influence the temporal variation of aerosol
 348 particles (e.g. Birmili et al., 2001; Mikkonen et al., 2011a). The annual means of possibly relevant
 349 properties and parameters in Table 2 – except for the particle number concentrations (which are under
 350 the investigation) and the fraction of diesel cars – did not show any obvious dependency; they virtually
 351 stayed constant over the years of interest. The possible effect of different weather conditions on the
 352 concentrations are studied separately by the GLMM and are discussed in Sect. 3.2.2. There were also
 353 no substantial and extensive urban constructions in the area (which could influence the urban air flow)
 354 nor larger systematic changes in the traffic circulation around the sampling site in the time interval
 355 considered. Therefore, the decline in the particle number concentrations ~~is~~ can most likely be interpreted
 356 as a consequence of the decreased anthropogenic particulate emissions in Budapest. The related source

sectors can include vehicular road traffic and household heating/cooking. The decline happened at an increasing share of the diesel passenger cars and straitened emission control on (diesel) vehicles, [as e.g. Platt et al. \(2017\) and Wihersaari et al. \(2020\)](#); [showed that modern diesel engines have smaller lower particle emissions than gasoline engines.](#)

The average decrease rates of particle number concentrations as derived from both the DLM and GLMM statistical approaches are summarised in Table 3. The rates are shown as obtained from the models and scaled for the 10-year measurement interval to ensure the comparability of the slopes. The relative mean changes in % per year were expressed with respect to the starting value (mean of the first year). There are some differences between the corresponding results of the two models, which were caused by standardising the concentrations with the predictors in the models and by handling the upgrades of measurement setup differently. The changes in all size fractions were on the same level and only minor differences could be seen. As the estimates always contain some uncertainty, these differences are not considered as statistically significant. The largest difference between the two models was observed for $N_{100-1000}$ (which had the lowest absolute concentrations). One possible cause for this might be that GLMM standardises the results for variables indicating anthropogenic emissions and thus the size fraction that is the most sensitive for the emissions has the strongest effect. Considering all these, the rates from the two statistical models agree well. Furthermore, the rates for N_{6-1000} and N_{6-100} were identical. This is explained by the fact that these two size fractions are strongly connected; the typical N_{6-100}/N_{6-1000} mean ratio in central Budapest is 75–80% (Salma and Németh, 2019). Small difference was also seen for N_{25-100} . In urban areas, this size fraction is mainly composed of particles from high-temperature emission sources. The source types responsible for the observed decline are further discussed in Sect. 3.2.1.

Table 3. Decrease rates of particle number concentrations in the diameter ranges from 6 to 1000 nm, from 6 to 100 nm, from 25 to 100 nm and from 100 to 1000 nm obtained by the dynamic linear model and generalized linear mixed model as a mean absolute change per year during the 10-year measurement interval and as a relative mean change per year with respect to the mean value of the first year.

Size fraction (nm)	Dynamic linear model		Generalized linear mixed model	
	Mean change/year (cm^{-3})	Relative mean change (%/year)	Mean change/year (cm^{-3})	Relative mean change (%/year)
6–1000	–510	–4	–660	–5
6–100	–400	–4	–480	–5
25–100	–310	–6	–360	–5
100–1000	–50	–3	–180	–8

Our results concerning the decennial change rates (and our conclusions with regard to their causes mainly discussed in Sect. 3.2.1) are comparable and are in line with some other very recent studies. Sun

386 et al. (2019,2020) investigated the statistical concentration trends in particle numbers (and equivalent
387 black carbon mass) at multiple urban, rural or background sites within the German Ultrafine Aerosol
388 Network. Decreasing annual slopes of $-(7.0-1.7)\%$ were obtained for several size fractions (which are
389 different from our intervals), and the most likely factors for the decreasing trends were assigned to
390 declining anthropogenic emissions due to emission mitigation policies of the EU. Masiol et al. (2018)
391 evaluated statistical time trends of particle number concentrations in various size fractions (which are
392 different again from the previous and present studies) in Rochester, NY, USA, and obtained a typical
393 decline rate of -4.6% per year for total particles. These outcomes and our data as well seem to be
394 different from the results obtained by Saha et al. (2018) in the urban Pittsburgh, PA, USA by comparing
395 two intervals of 2001–2002 and 2016–2017. It should be mentioned that in the latter research, the
396 experimental setup for measuring particle number size distributions had a lower diameter limit of
397 detection at 11 nm, some methodological approaches (e.g. classification of events) were different from
398 ours and that the time trend was not derived by statistical modelling. The authors concluded that both
399 the frequency of NPF events and their dynamic properties were reduced by (40–50)% over the past 15
400 years, resulting in ca. 48% reduction of UF concentrations. The changes were attributed to dramatic
401 reductions in SO₂ emissions in the larger region.

402 **3.2 Diurnal time scale**

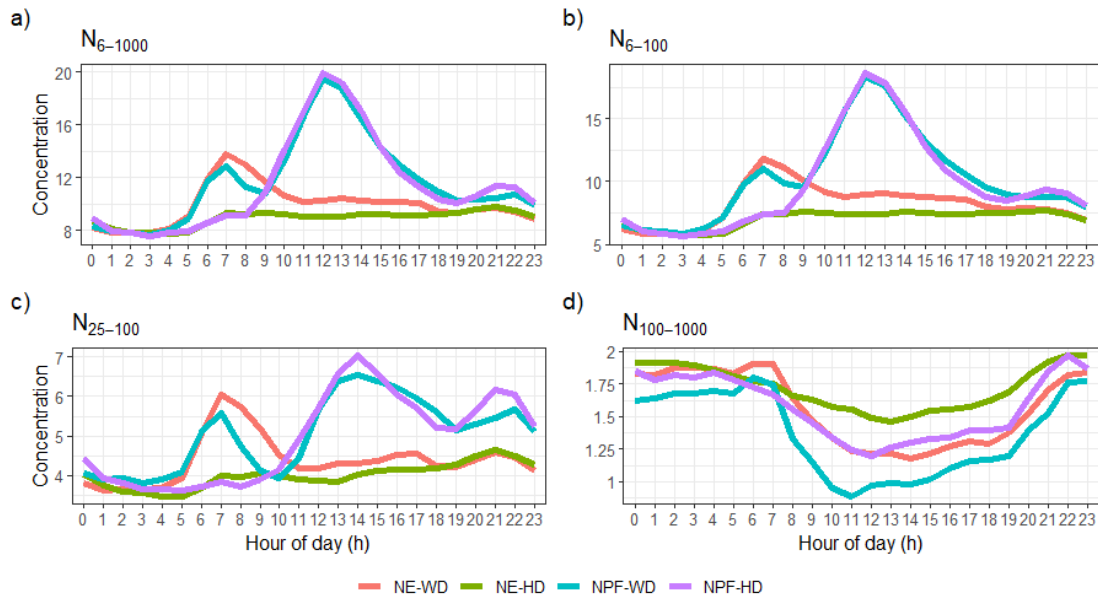
403 Diurnal statistical patterns of the particle number concentrations in different size fractions were
404 predicted by the GLMM considering the following variables: GRad, RH, concentrations of SO₂, NO₂,
405 O₃, and labels for workdays/holidays, for NPF event days/non-event days and for MCP codes. The initial
406 screening for possible prediction variables was done in earlier papers. Studies such as Hyvönen et al.
407 (2005), Mikkonen et al. (2006) and Nieminen et al. (2014) suggested that meteorological and trace gas
408 variables affect NPF. Furthermore, e.g. Mikkonen et al. (2011a), Guo et al. (2012) and Zaidan et al.
409 (2018) studied the factors which influence the growth of freshly formed particles as well as the
410 concentrations of particles in larger size fractions and specified the possible predictors. All variables
411 found in these screenings and measured at our site were tested one-by-one in the GLMM model in a
412 stepwise manner. In each step, the significance of the added or removed variable was investigated by a
413 likelihood ratio test (e.g. Pinheiro and Bates, 2000) until the final model shown in Eq. 4 was formed.
414 The effect of the H₂SO₄ proxy was also tested, and the results for the daytime concentrations were
415 similar to those obtained with the selection of variables above. The modelling results for night-time
416 were, however, biased since the proxy is defined for $\text{GRad} > 10 \text{ W m}^{-2}$, and, therefore, we decided not to
417 include the proxy into the final model.

418 **3.2.1 Diurnal statistical patterns**

419 Modelled diurnal pattern of particle number concentrations for event days on workdays, event days on
420 holidays, non-event days on workdays and non-event days on holidays separately for different size

421 fractions are shown in Fig. 3. The curves on Fig. 3a–c resemble tendentious variations, which can be
422 associated with typical diurnal activity–time pattern of inhabitants in cities, particularly with road traffic.
423 They are also perfectly in line with the mean diurnal tendencies of experimentally determined
424 concentrations in central Budapest (Salma et al., 2014; 2017) and are consistent with the time variations
425 in many other European cities (Hussein et al., 2004; Aalto et al., 2005; Moore et al., 2007; Avino et al.,
426 2011; Dall’Osto et al., 2013).

427 In the statistical diurnal patterns of UF particles (Fig. 3b), there is a huge peak from late morning to late
428 afternoon on event days. This is unambiguously caused by NPF and growth process. The peaks on
429 workdays and holidays are rather similar to each other in the position, shape and magnitude (area), which
430 means that the dynamics and timing of NPF events in general are not substantially influenced by
431 anthropogenic activities, which are more intensive on workdays than on holidays. It is worth mentioning
432 that the overall contribution of the NPF to particle number concentrations is less than what is seemingly
433 indicated by the diurnal patterns alone since NPF events occur on approximately 20% of days (Table 2).
434 Emissions from vehicular road traffic is represented by a notable peak during the morning rush hours
435 (between 05:30 and 08:30) on workdays. It is noted that the boundary layer mixing height is usually
436 increased during this interval because of the increasing solar radiation intensity and mixing intensity.
437 Another peak occurred around 21:00, thus later than the afternoon rush, which usually happens between
438 16:30 and 18:30. Under strong anti-cyclonic conditions, the evolution of the boundary layer mixing
439 height and mixing intensity can decrease the concentration levels in the afternoons until sunset, and this
440 can compensate the increased intensity of emissions. This all means that the afternoon peak is realised
441 in a fuzzy manner since it is more influenced by local meteorology than by vehicular emissions. The
442 effect of residential heating and combustion activities at evenings can also play a role. It is worth noting
443 that the early-morning rush-hour peak on event days was smaller than on non-event days, which agrees
444 with our earlier observation derived directly from experimental data (Salma et al., 2017) and is in line
445 with the overall picture on urban NPF events (Zhang et al., 2015; Kulmala et al., 2017). On holidays,
446 the modelled diurnal variation for non-event days contained an increasing part in the morning to a
447 modest concentration level, which remains fairly constant over the daytime. This is explained by the
448 differences in daily activities of citizens on workdays and holidays as far as both their intensity and
449 timing are concerned.



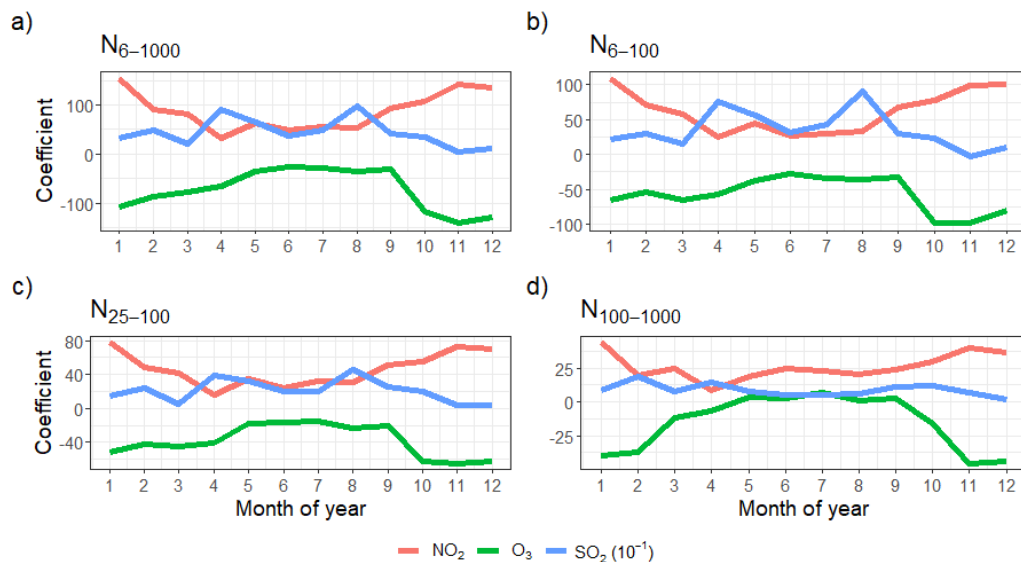
450
 451 **Figure 3.** Diurnal patterns of particle number concentrations in the diameter ranges from 6 to 1000 nm (N_{6-1000}),
 452 from 6 to 100 nm (N_{6-100}), from 25 to 100 nm (N_{25-100}) and from 100 to 1000 nm ($N_{100-1000}$) in units of 10^3 cm^{-3} .
 453 Red: non-event on workdays, green: non-event on holidays, cyan: event on workdays, purple: event on holidays.

454 The statistical diurnal patterns of N_{6-1000} trends (Fig. 3a) were very similar or analogous to those of the
 455 N_{6-100} . These two size fractions are strongly connected with each other as explained in Sect. 3.1. The
 456 diurnal curves for N_{25-100} (Fig. 3c) were also similar to the previous corresponding curves as far as the
 457 character and shape are concerned, while there were also evident differences between their relative
 458 structures. The peaks for the early morning and late afternoon rush hours were relatively larger than in
 459 the trends of 6–100- or 6–1000-nm size fractions due to the higher contribution of primary particles
 460 from high temperature sources in this size fraction. New particle formation generally occurs on days
 461 when N_{25-100} are smaller before the event onset (between 08:00 and 11:00). The maximum of the peaks
 462 associated with NPF events in Fig. 3a and b – which is between 12:00 and 13:00 – was also shifted to
 463 later, i.e. to ca. 14:00 in Fig. 3c. This can be explained by the time needed for freshly nucleated particles
 464 to reach the diameter range >25 nm.

465 The statistical diurnal patterns for $N_{100-1000}$ seem very different from the smaller size ranges. First, their
 466 time variations were rather small in comparison to the other size fractions. On workdays, they only
 467 showed a modest elevation from 06:00 to 08:00 (morning rush hours), which is mainly caused by
 468 resuspension of road/surface dust particles by moving vehicles or by emissions of coarse particles from
 469 material wear. This morning peak was even missing on holidays, but another small and broad elevation
 470 showed up from 21:00 to 22:00. This and the overall changes during the daylight time are primarily
 471 related to the daily cycling of local meteorological conditions, in particular of boundary layer mixing
 472 height under stable anti-cyclonic weather conditions, outlined above.

473 3.2.2 Effects of variables

474 Monthly mean coefficients (mean v_m slopes in Eq. 4) of NO₂, O₃ and SO₂ derived by GLMM, which
 475 express their partial effects on particle number concentrations are shown in Fig. 4 for different size
 476 fractions.



477
 478 **Figure 4.** Distribution of monthly mean coefficients (which are proportional to the partial effects) for NO₂, O₃ and
 479 SO₂ on particle number concentrations separately in the diameter ranges from 6 to 1000 nm (N_{6-1000}), from 6 to
 480 100 nm (N_{6-100}), from 25 to 100 nm (N_{25-100}) and from 100 to 1000 nm ($N_{100-1000}$).

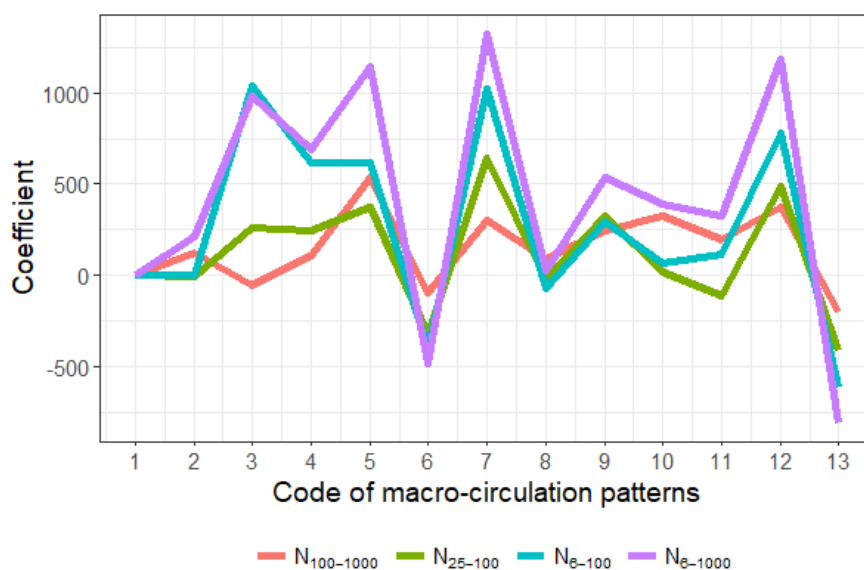
481 The coefficients of SO₂ and NO₂ are positive, while O₃ seems to have a decreasing effect on particle
 482 number concentrations. The coefficients all have seasonal patterns, which means that the magnitude of
 483 their effect on particle concentrations are of different magnitude in different months. This means for
 484 example that 1 $\mu\text{g m}^{-3}$ increase in NO₂ concentration increases N_{6-1000} concentration in January by 154
 485 m^{-3} but in June by 50 m^{-3} . This could, however, be partly caused by annual changes of boundary layer
 486 mixing height or some other variable affecting particle concentrations, and correlating with these, but
 487 not measured at the site. The boundary layer mixing height tends to be smaller in Budapest in winter
 488 than in the other seasons (Salma et al., 2011), which ordinarily results in higher atmospheric
 489 concentrations at steady-state absolute amounts of chemical species. The coefficients of NO₂ on N_{6-1000} ,
 490 N_{6-100} and N_{25-100} were higher in winter. This may indicate that large fractions of particles in these three
 491 size fractions originate from residential heating and NO₂ acts as an indicator for this source. Another
 492 major source of NO₂ and primary particles is the road traffic, but this does not show seasonal variation
 493 in Budapest. The seasonal effect of NO₂ on chemically aged, regional type particles ($N_{100-1000}$) may not
 494 be significant.

495 The partial effect of O₃ on N_{6-1000} , N_{6-100} and N_{25-100} was weaker in summer, late spring and early autumn.
 496 This interval coincides with relatively large O₃ concentrations in the area. Ozone has a strong seasonal
 497 variation (as shown in Fig. S1 in the Supplement). The negative correlation between O₃ concentration

498 and its effect on particle concentrations need further clarification since O_3 participates in a large variety
 499 of complex atmospheric processes and also serves as a marker for photochemical processes which
 500 influence secondary particle formation. The influence of O_3 on $N_{100-1000}$ was virtually negligible due
 501 likely to the regional character of these particles (which are usually chemically aged and often represent
 502 larger spatial scale due to their larger atmospheric residence time) similarly to NO_2 . In addition, O_3
 503 might act as an indicator of particulate pollution from traffic, power plants and other anthropogenic
 504 sources. Then more ozone would indicate higher number of larger particles and due to coagulation less
 505 smaller particles.

506 The partial effects of SO_2 on the particle number concentrations were the largest of the three gases
 507 considered. In the N_{6-1000} , N_{6-100} and N_{25-100} , two peaks appeared, one in spring and another one in late
 508 summer. This shape is in line with the average distribution of the monthly mean relative NPF occurrence
 509 frequency in Budapest (Salma and Németh, 2019). The latter distribution consists of an absolute and a
 510 local minimum in January (with a monthly mean occurrence frequency of 5.9%) and in August (17.0%),
 511 respectively, and an absolute and a local maximum in April (41%) and in September with (26%),
 512 respectively. The distribution of the SO_2 coefficient suggests and confirms that SO_2 , via NPF events
 513 contribute in a substantial extent to the particle number concentrations in cities. The influence of SO_2
 514 on $N_{100-1000}$ was virtually negligible due likely to the regional character of these particles similarly to the
 515 other two gases included into the model.

516 Figure 5 summarizes the effect of macro-circulation patterns on particle number concentrations in the
 517 different size fractions. It is seen that the larger regional-type particles are less affected by the MCPs
 518 than the smaller particles. The weather conditions favouring NPF events can be identified from the
 519 curves by looking at the largest coefficients for size fraction of 6–100 nm.

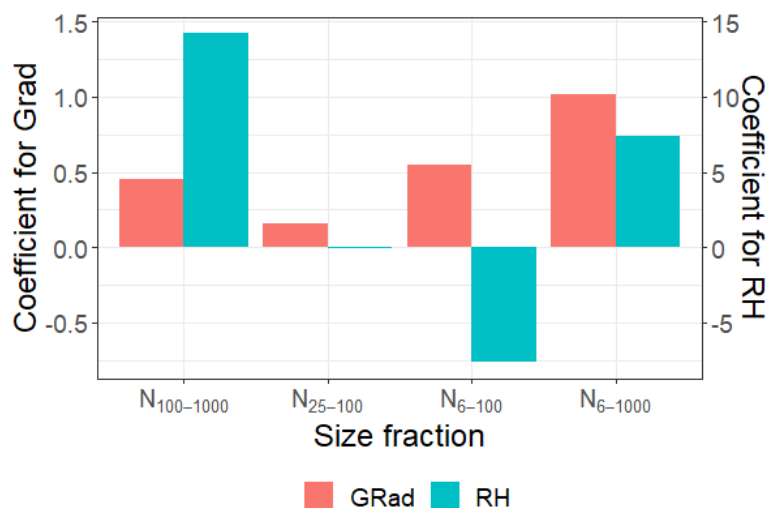


520

521 **Figure 5.** Distribution of monthly mean coefficients (which are proportional to the partial effects) for macro-
522 circulation patterns (Péczezy codes) on particle number concentrations separately in the diameter ranges from 100
523 to 1000 nm ($N_{100-1000}$), from 25 to 100 nm (N_{25-100}), from 6 to 100 nm (N_{6-100}) and from 6 to 1000 nm (N_{6-1000}).

524 It seems that the MCP no. 3 (Mediterranean cyclone with a cold front over S Europe, N wind), 7 (highly
525 developed cyclone over N Europe, W wind) and 12 (anticyclone over the Carpathian Basin, changing
526 wind direction) can represent favourable conditions for NPF events than the other MCPs. Under these
527 conditions, the weather in the area is typically windy, with average solar radiation (expect for MCP no.
528 3 in summer when it shows low daily values), with strong planetary bounding layer evolution and
529 consequently, iv) the pollutants concentrations are below the average (expect for the winter inversions
530 in MCP no. 12). The air pollution situations are better separated by MCP codes in summer than in winter.
531 The weather type classified as no. 6 (Mediterranean cyclone with a warm front over S Europe, S wind)
532 disfavour the events. Under these conditions, the weather is typically cloudy and rainy with lower than
533 average solar radiation. This situation is often associated with polluted air in Budapest. Proportions for
534 NPF days for different MCP codes, which are shown Table S1 in the Supplement, also confirm these
535 conclusions. In order to see if the decreasing concentrations are due to changes in meteorological
536 patterns, we investigated separately the occurrence of the MCP patterns during the measurement period.
537 We found no significant changes in the occurrence of the patterns and thus the decreasing particle
538 concentrations are due to something else than the meteorological patterns.

539 The coefficients for GRad and RH for different size fractions are shown in Fig. 6. It was found that these
540 variables do not have seasonal dependency, i.e. they contribute with equal strength to particle
541 concentrations throughout the year. Effect of GRad is positive for all size fractions, but it is weaker for
542 larger (regional-type or already chemically aged or processed) particles. The latter contribution could
543 be related to the bias in meteorological properties as well. The RH has negligible effect on size fraction
544 of 25–100 nm. It affects strongly and positively the largest particles, which means that the particles are
545 larger within higher humidity. This might be related to local meteorology, as higher RH probably means
546 more clouds and more clouds probably means less radiation and lower boundary layer and this could



547 cause higher particle concentration. In contrast, the effect of RH on the smallest particles was negative,
 548 which is probably caused by high RHs, which limit NPF (e.g. Hamed et al., 2011).

549 **Figure 6.** Distribution of monthly mean coefficients (which are proportional to the partial effects) for global
 550 radiation (GRad) and relative humidity (RH) separately in the diameter ranges from 100 to 1000 nm ($N_{100-1000}$),
 551 from 25 to 100 nm (N_{25-100}), from 6 to 100 nm (N_{6-100}) and from 6 to 1000 nm (N_{6-1000}).

552 3.2.3 Goodness-of-fit evaluation for GLMM

553 In order to estimate the uncertainty of the models for different size fractions, we calculated the mean
 554 absolute errors relative to the dependent variable mean, given by Willmot et al. (2009):

$$555 \text{Err} = (n^{-1} \sum_{i=1}^n |y_i - \hat{y}_i|) \cdot \bar{y}^{-1}, \quad (5)$$

556 where n is the number of observations, y_i are the observed particle number concentrations, \hat{y}_i are the
 557 predicted values given by the GLMM and \bar{y} is the mean of the observed values. In addition, we
 558 calculated Spearman's rank correlation coefficients between the observed and predicted values for all
 559 size fractions. Both goodness-of-fit estimates are shown in Table 4. As the relative errors for different
 560 size fractions are within a range of 0.30–0.34 and the correlations are higher than 0.70, it can be
 561 concluded that the model fitted the data with this size and measurement uncertainty well.

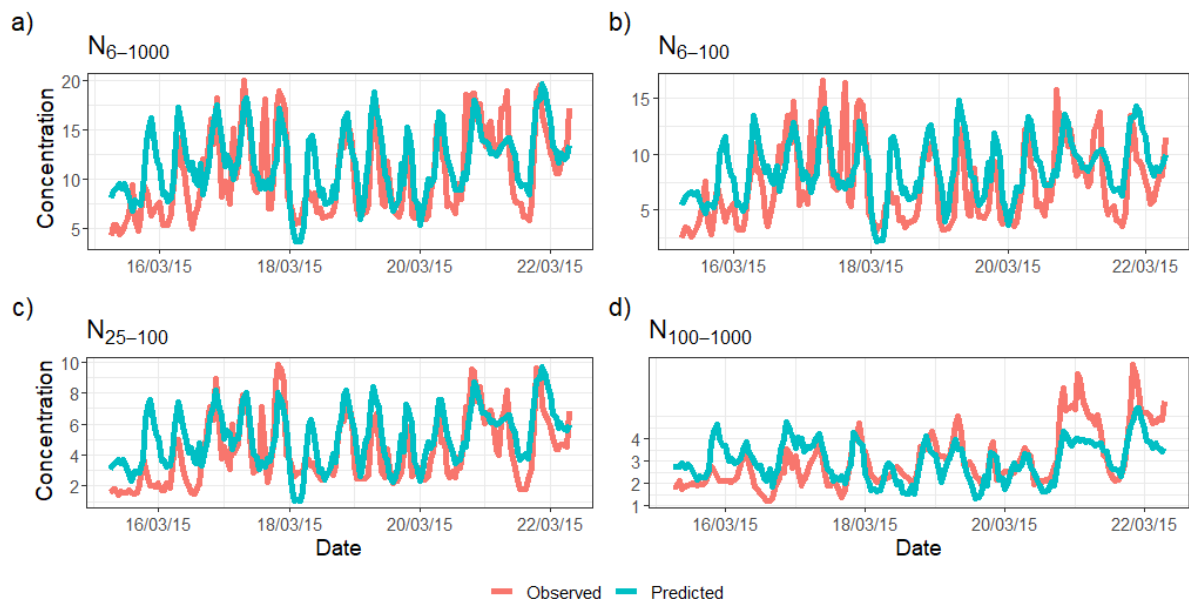
562

563 **Table 4.** Goodness-of-fit estimates for GLMM as expressed by the mean absolute error relative to the dependent
 564 variable mean and by Spearman's rank correlation coefficient separately in the size fractions of 6–1000, 6–100,
 565 25–100 and 100–1000 nm.

Size fraction	Error	Correlation
6–1000	0.30	0.73
6–100	0.32	0.72
25–100	0.34	0.71
100–1000	0.34	0.73

566

567 Figure 7 illustrates how well the GLMM model predicts the observations in all size fractions within a
 568 randomly selected period of one week in March 2015. The figure shows that the predicted values follow
 569 the observations fairly well in all size fractions. Overall, the statistical model finds the peaks of the
 570 concentration, but slightly underestimates the highest peaks and the fastest fluctuations and in some
 571 cases, overestimates the lowest concentrations.



572
 573 **Figure 7.** Observed (red line) and predicted (cyan line) time series for an illustrative example period separately in
 574 the size fractions of 6–1000, 6–100, 25–100 and 100–1000 nm.

575 4 Conclusions

576 In the present study, we determined decennial statistical time trends and diurnal statistical patterns of
 577 atmospheric particle number concentrations in various relevant size fractions in the city centre of
 578 Budapest in an interval of 2008–2018. The decennial statistical trends showed decreasing character
 579 ~~except for the size fraction representing the regional~~ in all applied size fractions of particle
 580 concentrations. The mean overall decrease rate was approximately –5% scaled for the 10-year
 581 measurement interval. One of the likely explanations of t ~~The decline can be interpreted as a consequence~~
 582 of is due to the decreased anthropogenic emissions in the city. The diurnal statistical patterns suggested
 583 that reduced traffic emissions were most likely an important factor in causing the observed changes. It
 584 is expected that traffic intensity changed in a modest manner in the city centre during the time interval
 585 of interest, so our results indicate that the reductions is most likely related to lower emission factors.
 586 This appears to follow some changes of sulfur content in fuels and control measures on emissions for
 587 on-road heavy-duty diesel vehicles. Introduction of better particle filters in diesel cars, cleaner fuel and
 588 more sophisticated diesel engines could also contribute. Modernised technologies in residential and
 589 household heating could also contribute. Our present interpretation ~~The magnitude of the reduced-traffic~~
 590 emission reductions cannot be completely conclusive in all aspects for the moment and further
 591 investigations are planned on the basis of the present results. The changes appear to have responded to
 592 both the policy on urban air quality and the influence of economic circumstances of inhabitants.
 593 Excitingly, the mean ages of passenger cars and busses in Hungary increased during the years under
 594 investigation. The exact explanation and confirmation of the decrease requires continuation of the

595 related measurements [with independent experimental systems](#) and further dedicated studies. The present
596 results can be also used for evaluating the effectiveness of present and prospective mitigation policies.

597 The diurnal statistical patterns can be also utilized in interpreting some properties of NPF events in urban
598 environments, and in explaining time evolution of particle number concentration. As a result of GLMM,
599 we could, for instance, give a parametrization for predicting particle concentrations in different size
600 fractions. Models similar to those developed in the present study could be used for other particle sizes or
601 locations as well. The same parameterization could be used at least in areas with similar concentration
602 levels of particles and pollutants, while the extrapolation of the results to cleaner or more polluted
603 environments needs to be confirmed before the use. Conjugate or linked parameterizations to be
604 developed for varying environments can be implemented as a part of atmospheric models to predict the
605 concentrations of climatically active particles in order to reduce their extensive computational times. In
606 addition, this could also contribute to solving some current uncertain issues in the theoretical description
607 of NPF and growth process, particularly when predicting cloud condensation nuclei concentrations.

608 **Data availability.** The observational data used in this paper are available on request from the corresponding author
609 Imre Salma.

610 **Author contributions.** IS and SM formulated the original concept; ZN, VV, TW and IS collected and processed
611 the experimental data; SM, VL and TY were responsible for the statistical data analyses and their physical basis;
612 SM and IS interpreted the results; IS and SM wrote the manuscript with contributions from all co-authors.

613 **Competing interest.** The authors declare that they have no conflict of interest.

614 **Financial support.** The research was supported by the National Research, Development and Innovation Office,
615 Hungary (contracts K116788, PD124283 and K132254), by the János Bolyai Research Scholarship of the
616 Hungarian Academy of Sciences (ZN) and by the European Regional Development Fund and the Hungarian
617 Government (GINOP-2.3.2-15-2016-00028), The Nessling Foundation, The Academy of Finland Centre of
618 Excellence (grant no. 307331) and The Academy of Finland Competitive funding to strengthen university research
619 profiles (PROFI) for the University of Eastern Finland (grant no. 325022) and Academy of Finland project (grant
620 no. 299544)

621 **References**

- 622 Aalto, P., Hämeri, K., Becker, E., Weber, R., Salm, J., Mäkelä, J., Hoell, C., O'Dowd, C., Karlsson, H., Väkevä,
623 M., Koponen, I. K., Buzorius, G., and Kulmala, M.: Physical characterization of aerosol particles during
624 nucleation events, *Tellus*, 53B, 344–358, 2001.
- 625 Aalto, P., Hämeri, K., Paatero, P., Kulmala, M., Bellander, T., Berglind, N., Bouso, L., Castaño-Vinyals, G.,
626 Sunyer, J., Cattani, G., Marconi, A., Cyrus, J., von Klot, S., Peters, A., Zetzsche, K., Lanki, T., Pekkanen, J.,
627 Nyberg, F., Sjövall, B., and Forastiere, F.: Aerosol particle number concentration measurements in five
628 European cities using TSI-3022 condensation particle counter over a three-year period during health effects of
629 air pollution on susceptible subpopulations, *J. Air Waste Manage. Assoc.*, 55, 1064–1076, 2005.

630 Asmi, A., Collaud Coen, M., Ogren, J. A., Andrews, E., Sheridan, P., Jefferson, A., Weingartner, E., Baltensperger,
631 U., Bukowiecki, N., Lihavainen, H., Kivekas, N., Asmi, E., Aalto, P. P., Kulmala, M., Wiedensohler, A.,
632 Birmili, W., Hamed, A., O'Dowd, C., Jennings, S. G., Weller, R., Flentje, H., Fjaeraa, A. M., Fiebig, M., Myhre,
633 C. L., Hallar, A. G., Swietlicki, E., Kristensson, A., and Laj, P.: Aerosol decadal trends - Part 2: In-situ aerosol
634 particle number concentrations at GAW and ACTRIS stations, *Atmos. Chem. Phys.*, 13, 895–916, 2013.

635 Avino, P., Casciardi, S., Fanizza, C., and Manigrasso, M.: Deep investigation of ultrafine particles in urban air,
636 *Aerosol Air Qual. Res.*, 11, 654–663, 2011.

637 Birmili, W., Wiedensohler, A., Heintzenberg, J., and Lehmann, K.: Atmospheric particle number size distribution
638 in central Europe: Statistical relations to air masses and meteorology, *J. Geophys. Res., Atmospheres*,
639 106(D23), 32005-18, 2001.

640 Braakhuis, H. M., Park, M. V., Gosens, I., De Jong, W. H., and Cassee, F. R.: Physicochemical characteristics of
641 nanomaterials that affect pulmonary inflammation, *Part. Fibre Toxicol.*, 11:18, doi: 10.1186/1743-8977-11-18,
642 2014.

643 Brines, M., Dall'Osto, M., Beddows, D. C. S., Harrison, R. M., Gómez-Moreno, F., Núñez, L., Artñano, B.,
644 Costabile, F., Gobbi, G. P., Salimi, F., Morawska, L., Sioutas, C., and Querol, X.: Traffic and nucleation events
645 as main sources of ultrafine particles in high-insolation developed world cities, *Atmos. Chem. Phys.* 15, 5929–
646 5945, 2015.

647 Cassee, F. R., Héroux, M.-E., Gerlofs-Nijland, M. E., and Kelly, F. J.: Particulate matter beyond mass: recent
648 health evidence on the role of fractions, chemical constituents and sources of emission, *Inhal. Toxicol.* 25,
649 802–812, 2013.

650 Carslaw, K. S., Lee, L. A., Reddington, C. L., Pringle, K. J., Rap, A., Forster, P. M., Mann, G. W., Spracklen, D.
651 V., Woodhouse, M. T., Regayre, L. A., and Pierce, J. R.: Large contribution of natural aerosols to uncertainty
652 in indirect forcing, *Nature*, 503, 67–71, 2013.

653 Dada, L., Ylivinkka, I., Baalbaki, R., Li, Ch., Guo, Y., Yan, Ch., Yao, L., Sarnela, N., Jokinen, T., Daellenbach,
654 K. D., Yin, R., Deng, Ch., Chu, B., Nieminen, T., Kontkanen, J., Stolzenburg, D., Sipilä, M., Hussein, T.,
655 Paasonen, P., Bianchi, F., Salma, I., Weidinger, T., Pikridas, M., Sciare, J., Jiang, J., Liu, Y., Petäjä, T.,
656 Kerminen, V.-M., and Kulmala, M.: Sources and sinks driving sulphuric acid concentrations in contrasting
657 environments: implications on proxy calculations, *Atmos. Chem. Phys. Discuss.*, under evaluation, 2020.

658 Dal Maso, M., Kulmala, M., Lehtinen, K. E. J., Mäkelä, J. M., Aalto, P. P., and O'Dowd, C.: Condensation and
659 coagulation sinks and formation of nucleation mode particles in coastal and boreal forest boundary layers, *J.*
660 *Geophys. Res.*, 107(19D), 8097, 10.1029/2001jd001053, 2002.

661 Dal Maso, M., Kulmala, M., Riipinen, I., Wagner, R., Hussein, T., Aalto, P. P., and Lehtinen, K. E. J.: Formation
662 and growth of fresh atmospheric aerosols: eight years of aerosol size distribution data from SMEAR II,
663 Hyytiälä, Finland, *Boreal Environ. Res.*, 10, 323–336, 2005.

664 Dall'Osto, M., Querol, X., Alastuey, A., O'Dowd, C., Harrison, R. M., Wenger, J., and Gómez-Moreno, F. J.: On
665 the spatial distribution and evolution of ultrafine particles in Barcelona, *Atmos. Chem. Phys.*, 13, 741–759,
666 2013.

667 Directive 2009/30/EC, Official Journal of the European Union, L 140, EN, 88–113, 5. 6. 2009.

668 Dunne, E. M., Gordon, H., Kürten, A., Almeida, J., Duplissy, J., Williamson, C., Ortega, I. K., Pringle, K. J.,
669 Adamov, A., Baltensperger, U., Barmet, P., Benduhn, F., Bianchi, F., Breitenlechner, M., Clarke, A., Curtius,
670 J., Dommen, J., Donahue, N. M., Ehrhart, S., Flagan, R. C., Franchin, A., Guida, R., Hakala, J., Hansel, A.,
671 Heinritzi, M., Jokinen, T., Kangasluoma, J., Kirkby, J., Kulmala, M., Kupc, A., Lawler, M. J., Lehtipalo, K.,
672 Makhmutov, V., Mann, G., Mathot, S., Merikanto, J., Miettinen, P., Nenes, A., Onnela, A., Rap, A.,
673 Reddington, C. L. S., Riccobono, F., Richards, N. A. D., Rissanen, M. P., Rondo, L., Sarnela, N.,
674 Schobesberger, S., Sengupta, K., Simon, M., Sipilä, M., Smith, J. N., Stozkhov, Y., Tomé, A., Tröstl, J.,
675 Wagner, P. E., Wimmer, D., Winkler, P. M., Worsnop, D. R., and Carslaw, K. S.: Global atmospheric particle
676 formation from CERN CLOUD measurements, *Science* 354, 1119–1124, 2016.

677 Durbin, J. and Koopman, S. J.: Time series analysis by state space methods, Oxford University Press, Oxford,
678 2012.

679 Giechaskiel, B., Lahde, T., Suarez-Bertoa, R., Clairotte, M., Grigoratos, T., Zardini, A., Perujo, A., and Martini,
680 G.: Particle number measurements in the European legislation and future JRC activities, *Combustion Engines*,
681 174, 3–16, 2018.

682 Gordon, H., Sengupta, K., Rap, A., Duplissy, J., Frege, C., Williamson, C., Heinritzi, M., Simon, M., Yan, C.,
683 Almeida, J., Tröstl, J., Nieminen, T., Ortega, I. K., Wagner, R., Dunne, E. M., Adamov, A., Amorim, A.,
684 Bernhammer, A. K., Bianchi, F., Breitenlechner, M., Brilke, S., Chen, X., Craven, J. S., Dias, A., Ehrhart, S.,
685 Fischer, L., Flagan, R. C., Franchin, A., Fuchs, C., Guida, R., Hakala, J., Hoyle, C. R., Jokinen, T., Junninen,
686 H., Kangasluoma, J., Kim, J., Kirkby, J., Krapf, M., Kürten, A., Laaksonen, A., Lehtipalo, K., Makhmutov, V.,
687 Mathot, S., Molteni, U., Monks, S. A., Onnela, A., Peräkylä, O., Piel, F., Petäjä, T., Praplan, A. P., Pringle, K.
688 J., Richards, N. A. D., Rissanen, M. P., Rondo, L., Sarnela, N., Schobesberger, S., Scott, C. E., Seinfeld, J. H.,
689 Sharma, S., Sipilä, M., Steiner, G., Stozhkov, Y., Stratmann, F., Tomé, A., Virtanen, A., Vogel, A. L., Wagner,
690 A. C., Wagner, P. E., Weingartner, E., Wimmer, D., Winkler, P. M., Ye, P., Zhang, X., Hansel, A., Dommen,
691 J., Donahue, N. M., Worsnop, D. R., Baltensperger, U., Kulmala, M., Curtius, J., and Carslaw, K. S.: Reduced
692 anthropogenic aerosol radiative forcing caused by biogenic new particle formation, *Proc. Natl. Acad. Sci.*
693 *U.S.A.*, 113, 12053–12058, 2016.

694 Guo, H., Wang, D. W., Cheung, K., Ling, Z. H., Chan, C. K., and Yao, X. H.: Observation of aerosol size
695 distribution and new particle formation at a mountain site in subtropical Hong Kong, *Atmos. Chem. Phys.*, 12,
696 9923–9939, <https://doi.org/10.5194/acp-12-9923-2012>, 2012.

697 Hamed, A., H. Korhonen, S.-L. Sihto, J. Joutsensaari, H. Järvinen, T. Petäjä, F. Arnold, T. Nieminen, M. Kulmala,
698 J. N. Smith, K. E. J. Lehtinen, A. Laaksonen: The role of relative humidity in continental new particle
699 formation, *J. Geophys. Res.*, 116, D03202, doi:10.1029/2010JD014186, 2011.

700 Hussein, T., Puustinen, A., Aalto, P. P., Mäkelä, J. M., Hämeri, K., and Kulmala, M.: Urban aerosol number size
701 distributions, *Atmos. Chem. Phys.*, 4, 391–411, 2004.

702 Hyvönen, S., Junninen, H., Laakso, L., Dal Maso, M., Grönholm, T., Bonn, B., Keronen, P., Aalto, P., Hiltunen,
703 V., Pohja, T., Launiainen, S., Hari, P., Mannila, H., and Kulmala, M.: A look at aerosol formation using data
704 mining techniques, *Atmos. Chem. Phys.*, 5, 3345–3356, 2005.

705 Károssy, Cs.: A Kárpát-medence Péczely-féle makroszinoptikus időjárás helyzeteinek katalógusa 1881–2015
706 (Catalogue of the Péczely macrosynoptic weather types for the Carpathian Basin 1881–2015, in Hungarian),
707 OSKAR Kiadó, Budapest, 2016.

708 Kerminen, V.-M., Paramonov, M., Anttila, T., Riipinen, I., Fountoukis, C., Korhonen, H., Asmi, E., Laakso, L.,
709 Lihavainen, H., Swietlicki, E., Svenningsson, B., Asmi, A., Pandis, S. N., Kulmala, M., and Petäjä, T.: Cloud
710 condensation nuclei production associated with atmospheric nucleation: a synthesis based on existing literature
711 and new results, *Atmos. Chem. Phys.*, 12, 12037–12059, 2012.

712 Kerminen, V.-M., Chen, X., Vakkari, V., Petäjä, T., Kulmala, M., and Bianchi, F.: Atmospheric new particle
713 formation and growth: review of field observations, *Environ. Res. Lett.*, 13 (2018) 103003, 2018.

714 KSH, National register of road vehicles (in Hungarian), Hungarian Central Statistical Office, Budapest, 2019.

715 Kulmala, M., Dal Maso, M., Mäkelä, J. M., Pirjola, L., Väkevä, M., Aalto, P., Miiikkulainen, P., Hämeri, K., and
716 O'Dowd, C. D.: On the formation, growth and composition of nucleation mode particles, *Tellus B*53, 479–490,
717 2001.

718 Kulmala, M., Petäjä, T., Nieminen, T., Sipilä, M., Manninen, H. E., Lehtipalo, K., Dal Maso, M., Aalto, P. P.,
719 Junninen, H., Paasonen, P., Riipinen, I., Lehtinen, K. E. J., Laaksonen, A., and Kerminen, V.-M.: Measurement
720 of the nucleation of atmospheric aerosol particles, *Nat. Protoc.*, 7, 1651–1667, doi:10.1038/nprot.2012.091,
721 2012.

722 Kulmala, M., Kontkanen, J., Junninen, H., Lehtipalo, K., Manninen, H. E., Nieminen, T., Petäjä, T., Sipilä, M.,
723 Schobesberger, S., Rantala, P., Franchin, A., Jokinen, T., Järvinen, E., Äijälä, M., Kangasluoma, J., Hakala, J.,
724 Aalto, P. P., Paasonen, P., Mikkilä, J., Vanhanen, J., Aalto, J., Hakola, H., Makkonen, U., Ruuskanen, T.,
725 Mauldin, R. L. III, Duplissy, J., Vehkamäki, H., Bäck, J., Kortelainen, A., Riipinen, I., Kurtén, T., Johnston,
726 M. V., Smith, J. N., Ehn, M., Mentel, T. F., Lehtinen, K. E. J., Laaksonen, A., Kerminen, V.-M., and Worsnop,
727 D. R.: Direct observations of atmospheric aerosol nucleation, *Science*, 339, 943–946, 2013.

728 Kulmala, M., Petäjä, T., Ehn, M., Thornton, J., Sipilä, M., Worsnop, D. R., and Kerminen, V.-M.: Chemistry of
729 atmospheric nucleation: On the recent advances on precursor characterization and atmospheric cluster
730 composition in connection with atmospheric new particle formation, *Annu. Rev. Phys. Chem.*, 65, 21–37,
731 2014.

732 Kulmala, M., Kerminen, V. M., Petäjä, T., Ding, A. J., and Wang, L.: Atmospheric gas-to-particle conversion:
733 why NPF events are observed in megacities, *Faraday Discuss.*, doi:10.1039/C6FD00257A, 2017.

734 Laine, M.: Introduction to Dynamic Linear Models for Time Series Analysis. In: Montillet, J. P., Bos, M. (eds),
735 Geodetic Time Series Analysis in Earth Sciences, Springer, pp. 139–156, 2020.

736 Maheras, P., Tolika, K., Tegoulis, I., Anagnostopoulou, Ch., Szpirosz, K. Károssy, Cs., and Makra, L.:
737 Comparison of an automated classification system with an empirical classification of circulation patterns over
738 the Pannonian basin, Central Europe, Meteorol. Atmos. Phys., <https://doi.org/10.1007/s00703-018-0601-x>,
739 2018.

740 Makkonen, R., Asmi, A., Korhonen, H., Kokkola, H., Järvenoja, S., Räisänen, P., Lehtinen, K. E. J., Laaksonen,
741 A., Kerminen, V.-M., Järvinen, H., Lohmann, U., Bennartz, R., Feichter, J., and Kulmala, M.: Sensitivity of
742 aerosol concentrations and cloud properties to nucleation and secondary organic distribution in ECHAM5-
743 HAM global circulation model, Atmos. Chem. Phys., 9, 1747–1766, 2009.

744 Masiol, M., Squizzato, S., Chalupa, D., Utell, M. J., Rich, D. Q., and Hopke, P. K.: Long-term trends in submicron
745 particle concentrations in a metropolitan area of the northeastern United States, Sci. Total Environ., 633, 59–
746 70, 2018.

747 McCulloch, C. E., Searle, S. R., and Neuhaus, J. M.: Generalized, linear, and mixed models, 2nd ed., Wiley, New
748 York, 2008.

749 McFiggans, G., Mentel, T. F., Wildt, J., Pullinen, I., Kang, S., Kleist, E., Schmitt, S., Springer, M., Tillmann, R.,
750 Wu, C., Zhao, D., Hallquist, M., Faxon, C., Le Breton, M., Hallquist, A. M., Simpson, D., Bergstroem, R.,
751 Jenkin, M. E., Ehn, M., Thornton, J. A., Alfarra, M. R., Bannan, T. J., Percival, C. J., Priestley, M., Topping,
752 D., and Kiendler-Scharr, A.: Secondary organic aerosol reduced by mixture of atmospheric vapours, Nature,
753 565, 587–593, 2019.

754 Merikanto, J., Spracklen, D. V., Mann, G. W., Pickering, S. J., and Carslaw, K. S.: Impact of nucleation on global
755 CCN, Atmos. Chem. Phys., 9, 8601–8616, 2009.

756 Mikkonen, S., Lehtinen, K. E. J., Hamed, A., Joutsensaari, J., Facchini, M. C., and Laaksonen, A.: Using
757 discriminant analysis as a nucleation event classification method, Atmos. Chem. Phys., 6, 5549–5557,
758 <https://doi.org/10.5194/acp-6-5549-2006>, 2006.

759 Mikkonen, S., Korhonen, H., Romakkaniemi, S., Smith, J. N., Joutsensaari, J., Lehtinen, K. E. J., Hamed, A.,
760 Breider, T. J., Birmili, W., Spindler, G., Plass-Duelmer, C., Facchini, M. C., and Laaksonen, A.:
761 Meteorological and trace gas factors affecting the number concentration of atmospheric Aitken ($D_p=50$ nm)
762 particles in the continental boundary layer: parameterization using a multivariate mixed effects model, Geosci.
763 Model Dev., 4, 1–13, <https://doi.org/10.5194/gmd-4-1-2011>, 2011a.

764 Mikkonen, S., Romakkaniemi, S., Smith, J. N., Korhonen, H., Petäjä, T., Plass-Duelmer, C., Boy, M., McMurry,
765 P. H., Lehtinen, K. E. J., Joutsensaari, J., Hamed, A., Mauldin III, R. L., Birmili, W., Spindler, G., Arnold, F.,
766 Kulmala, M., and Laaksonen, A.: A statistical proxy for sulphuric acid concentration, Atmos. Chem. Phys., 11
767 11319–11334, <https://doi.org/10.5194/acp-11-11319-2011>, 2011b.

768 Mikkonen, S., Laine, M., Mäkelä, H. M., Gregow, H., Tuomenvirta, H., Lahtinen, M., Laaksonen, A.: Trends in
769 the average temperature in Finland, 1847–2013, Stoch. Environ. Res. Risk Ass., 29, 1521–1529, 2015.

770 Moore, K. F., Ning, Z., Ntziachristos, L., Schauer, J. J., and Sioutas, C.: Daily variation in the properties of urban
771 ultrafine aerosol - Part I: Physical characterization and volatility, Atmos. Environ., 41, 8633–8646, 2007.

772 Moosmuller, H., Chakrabarty, R. K. and Arnott, W.: Aerosol light absorption and its measurement: A review, J.
773 Quant. Spectrosc. Radiat. Transf., 110, 844–878, 2009.

774 Németh, Z. and Salma, I.: Spatial extension of nucleating air masses in the Carpathian Basin, Atmos. Chem. Phys.,
775 14, 8841–8848, 2014.

776 Németh, Z., Rosati, B., Ziková, N., Salma, I., Bozó, L., Dameto de España, C., Schwarz, J., Ždímal, V., and
777 Wonašchütz, A.: Comparison of atmospheric new particle formation and growth events in three Central
778 European cities, Atmos. Environ., 178, 191–197, 2018.

779 Nieminen, T., Asmi, A., Dal Maso, M., P. Aalto, P., Keronen, P., Petäjä, T., Kulmala, M. & Kerminen, V.-M.:
780 Trends in atmospheric new-particle formation: 16 years of observations in a boreal-forest environment. Boreal
781 Env. Res. 19 (suppl. B): 191–214, 2014.

782 Nieminen, T., Kerminen, V.-M., Petäjä, T., Aalto, P. P., Arshinov, M., Asmi, E., Baltensperger, U., Beddows, D.
783 C. S., Beukes, J. P., Collins, D., Ding, A., Harrison, R. M., Henzing, B., Hooda, R., Hu, M., Hörrak, U.,
784 Kivekäs, N., Komsaare, K., Krejci, R., Kristensson, A., Laakso, L., Laaksonen, A., Leaitch, W. R., Lihavainen,
785 H., Mihalopoulos, N., Németh, Z., Nie, W., O'Dowd, C., Salma, I., Sellegri, K., Svenningsson, B., Swietlicki,
786 E., Tunved, P., Ulevicius, V., Vakkari, V., Vana, M., Wiedensohler, A., Wu, Z., Virtanen, A., and Kulmala,

787 M.: Global analysis of continental boundary layer new particle formation based on long-term measurements,
788 Atmos. Chem. Phys., 18, 14737–14756, 2018.

789 Oberdörster, G., Oberdörster, E., and Oberdörster, J.: Nanotoxicology: an emerging discipline evolving from
790 studies of ultrafine particles, Environ. Health Perspect., 113, 823–839, 2005.

791 Ohlwein, S., Kappeler, R., Joss, M. K., Künzli, N., and Hoffmann, B.: Health effects of ultrafine particles: a
792 systematic literature review update of epidemiological evidence, Int. J. Public Health, 685, 547–559, 2019.

793 Ostro, B., Hu, J., Goldberg, D., Reynolds, P., Hertz, A., Bernstein, L., and Kleeman, M. J.: Associations of
794 mortality with long-term exposures to fine and ultrafine particles, species and sources: results from the
795 California teachers study cohort, Environ. Health Perspect., 123, 549–556, 2015.

796 Paasonen, P., Kupiainen, K., Klimont, Z., Visschedijk, A., Denier van der Gon, H. A. C., and Amann, M.:
797 Continental anthropogenic primary particle number emissions, Atmos. Chem. Phys., 16, 6823–6840, 2016.

798 Péczely, Gy.: Grosswetterlagen in Ungarn (Large-scale weather situations in Hungary, in German), Publication of
799 the Hungarian Meteorological Institute, 30, pp. 86, Budapest, 1957.

800 Petäjä, T., Mauldin, III, R. L., Kosciuch, E., McGrath, J., Nieminen, T., Paasonen, P., Boy, M., Adamov, A.,
801 Kotiaho, T., and Kulmala, M.: Sulfuric acid and OH concentrations in a boreal forest site, Atmos. Chem. Phys.,
802 9, 7435–7448, 2009.

803 Petris, G., Petrone, S., and Campagnoli, P.: Dynamic linear models, Springer, New York, 2009.

804 Pinheiro, J.C., and Bates, D.M.: Mixed-Effects Models in S and S-PLUS, Springer, 2000.

805 Platt, S. M., El Haddad, I., Pieber, S. M., Zardini, A. A., Suarez-Bertoa, R., Clairotte, M., Daellenbach, K. R.,
806 Huang, R.-J., Slowik, J. G., Hellebust, S., Temime-Roussel, B., Marchand, N., de Gouw, J., Jimenez, J. L.,
807 Hayes, P. L., Robinson, A. L., Baltensperger, U., Astorga, C., and Prévôt, A. S. H.: Gasoline cars produce
808 more carbonaceous particulate matter than modern filter-equipped diesel cars, Sci. Rep., 7, 4926, 2017,
809 <https://doi.org/10.1038/s41598-017-03714-9>.

810 Pöschl, U., Rudich, Y., and Ammann, M.: Kinetic model framework for aerosol and cloud surface chemistry and
811 gas-particle interactions – Part 1: General equations, parameters, and terminology, Atmos. Chem. Phys., 7,
812 5989–6023, 2007.

813 Raes, F., Van Dingenen, R., Vignati, E., Wilson, J., Putaud, J. P., Seinfeld, J. H., and Adams, P.: Formation and
814 cycling of aerosol in the global troposphere, Atmos. Environ., 34, 4215–4240, 2000.

815 Rich, D. Q., Zareba, W., Beckett, W., Hopke, P. K., Oakes, D., Frampton, M. W., Bisognano, J., Chalupa, D.,
816 Bausch, J., O'Shea, K., Wang, Y., and Utell, M. J.: Are ambient ultrafine, accumulation mode, and fine particles
817 associated with adverse cardiac responses in patients undergoing cardiac rehabilitation?, Environ. Health
818 Perspect., 120, 1162–1169, 2012.

819 Saha, P. K., Robinson, E. S., Shah, R. U., Zimmerman, N., Apte, J. S., Robinson, A. L., and Presto, A. A.: Reduced
820 ultrafine particle concentration in urban air: changes in nucleation and anthropogenic emissions, Environ. Sci.
821 Technol., 52, 6798–6806, 2018.

822 Salma, I., Borsós, T., Weidinger, T., Aalto, P., Hussein, T., Dal Maso, M., and Kulmala, M.: Production, growth
823 and properties of ultrafine atmospheric aerosol particles in an urban environment, Atmos. Chem. Phys., 11,
824 1339–1353, 2011.

825 Salma, I., Borsós, T., Németh, Z., Weidinger, T., Aalto, T., and Kulmala, M.: Comparative study of ultrafine
826 atmospheric aerosol within a city, Atmos. Environ., 92, 154–161, 2014.

827 Salma, I., Németh, Z., Weidinger, T., Kovács, B., and Kristóf, G.: Measurement, growth types and shrinkage of
828 newly formed aerosol particles at an urban research platform, Atmos. Chem. Phys., 16, 7837–7851, 2016a.

829 Salma, I., Németh, Z., Kerminen, V. M., Aalto, P., Nieminen, T., Weidinger, T., Molnár, Á., Imre, K., and
830 Kulmala, M.: Regional effect on urban atmospheric nucleation, Atmos. Chem. Phys., 16, 8715–8728, 2016b.

831 Salma, I., Varga, V., and Németh, Z.: Quantification of an atmospheric nucleation and growth process as a single
832 source of aerosol particles in a city, Atmos. Chem. Phys., 17, 15007–15017, 2017.

833 Salma, I. and Németh, Z.: Dynamic and timing properties of new aerosol particle formation and consecutive
834 growth events, Atmos. Chem. Phys., 19, 5835–5852, 2019.

835 Salvo, A., Brito, J., Artaxo, P., and Geiger, F. M.: Reduced ultrafine particle levels in São Paulo's atmosphere
836 during shifts from gasoline to ethanol use, Nat. Commun., 8, 77, DOI: 10.1038/s41467-017-00041-5, 2017.

837 Schmid, O. and Stoeger, T.: Surface area is the biologically most effective dose metric for acute nanoparticle
838 toxicity in the lung, J. Aerosol Sci., 99, 133–143, 2016.

839 Sihto, S.-L., Mikkilä, J., Vanhanen, J., Ehn, M., Liao, L., Lehtipalo, K., Aalto, P. P., Duplissy, J., Petäjä, T.,
840 Kerminen, V.-M., Boy, M., and Kulmala, M.: Seasonal variation of CCN concentrations and aerosol activation
841 properties in boreal forest, *Atmos. Chem. Phys.*, 11, 13269–13285, 2011.

842 Sipilä, M., Berndt, T., Petäjä, T., Brus, D., Vanhanen, J., Stratmann, F., Patokoski, J., Mauldin, R. L. 3rd,
843 Hyvärinen, A. P., Lihavainen, H., and Kulmala, M.: The role of sulfuric acid in atmospheric nucleation,
844 *Science*, 327(5970), 1243–6. doi: 10.1126/science.1180315, 2010.

845 Spracklen, D. V., Carslaw, K. S., Merikanto, J., Mann, G. W., Reddington, C. L., Pickering, S., Ogren, J. A.,
846 Andrews, E., Baltensperger, U., Weingartner, E., Boy, M., Kulmala, M., Laakso, L., Lihavainen, H., Kivekäs,
847 N., Komppula, M., Mihalopoulos, N., Kouvarakis, G., Jennings, S. G., O'Dowd, C., Birmili, W., Wiedensohler,
848 A., Weller, R., Gras, J., Laj, P., Sellegri, K., Bonn, B., Krejčí, R., Laaksonen, A., Hamed, A., Minikin, A.,
849 Harrison, R. M., Talbot, R., and Sun, J.: The contribution of boundary layer nucleation events to total particle
850 concentrations on regional and global scales, *Atmos. Chem. Phys.*, 6, 5631–5648, 2006.

851 Sun, J., Birmili, W., Hermann, M., Tuch, T., Weinhold, K., Merkel, M., Rasch, F., Müller, T., Schladitz, A.,
852 Bastian, S., Löschau, G., Cyrus, J., Gu, J., Flentje, H., Briel, B., Asbach, C., Kaminski, H., Ries, L., Sohmer,
853 R., Gerwig, H., Wirtz, K., Meinhardt, F., Schwerin, A., Bath, O., Ma, N., and Wiedensohler, A.: Decreasing
854 trends of particle number and black carbon mass concentrations at 16 observational sites in Germany from
855 2009 to 2018, [Atmos. Chem. Phys.](https://doi.org/10.5194/acp-20-7049-2020), 20, 7049–7068, doi:10.5194/acp-20-7049-2020, 2020. [Atmos.](https://doi.org/10.5194/acp-2019-754)
856 [Chem. Phys. Discuss.](https://doi.org/10.5194/acp-2019-754), doi:10.5194/acp-2019-754, 2019.

857 Wehner, B. and Wiedensohler, A.: Long term measurements of submicrometer urban aerosols: statistical analysis
858 for correlations with meteorological conditions and trace gases, *Atmos. Chem. Phys.*, 3, 867–879, 2003

859 [Wiheraari, H., Pirjola, L., Karjalainen, P., Saukko, E., Kuuluvainen, H., Kulmala, K., Keskinen, J. and Rönkkö,](https://doi.org/10.1016/j.envpol.2020.114948)
860 [T.: Particulate emissions of a modern diesel passenger car under laboratory and real-world transient driving](https://doi.org/10.1016/j.envpol.2020.114948)
861 [conditions, Environ. Pollut.](https://doi.org/10.1016/j.envpol.2020.114948), 265, 114948, doi:10.1016/j.envpol.2020.114948, 2020.

862 Wiedensohler, A., Cheng, Y. F., Nowak, A., Wehner, B., Achtert, P., Berghof, M., Birmili, W., Wu, Z. J., Hu, M.,
863 Zhu, T., Takegawa, N., Kita, K., Kondo, Y., Lou, S. R., Hofzumahaus, A., Holland, F., Wahner, A., Gunthe,
864 S. S., Rose, D., Su, H., and Pöschl, U.: Mobility particle size spectrometers: harmonization of technical
865 standards and data structure to facilitate high quality long-term observations of atmospheric particle number
866 size distributions, *Atmos. Meas. Tech.*, 5, 657–685, 2012.

867 Willmott, C. J., Matsuura, K., and Robeson, S. M.: Ambiguities inherent in sums-of-squares-based error statistics,
868 *Atmos. Environ.*, 43, 749–752, doi:10.1016/j.atmosenv.2008.10.005, 2009.

869 Yu, F., Luo, G., Bates, T. S., Anderson, B., Clarke, A., Kapustin, V., Yantosca, R. M., Wang, Y., and Wu, S.:
870 Spatial distributions of particle number concentrations in the global troposphere: simulations, observations,
871 and implications for nucleation mechanisms, *J. Geophys. Res.*, 115, D17205, doi:10.1029/2009JD013473,
872 2010.

873 Zaidan, M. A., Haapasilta, V., Relan, R., Paasonen, P., Kerminen, V.-M., Junninen, H., Kulmala, M., and Foster,
874 A. S.: Exploring non-linear associations between atmospheric new-particle formation and ambient variables: a
875 mutual information approach, *Atmos. Chem. Phys.*, 18, 12699–12714, 2018.

876 Zhang, R., Wang, G., Guo, S., Zamora, M. L., Ying, Q., Lin, Y., Wang, W., Hu, M., and Wang, Y.: Formation of
877 urban fine particulate matter, *Chem. Rev.*, 115, 3803–3855, 2015.

Decennial time trends and diurnal patterns of particle number concentrations in a Central European city between 2008 and 2018

Santtu Mikkonen^{1,2}, Zoltán Németh³, Veronika Varga³, Tamás Weidinger⁴, Ville Leinonen¹,
Taina Yli-Juuti¹, and Imre Salma³

¹ Department of Applied Physics, University of Eastern Finland, P.O. Box 1627, 70211 Kuopio, Finland

² Department of Environmental and Biological Sciences, University of Eastern Finland, P.O. Box 1627,
70211 Kuopio, Finland

³ Institute of Chemistry, Eötvös University, H-1518 Budapest, P.O. Box 32, Hungary

⁴ Department of Meteorology, Eötvös University, H-1518 Budapest, P.O. Box 32, Hungary

Correspondence to: Imre Salma (salma@chem.elte.hu) and Santtu Mikkonen (santtu.mikkonen@uef.fi)

Abstract. Multiple atmospheric properties were measured semi-continuously in the Budapest platform for Aerosol Research and Training Laboratory which represents the urban background for a time interval of 2008-2018. Dataset of 6 full measurement years during a decennial time interval were subjected to statistical time trend analyses by an advanced dynamic linear model and a generalized linear mixed model. The main interest in the analysed data set was on particle number concentrations in the diameter ranges from 6 to 1000 nm (N_{6-1000}), from 6 to 100 nm (N_{6-100} , ultrafine particles), from 25 to 100 nm (N_{25-100}) and from 100 to 1000 nm ($N_{100-1000}$). These data were supported by concentrations of SO₂, CO, NO, NO_x, O₃, PM₁₀ mass, air temperature, relative humidity, wind speed, atmospheric pressure, global solar radiation, condensation sink, gas-phase H₂SO₄ proxy, classes of new aerosol particle formation (NPF) and growth events and meteorological macro-circulation patterns. The trend of the particle number concentrations derived as a change in the statistical properties of background state of the data set decreased in all size fractions over the years. Most particle number concentrations showed decreasing decennial statistical trends. The estimated annual mean decline of N_{6-1000} was (4–5)% during the 10-year measurement interval, which corresponds to a mean absolute change of -590 cm^{-3} in a year. This was interpreted as a consequence of the decreased anthropogenic emissions mainly at least partly from road traffic alongside to household heating and industry. Similar trends were not observed for the air pollutant gases. Diurnal statistical patterns of particle number concentrations showed tendentious variations, which were associated with typical diurnal activity–time pattern of inhabitants in cities, particularly of vehicular road traffic. The trend patterns for NPF event days contained a huge peak from late morning to late afternoon, which is unambiguously caused by NPF and growth processes. These peaks were rather similar to each other in the position, shape and area on workdays and holidays, which implies that the dynamic and timing properties of NPF events are not substantially influenced by anthropogenic activities in central Budapest. Diurnal pattern for N_{25-100} exhibited the largest relative changes, which were related to particle emissions from high-temperature sources. The diurnal pattern for $N_{100-1000}$ – which represents chemically and physically aged particles of larger spatial scale – were different from the diurnal patterns for the other size fractions.

37 **1 Introduction**

38 Atmospheric aerosol can be characterised by various properties. There are several important phenomena
39 and processes in which individual particles play a role. In these cases, particle number concentrations
40 or particle number size distributions are the relevant metrics. Number concentrations of (insoluble)
41 particles produce adverse effects on human health (Oberdörster et al., 2005; Rich et al., 2012; Cassee et
42 al., 2013; Braakhuis et al., 2014; Ostro et al., 2015; Schmid and Stoeger, 2016; Ohlwein et al., 2019).
43 Individual particles and their properties are also important in cloud formation processes and, therefore,
44 in indirect aerosol climate forcing (Makkonen et al., 2009; Merikanto et al., 2009; Sihto et al., 2011;
45 Kerminen et al., 2012; Carslaw et al., 2013; Gordon et al., 2016). Particle numbers and associated size
46 distributions are relevant properties in several optical interactions in the atmosphere (e.g. Moosmuller
47 et al., 2009) and in various surface-controlled chemical reactions (e.g. Pöschl et al., 2007).

48 In the global troposphere, it is the new aerosol particle formation (NPF) and consecutive growth process
49 that is the dominant source of particle numbers (Spracklen et al., 2006; Yu et al., 2010; Kulmala et al.,
50 2013; Dunne et al., 2016). This source type occurs in various atmospheric environments around the
51 world and produces secondary particles (Kerminen et al., 2018 and references therein). The major
52 anthropogenic source of (primary) particles is combustion. It includes traffic exhaust mainly from diesel
53 engines, fuel or waste burning in industrial and domestic installations, residential heating and cooking
54 (Paasonen et al., 2016; Masiol et al., 2018). Nanotechnology and its products can have importance in
55 some limited or occupational environments. In large cities and in longer time intervals, primary particles
56 often prevail over secondary particles (Brines et al., 2015; Salma et al., 2017; Saha et al., 2018).

57 Ultrafine (UF) particles (with a diameter $d < 100$ nm) account for most of the particle number
58 concentrations but have usually negligible contribution to particulate matter (PM) mass. This implies
59 that particle numbers are not covered by legislative regulations on the ambient air quality, which are
60 ordinary based on the PM mass. Particle number concentrations have not been promulgated among the
61 air quality standards yet. There are, however, mitigation policies and control regulations, which intend
62 to reduce their ambient levels as part of an overall air-quality improvement strategy since 1990s. The
63 legislations, for instance in the EU including Hungary, focus on the particle emissions from diesel
64 engines (Giechaskiel et al., 2018). There were some important changes in the car emissions during the
65 time interval under the investigation in this study. These included the introduction of Euro 5 and 6
66 regulations for light-duty vehicles in January 2011 and Euro VI regulations for heavy-duty vehicles in
67 September 2015 (the number of emitted particles with diameters > 23 nm should be $< 6 \times 10^{11}$ km⁻¹ for
68 type approval). A prerequisite for the efficient operation of exhaust after treatment devices is having
69 fuel with low sulfur content. The reduction of sulfur in diesel fuel for on-road transport was decreased
70 after several previous phases to < 10 ppm in January 2009 (Directive 2009/30/EC). Sulfur content in
71 fuels for mobile non-road diesel vehicles – including mobile machinery, agricultural and forestry

72 tractors, inland waterway vessels and recreational crafts – was limited at a level of 1000 ppm from 2008
73 and at 10 ppm from 2011. The unsuitable/dangerous fuel types for domestic heating are also listed, their
74 emission factors are determined, and the accumulated information is disseminated among potential
75 users. As far as secondary particles are concerned, it is not straightforward to reduce their concentration
76 levels because the effects of gaseous and aerosol species on the NPF are complex and uncertain due to
77 nonlinear relationship and feedbacks in their related processes.

78 It is relevant to investigate the potential changes, namely overall and diurnal tendencies of particle
79 number concentrations from different sources on longer run because of their role in both health-risk and
80 climate-change issues. The major source types of particle numbers can be separated by measuring their
81 size distributions. Atmospheric NPF events produce particles of the nucleation mode, which occurs
82 intermittently, and which gradually merges into the larger Aitken mode. High temperature emission
83 sources ordinarily produce Aitken-mode particles, while transformation processes (physical and
84 chemical aging) of existing particles in the atmosphere give rise to the accumulation mode. An important
85 property of the nucleation- and Aitken-mode particles is that their residence time is limited to several
86 hours (Raes et al., 2000; Salma et al., 2011). This is different from accumulation-mode particles, which
87 reside in the air up to 7 days. This means that the particles of the former two modes are present in the
88 air until their sources are active, and that their concentrations can change substantially and rapidly over
89 a day (e.g. Mikkonen et al., 2011a, Salma et al., 2014, 2017; Paasonen et al., 2016). This is advantageous
90 when source types are to be identified or quantified. At the same time, the relatively short residence time
91 is not beneficial when time trends are to be studied and derived. The limited residence time can cause
92 additional, substantial and sudden variability in time with or without time patterns, which can complicate
93 the evaluation.

94 Particle number concentrations or particle number size distributions in the relevant diameter range (i.e.
95 from few nanometers to ca. 1 μm) are measured for various purposes. They include fundamental studies
96 on atmospheric nucleation and particle growth phenomena, which usually require semi-continuous long-
97 term measurements. The related experimental data sets have been accumulating gradually (Wehner and
98 Wiedensohler, 2003; Asmi et al., 2013; Kerminen et al., 2018; Nieminen et al., 2018). They can also be
99 exploited for time trend analysis by using appropriate statistical models. At present, however, knowledge
100 on time trends particularly in various size fractions and over several years is largely lacking with few
101 recent exceptions (Masiol et al., 2018; Saha et al., 2018; Sun et al., ~~2019~~2020).

102 Research activities dedicated to NPF and growth events in Budapest have been going on since November
103 2008. Measurements for 6 full years were realised in the city centre at a single fixed location. Semi-
104 continuous and critically evaluated data sets consisting of particle number size distributions,
105 concentrations of criteria air pollutants and meteorological data were available for the study. They were
106 combined in a coherent set, which was utilised in two statistical models developed specifically to

107 determine the time trends for particle number concentrations in several important size fractions from
108 2008 to 2018. The main objectives of this study are to present and discuss the statistical models, to
109 interpret their results on time trends and diurnal variability, to quantify the change rates, and to relate
110 the temporal tendencies to different atmospheric sources, processes and environmental circumstances.

111 **2 Methods**

112 **2.1 Measurements**

113 Most experimental data dealt with in the present study were obtained at a single urban site, namely at
114 the Budapest platform for Aerosol Research and Training (BpART) research laboratory (N 47° 28' 29.9",
115 E 19° 3' 44.6", 115 m above mean sea level). This location represents a well-mixed, average atmospheric
116 environment for the city centre of Budapest due to its geographical and meteorological conditions
117 (Salma et al., 2016a), thus it can be regarded as an urban background site. The local emissions include
118 diffuse urban traffic exhaust, household/residential emissions and limited industrial sources together
119 with some off-road transport (diesel rail, shipping and airplane emissions). Experimental data for 6 full-
120 year-long time intervals, i.e. from 3 November 2008 to 2 November 2009, from 13 November 2013 to
121 12 November 2014, from 13 November 2014 to 12 November 2015, from 13 November 2015 to 12
122 November 2016, from 28 January 2017 to 27 January 2018 and from 28 January 2018 to 27 January
123 2019 were available for this single site. A decennial time interval from 03 November 2008 to 02
124 November 2018 was considered in the statistical analysis. Local time (LT=UTC+1 or daylight-saving
125 time, UTC+2) was chosen as the time base of the data processing because the ordinary daily activities
126 of inhabitants substantially influence the atmospheric concentrations and several processes in cities
127 (Salma et al., 2014).

128 The major aerosol measuring system was a flow-switching type differential mobility particle sizer
129 (DMPS, Alto et al., 2001). It records particle number concentrations in an electrical mobility diameter
130 range from 6 to 1000 nm in the dry state of particles (with a relative humidity of RH<30%) in 30
131 channels (Salma et al., 2011). The measuring system was updated twice; in spring 2013 and winter 2016.
132 Its major parts including a differential mobility analyser (DMA, Hauke-type with a length of 28 cm) and
133 a condensation particle counter (CPC, TSI model 3775) remained, however, unchanged. They were
134 cleaned and serviced. The diameter resolution of the DMA was also calibrated during the updates.
135 Several data validation or comparative exercises were realised over the years; the most extensive inter-
136 comparison was realised in summer 2015 (~~Salma et al., 2016a~~) and autumn 2019. First, the measured
137 data by the CPC deployed in the DMPS system were compared to that of an identical stand-alone CPC
138 operated in parallel. The agreement between the instruments was in accordance with the nominal
139 specification of CPCs. As the next step, the integrated concentrations obtained from the size-resolved
140 DMPS data were compared to the concentrations measured directly by the stand-alone CPC. The two

141 instruments were again operated in parallel. The median CPC/DMPS ratio was utilised as correction
142 factor for particle diffusion losses in the DMPS system (Salma et al., 2016a). The time resolution of the
143 DMPS measurements was approximately 10 min in the year 2008–2009 and it was 8 min from 13
144 November 2013 on. The sampling inlet was installed at a height of 12.5 m above the street level. There
145 was no upper-size cut-off inlet applied to the sampling line, and a rain shield and insect net were only
146 adopted. The measurements were performed according to the international technical standard
147 (Wiedensohler et al., 2012).

148 Meteorological data for air temperature (T), relative humidity (RH), wind speed (WS), wind direction
149 and atmospheric pressure (p) were obtained from a measurement station of the Hungarian
150 Meteorological Service (HMS) operated in a distance of ca. 70 m from the BpART laboratory by
151 standardised methods (Vaisala HMP45D humidity and temperature probe, Vaisala WAV15A
152 anemometer, Vaisala pressure, all Finland) with a time resolution of 10 min. Global solar radiation
153 (GRad) data were measured by a CMP11 pyranometer (Kipp and Zonnen, The Netherlands) at another
154 station of the HMS situated in 10 km in Eastern direction with a time resolution of 1 h. Concentrations
155 of pollutants SO₂, CO, NO, NO_x, O₃, and PM₁₀ mass were acquired from a measurement station of the
156 National Air Quality Network in Budapest in Széna Square, which is located in the upwind prevailing
157 wind direction in a distance of 4.5 km from the BpART laboratory. This station ordinarily measures the
158 smallest levels of the criteria air pollutants among the four monitoring stations located in the city centre.
159 It can, therefore, be considered to represent the air pollution in between the urban background and street
160 level/kerbside site. They are measured by UV fluorescence (Ysselbach 43C), IR absorption (Ysselbach
161 48C), chemiluminescence (Thermo 42C), UV absorption (Ysselbach 49C) and beta-ray attenuation
162 (Thermo 5014I) methods, respectively with a time resolution of 1 h.

163 The availability of the DMPS data over the six one-year-long time intervals were 95, 99, 95, 73, 99 and
164 90%, respectively. The meteorological data were accessible in >90% of time in each year, while the
165 concentration data for key pollutants were available in >85% of the yearly time intervals.

166 **2.2 Data treatment**

167 Particle number concentrations in the diameter ranges 1) from 6 to 1000 nm (N_{6-1000}), 2) from 6 to 100
168 nm (N_{6-100}), 3) from 25 to 100 nm (N_{25-100}) and 4) from 100 to 1000 nm ($N_{100-1000}$) were calculated from
169 the measured and inverted DMPS data. The size ranges were selected to represent 1) the total particles,
170 2) UF particles, 3) UF particles emitted mainly from incomplete combustion (and partially grown by
171 condensation; this size ranges is dominated by primary particles in cities in most of the time) and 4)
172 physically and chemically aged particles which usually represent larger spatial extent, respectively
173 (Salma et al., 2014, 2017).

174 Condensation sink (CS) for vapour molecules onto the surface of existing aerosol particles was
 175 calculated for discrete size distributions (Kulmala et al., 2001, 2012; Dal Maso et al., 2002, 2005). Dry
 176 particle diameters were considered in the calculations and condensing vapour was assumed to have
 177 sulphuric acid properties.

178 One of the key components for NPF events is the gas-phase H_2SO_4 (Sipilä et al., 2010; Sihto et al.,
 179 2011). It is challenging to measure its atmospheric concentration and, therefore, the experimental data
 180 for long time intervals are rare. The relative effects of gas-phase H_2SO_4 are, however, often estimated
 181 by deriving its proxy value. In this study, the H_2SO_4 proxy was calculated according to Mikkonen et al.
 182 (2011b), where the best proxy was based on GRad, SO_2 concentration, RH and CS. The proxy is defined
 183 for $\text{GRad} > 10 \text{ W m}^{-2}$. Other widely used proxy was introduced by Petäjä et al. (2009), but that was
 184 created for clean boreal forest environment. The most recent proxy from Dada et al. (2020) is currently
 185 under review and has not been tested against the proxy used here. All experimental data were used with
 186 their maximum time resolution.

187 The influence of large-scale weather types was considered on a daily basis by including codes for macro-
 188 circulation patterns (MCPs) invented specifically for the Carpathian Basin (Péczely, 1957; Károssy,
 189 2016). The classification is based on the extension and development of cyclones and anticyclones
 190 relative to the Carpathian Basin via the daily sea-level pressure maps constructed for 00:00 UTC in the
 191 North-Atlantic–European region. Thus defined MCP was assigned to the following day in the data.
 192 Basic information on the MCPs are summarised in Table 1.

193 **Table 1.** Macro-circulation patterns (Péczely codes) and their seasonal and annual occurrences in the Carpathian
 194 Basin for years 1958–2010 (Maheras et al., 2018).

No.	Code	Description	Occurrence (%)				
			Winter	Spring	Summer	Autumn	Annual
1	mCc	Cyclone with a cold front over NE Europe, N wind	7.3	11.3	12.1	8.0	9.7
2	AB	Anticyclone over the British Isles, N wind	5.6	7.1	8.6	6.4	6.9
3	CMc	Mediterranean cyclone with a cold front over S Europe, N wind	2.5	3.5	1.8	1.9	2.4
4	mCw	Mediterranean cyclone with a warm front over NE Europe, S wind	9.2	9.7	5.7	7.2	7.9
5	Ae	Anticyclone over E Europe, S wind	14.2	11.3	7.3	17.6	12.6
6	CMw	Mediterranean cyclone with a warm front over S Europe, S wind	8.9	8.7	3.7	8.3	7.4
7	zC	Highly developed cyclone over N Europe, W wind	5.0	3.2	2.7	2.9	3.5
8	Aw	Anticyclone over W Europe, W wind	13.1	11.2	20.8	12.8	14.6

9	As	Anticyclone over S Europe, W wind	7.0	4.4	2.9	5.6	4.9
10	An	Anticyclone over N Europe, E wind	10.9	12.8	11.3	10.1	11.3
11	AF	Anticyclone over Fennoscandia, E wind	2.8	5.2	5.9	3.7	4.4
12	A	Anticyclone over the Carpathian Basin, changing wind direction	11.8	7.3	13.3	13.3	11.4
13	C	Cyclone over the Carpathian Basin, changing wind direction	1.7	4.3	3.9	2.2	3.0

195
196 Each data line containing the date and time, concentrations, CS, H₂SO₄ proxy, meteorological data and
197 MCP codes was further labelled by several indices on a daily basis. These labels served to differentiate
198 between various environmental conditions, which can lead to substantial changes in some variables
199 (Salma et al., 2014). The workdays were marked by label WD, while the holidays were denoted by label
200 HD. Varying classes of NPF event days were also labelled differently. The classification was
201 accomplished via the particle number size distribution surface plots (Dal Maso et al., 2005; refined in
202 Németh et al., 2018 for urban sites) on a daily basis. The main classes were: NPF event days (marked
203 by label NPF), non-event days (label NE), days with undefined character and days with missing data.
204 The earliest estimated time of the beginning of a nucleation (t_1) was also derived (Németh and Salma,
205 2014) and was added to the data record as a parameter. Finally, the data lines were labelled according
206 to the actual technical status of the DMPS system. The data obtained from the beginning of the
207 measurements to the 1st update was labelled as S1, the data derived between the 1st and 2nd updates were
208 label as S2, and label S3 was given to the data obtained after the 2nd update.

209 2.3 Statistical modelling

210 Atmospheric data are usually not normally distributed, and, therefore, non-parametric methods are often
211 used to detect their long-term trends (Asmi et al., 2013; Masiol et al., 2018). The coherent data set
212 prepared as described in Sect. 2.2 was analysed in two ways. First, time trends for concentrations of
213 particles and air pollutants were estimated by using a dynamic linear model (DLM) method. Secondly,
214 the factors affecting the changes in particle concentrations were detected with a generalized linear mixed
215 model (GLMM).

216 2.3.1 Dynamic linear model

217 Dynamic linear models (Durbin and Koopman, 2012; Petris et al., 2009; Laine, 2020) are state-of-the-
218 art tools for time trend detection. The trend is seen as a statistical change in the properties of the
219 background state of the system. Although changes in aerosol concentrations have previously been
220 approximated with linear trends (e.g. Sun et al., ~~2019~~2020), this is not always the most suitable method
221 since the processes affecting the concentrations are continuously evolving over time. Additionally, time
222 series of atmospheric measurements can include multiple time-dependent cycles (e.g. seasonal and
223 diurnal cycles) which are typically non-stationary – meaning that their distributional properties change

224 over time. The DLM approach effectively decomposes the data series into basic components such as
 225 level, trend, seasonality and effect of external forcing by describing statistically the underlying structure
 226 of the process that generated the measured data. All these components are defined by Gaussian
 227 distributions, and they are allowed to vary in time, and the significance and magnitude of this variation
 228 can also be modelled and estimated. In the basic setup of DLM, the sign or the magnitude of the trend
 229 is not defined in advance by the model formulation but estimated from the data. The method can detect
 230 and quantify trends, but the explanations for the observed changes is provided by the user. Nevertheless,
 231 it determines if the observations are consistent with the selected model. We used the DLM to explain
 232 variability in the particle concentration time series using following components: locally linear mean
 233 level, trend, seasonal effect, autoregressive component and noise. The autoregressive component is
 234 added to the model in order to take account the autocorrelation in the data, i.e. the correlation between
 235 subsequent observations. Here it refers to first order autoregressive model (AR(1)). The evolution of the
 236 investigated concentrations – after the seasonal and noise components were filtered out – is modelled
 237 by using the smoothed mean level. Here, the change in the mean level is the trend of the variable. The
 238 statistical model can be described by the following equations (Mikkonen et al., 2015):

$$239 \quad y_t = \mu_t + \gamma_t + \eta_t + \varepsilon_{obs}, \varepsilon_{obs} \sim N(0, \sigma_t^2), \quad (1)$$

$$240 \quad \mu_t = \mu_{t-1} + \alpha_t + \varepsilon_{level}, \varepsilon_{level} \sim N(0, \sigma_{level}^2), \quad (2)$$

$$241 \quad \alpha_t = \alpha_{t-1} + \varepsilon_{trend}, \varepsilon_{trend} \sim N(0, \sigma_{trend}^2), \quad (3)$$

$$242 \quad \eta_t = \rho\eta_{t-1} + \varepsilon_{AR}, \varepsilon_{AR} \sim N(0, \sigma_{AR}^2), \quad (4)$$

243 where y_t is the investigated concentration at time t , μ_t is the mean level and α_t is the change in the level
 244 from time $t-1$ to time t , γ_t is the seasonal component, ~~and~~ η_t is an autoregressive error component and
 245 ρ is the coefficient for autoregressive component, here fixed to $\rho = 0.6$. Here, this latter level is fixed.
 246 The Gaussian stochastic ε terms are used for the observation uncertainty and for random dynamics of
 247 the level and the trend. The seasonal component γ_t contains dummy variables for each month, so it has
 248 a different value for each month with a condition that 12 consecutive months sum to zero. More detailed
 249 description on how the model is written through state space equation can be found in Mikkonen et al.
 250 (2015).

251 2.3.2 Generalized linear mixed model

252 Linear mixed models (McCulloch et al., 2008) belong to the family of models that combine several
 253 different kinds of models used in multivariate analysis when the data do not fulfil the standard
 254 independency and homogeneity assumptions. This is the normal case with atmospheric and
 255 climatological measured variables (e.g. Mikkonen et al., 2011a). The main goal of the mixed models is
 256 to estimate not only the mean of the measured response variable but also the variance-covariance

257 structure of the data, which makes the model more valid for complex atmospheric data. In addition,
 258 modelling the (co)variances of the variables reduces the bias of the estimates, and prevents
 259 autocorrelation of the residuals. The model is constructed from general linear model, written in matrix
 260 format as $y = \mathbf{X}\boldsymbol{\beta} + \boldsymbol{\varepsilon}$, by adding a so-called random component (denoted $\mathbf{Z}\mathbf{u}$) to the model, thus the model
 261 is given by $y = \mathbf{X}\boldsymbol{\beta} + \mathbf{Z}\mathbf{u} + \boldsymbol{\varepsilon}$. Here, if we let n equal to number of observations, p equal to number of fixed
 262 parameters and q equal to number of random parameters in the model, \mathbf{y} is the $(n \times 1)$ vector of
 263 measurements of the variable of interest, $\boldsymbol{\beta}$ denotes the unknown $(p \times 1)$ vector of intercept and slope
 264 estimates of the model, \mathbf{X} is the $(n \times p)$ matrix of observations from predictor variables and $\boldsymbol{\varepsilon}$ contains
 265 the residuals of the model. In the random part, \mathbf{Z} is the $(n \times q)$ design matrix for the $(q \times 1)$ vector of
 266 random covariates \mathbf{u} with a q -dimensional normal distribution. With adequate choices of the matrix \mathbf{Z} ,
 267 different covariance structures $\text{Cov}(\mathbf{u}) = \mathbf{G}$ and $\text{Cov}(\boldsymbol{\varepsilon}) = \mathbf{R}$ can be defined and fitted. Successful modelling
 268 of variances and covariances of the observations provides valid statistical inference for the fixed effects
 269 $\boldsymbol{\beta}$ of the mixed model. In contrast to general linear models, the error terms $\boldsymbol{\varepsilon}$ can be correlated, which
 270 makes the modelling more robust. It follows from this that the distribution of observations can be
 271 described by a normal distribution with the expectation of $\bar{\mathbf{X}}$ and covariance matrix \mathbf{V} , which is given
 272 by $\mathbf{V} = \mathbf{Z}\mathbf{G}\mathbf{Z}' + \mathbf{R}$. With GLMM, it is possible to reliably detect the factors which affect particle number
 273 concentrations or which act as indicators for their different sources. The model can be expressed in a
 274 mathematical form as (Mikkonen et al., 2011a):

$$275 \quad N_{Di} = (\beta_0 + \beta_{setup} + u_m) + \alpha_d + (\beta_{wd} \cdot \beta_E) \cdot X_{Ti} + (\beta_1 + v_{1m}) \cdot SO_{2,i} + (\beta_2 + v_{2m}) \cdot NO_{2,i} + \\ 276 \quad (\beta_3 + v_{3m}) \cdot O_{3,i} + \beta_4 \cdot GRad_i + \beta_5 \cdot RH_i + \beta_6 \cdot MCP_i, \quad (45)$$

277 where N_{Di} is the number concentration in selected size range in time i , β_0 is a model intercept, β_{setup} is
 278 a correction term for changes in the measurement system due to two major upgrades, u_m is vector of
 279 random intercepts different for each month, α_d is average change of N_{Di} per day (i.e. slope of trend),
 280 β_{wd} and β_E are coefficients for workday and NPF event day, respectively, and X_{Ti} is the corresponding
 281 vector showing the type of the day (in both means: WD/HD and E/NE) in time i , $\beta_1 - \beta_5$ are fixed
 282 coefficients for SO_2 , NO_2 , O_3 , $GRad$ and RH , respectively, β_6 is the (13×1) vector of coefficients for
 283 different macro-circular patterns (MCP) [indicating the characteristic level of number concentration](#)
 284 during each MCP type, which are treated here as categorical variable, and v_m are the random, month
 285 specific slopes for SO_2 , NO_2 , O_3 and $GRad$. The coefficients of the model can be interpreted in a similar
 286 manner as multivariate regression or general linear models, just with an addition of month-specific
 287 effects for given variables.

288 3 Results and discussion

289 Annual insolation (Q), which expresses the total energy density at a receptor site, was derived from the
 290 individual hourly mean $\text{GRad}_{i,j}$ data, where index i represents the hour of day (from 0 to 23) and index
 291 j stands for the day of year (from 1 to 365) as $Q = 3.6 \times 10^{-6} \times \sum_{i,j} \text{GRad}_{i,j}$. The dimensions of the
 292 individual $\text{GRad}_{i,j}$ data and Q are W m^{-2} and $\text{GJ m}^{-2} \text{y}^{-1}$, respectively. The few randomly missing
 293 datapoints were interpolated linearly. An overview on annual averages of the data analysed in this study
 294 is given in Table 2. Annual insolation, which expresses the total energy density at the receptor site, was
 295 derived from the individual GRad_i data as $Q = n_d \times 24 \times 3600 \times \sum_i \text{GRad}_i$ over the year of interest (n_d is
 296 the number of day in the year). Since the major sources of particles in cities include road vehicles and
 297 atmospheric nucleation, we added some indicative data on these specific sources as well. The median
 298 particle number concentrations are basically in line with many other comparable cities in the world (e.g.
 299 Kerminen et al., 2018; Masiol et al., 2018). They indicate a decreasing change (except for $N_{100-1000}$) over
 300 the years 2008–2018. At the same time, the annual averages of the other concentrations, meteorological
 301 data and auxiliary variables did not change substantially. Annual mean relative occurrence frequency of
 302 NPF events stayed almost constant with a mean and SD of $(20 \pm 4)\%$, except for the measurement year
 303 2015–2016 when it was unusually small. It is worth adding that the NPF increases the existing particle
 304 number concentrations in Budapest by a factor of approximately 2 on event days (Salma et al., 2017).
 305 The annual medians for the particle formation rate and particle growth rate also stayed constant and
 306 seemingly varied only as fluctuations within ca. $\pm 20\%$ and $\pm 8\%$, respectively. The number of passenger
 307 cars was registered in Budapest remained constant within $\pm 5\%$, while the share of the diesel-powered
 308 passenger cars increased modestly by a rate of approximately 12% from 2008 to 2018 (KSH, 2019). The
 309 number (ca. 4000) of buses registered in Budapest and the share (98%) of the diesel-power buses on the
 310 national bus fleet remained constant.

311 **Table 2.** Annual medians of particle number concentrations in the diameter ranges from 6 to 1000 nm (N_{6-1000}),
 312 from 6 to 100 nm (N_{6-100}), from 25 to 100 nm (N_{25-100}) and from 100 to 1000 nm ($N_{100-1000}$), concentrations of SO_2 ,
 313 CO , NO , NO_x , O_3 , PM_{10} mass, annual means of air temperature (T), relative humidity (RH), wind speed (WS),
 314 atmospheric pressure (P) and annual insolation (Q), annual mean relative occurrence frequency of nucleation
 315 (f_{NPF}), annual median formation rate of particles with a diameter of 6 nm (J_6), annual median growth rate of
 316 particles with a diameter of 10 nm (GR_{10} ; for the rates, see Salma and Németh, 2019), number of passenger cars
 317 registered in Budapest (Cars), the mean age and the share of diesel-powered vehicles (Diesel) separately for the 1-
 318 year-long measurement time intervals.

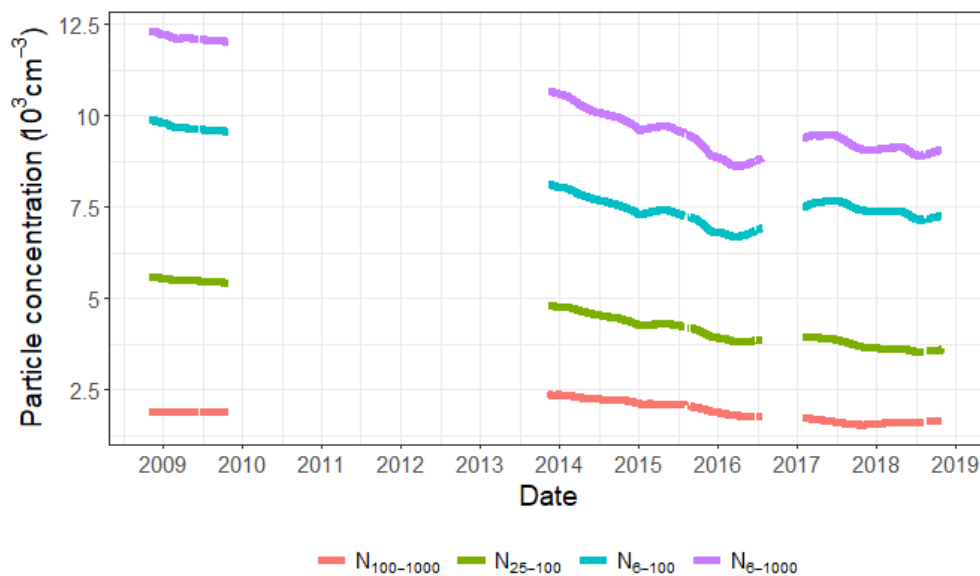
Variable	Unit	2008–2009	2013–2014	2014–2015	2015–2016	2017–2018	2018–2019
N_{6-1000}	10^3 cm^{-3}	11.5	9.7	9.3	7.5	8.6	8.3
N_{6-100}	10^3 cm^{-3}	9.1	7.2	6.9	5.7	6.8	6.5
N_{25-100}	10^3 cm^{-3}	5.1	4.3	4.1	3.3	3.6	3.2
$N_{100-1000}$	10^3 cm^{-3}	1.79	2.2	2.0	1.56	1.49	1.53
SO_2	$\mu\text{g m}^{-3}$	5.0	4.8	4.6	4.8	4.5	5.2

CO	$\mu\text{g m}^{-3}$	547	488	577	513	534	624
NO	$\mu\text{g m}^{-3}$	13.3	19.2	23	17.6	20	17.0
NO _x	$\mu\text{g m}^{-3}$	58	80	89	72	79	73
O ₃	$\mu\text{g m}^{-3}$	23	14.8	19.6	25	20	21
PM ₁₀	$\mu\text{g m}^{-3}$	33	31	39	29	28	36
<i>T</i>	°C	12.0	13.2	13.2	12.9	13.2	13.3
RH	%	64	69	64	69	63	67
WS	m s^{-1}	2.5	2.6	2.8	2.7	2.9	2.5
<i>P</i>	hPa	1001	1003	1005	1004	1004	1004
<i>Q</i>	$\text{GJ m}^{-2} \text{y}^{-1}$	4.45	4.39	4.58	4.52	4.77	4.66
<i>f</i> _{NPF}	%	24	20	23	13.0	23	20
<i>J</i> ₆	$\text{cm}^{-3} \text{s}^{-1}$	4.2	3.5	4.4	4.6	6.3	4.6
GR ₁₀	nm h^{-1}	7.6	6.6	6.5	8.0	7.5	7.0
Cars*	10 ³ pcs	582	573	584	597	634	659
Age*	y	10.8	13.0	13.4	13.7	14.1	14.2
Diesel*	%	20	24	26	28	29	n.a.

319 * Status at the end of years 2009, 2013, 2014, 2015, 2017 and 2018, respectively.
320 n.a.: not yet available.

321 3.1 Decennial time scale

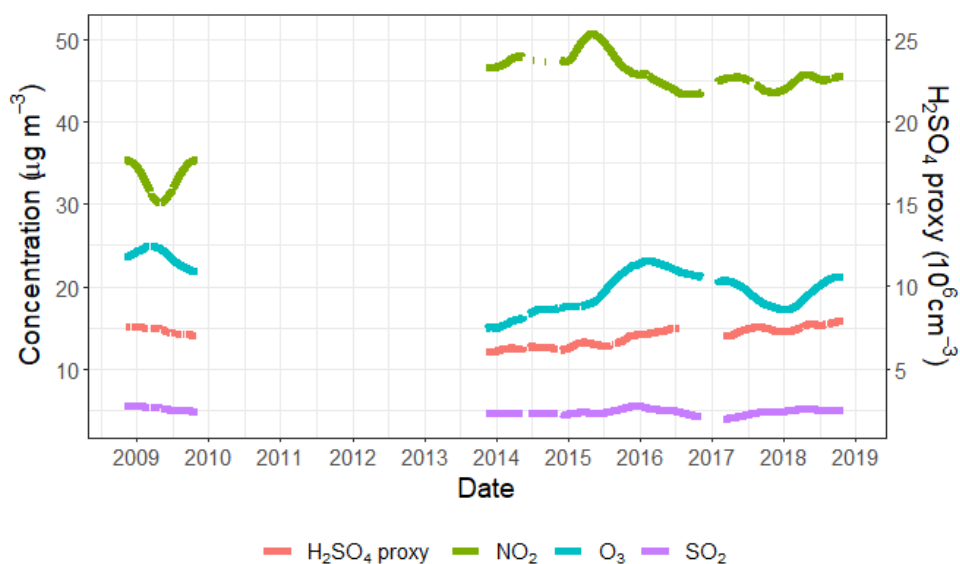
322 Overall statistical time trends for particle number concentrations in various size fractions obtained by
323 the DLM are displayed in Figure 1. The curves confirm that the N_{6-1000} , N_{6-100} and N_{25-100} indeed
324 decreased in Budapest between 2008 and 2018, while the change in $N_{100-1000}$ was not significant. The
325 decline mostly took place in a monotonical manner except for perhaps the interval of summer 2016–
326 spring 2017, when some partial/local increase could be realised for N_{6-1000} and N_{6-100} .



327 **Figure 1.** Statistical time trends of particle number concentrations in the diameter ranges from 6 to 1000 nm (N_{6-1000}),
328 from 6 to 100 nm (N_{6-100}), from 25 to 100 nm (N_{25-100}) and from 100 to 1000 nm ($N_{100-1000}$) derived by DLM
329 over a decennial interval.

330 There are several important sources, sinks and atmospheric transformation processes including
331 environmental conditions which can influence the atmospheric concentrations. The major sources

332 include both high-temperature emissions and NPF events as discussed in Sect. 1. The latter source is
 333 affected by concentrations of precursor and other trace gases, meteorological properties for
 334 photochemical reactions, and the interactions among gas-phase chemical species of different origin/type
 335 with respect the formation yield of condensing vapours (Kulmala et al., 2014; McFiggans et al., 2019).
 336 The air pollutants listed in Table 2 and gas-phase H_2SO_4 proxy – which are known or expected to affect
 337 particle number concentrations – did not exhibit decreasing statistical trend between 2008 and 2018
 338 (Fig. 2). On one hand, this decoupling ~~confirms~~ suggests that the causes of the decrease in particle
 339 number concentrations are not primarily related to meteorological conditions because they would jointly
 340 affect the gas concentrations as well (if their sources are more-or-less constant over a certain time
 341 interval). On the other hand, the constant gas concentrations suggest that the decreasing trend in particles
 342 does not seem to be related to the major precursors or interacting gaseous chemical species (such as
 343 SO_2 , H_2SO_4 or NO_2).



344 **Figure 2.** Statistical time trends of gas-phase H_2SO_4 proxy, SO_2 , O_3 and NO_2 derived by DLM over the decennial
 345 interval.

346 As far as the meteorological conditions are concerned, some of them such as WS, atmospheric boundary
 347 mixing layer height and T have previously been shown to influence the temporal variation of aerosol
 348 particles (e.g. Birmili et al., 2001; Mikkonen et al., 2011a). The annual means of possibly relevant
 349 properties and parameters in Table 2 – except for the particle number concentrations (which are under
 350 the investigation) and the fraction of diesel cars – did not show any obvious dependency; they virtually
 351 stayed constant over the years of interest. The possible effect of different weather conditions on the
 352 concentrations are studied separately by the GLMM and are discussed in Sect. 3.2.2. There were also
 353 no substantial and extensive urban constructions in the area (which could influence the urban air flow)
 354 nor larger systematic changes in the traffic circulation around the sampling site in the time interval
 355 considered. Therefore, the decline in the particle number concentrations ~~is~~ can most likely be interpreted
 356 as a consequence of the decreased anthropogenic particulate emissions in Budapest. The related source

sectors can include vehicular road traffic and household heating/cooking. The decline happened at an increasing share of the diesel passenger cars and straitened emission control on (diesel) vehicles, [as e.g. Platt et al. \(2017\) and Wihersaari et al. \(2020\)](#); [showed that modern diesel engines have smaller lower particle emissions than gasoline engines.](#)

The average decrease rates of particle number concentrations as derived from both the DLM and GLMM statistical approaches are summarised in Table 3. The rates are shown as obtained from the models and scaled for the 10-year measurement interval to ensure the comparability of the slopes. The relative mean changes in % per year were expressed with respect to the starting value (mean of the first year). There are some differences between the corresponding results of the two models, which were caused by standardising the concentrations with the predictors in the models and by handling the upgrades of measurement setup differently. The changes in all size fractions were on the same level and only minor differences could be seen. As the estimates always contain some uncertainty, these differences are not considered as statistically significant. The largest difference between the two models was observed for $N_{100-1000}$ (which had the lowest absolute concentrations). One possible cause for this might be that GLMM standardises the results for variables indicating anthropogenic emissions and thus the size fraction that is the most sensitive for the emissions has the strongest effect. Considering all these, the rates from the two statistical models agree well. Furthermore, the rates for N_{6-1000} and N_{6-100} were identical. This is explained by the fact that these two size fractions are strongly connected; the typical N_{6-100}/N_{6-1000} mean ratio in central Budapest is 75–80% (Salma and Németh, 2019). Small difference was also seen for N_{25-100} . In urban areas, this size fraction is mainly composed of particles from high-temperature emission sources. The source types responsible for the observed decline are further discussed in Sect. 3.2.1.

Table 3. Decrease rates of particle number concentrations in the diameter ranges from 6 to 1000 nm, from 6 to 100 nm, from 25 to 100 nm and from 100 to 1000 nm obtained by the dynamic linear model and generalized linear mixed model as a mean absolute change per year during the 10-year measurement interval and as a relative mean change per year with respect to the mean value of the first year.

Size fraction (nm)	Dynamic linear model		Generalized linear mixed model	
	Mean change/year (cm^{-3})	Relative mean change (%/year)	Mean change/year (cm^{-3})	Relative mean change (%/year)
6–1000	–510	–4	–660	–5
6–100	–400	–4	–480	–5
25–100	–310	–6	–360	–5
100–1000	–50	–3	–180	–8

Our results concerning the decennial change rates (and our conclusions with regard to their causes mainly discussed in Sect. 3.2.1) are comparable and are in line with some other very recent studies. Sun

386 et al. (2019,2020) investigated the statistical concentration trends in particle numbers (and equivalent
387 black carbon mass) at multiple urban, rural or background sites within the German Ultrafine Aerosol
388 Network. Decreasing annual slopes of $-(7.0-1.7)\%$ were obtained for several size fractions (which are
389 different from our intervals), and the most likely factors for the decreasing trends were assigned to
390 declining anthropogenic emissions due to emission mitigation policies of the EU. Masiol et al. (2018)
391 evaluated statistical time trends of particle number concentrations in various size fractions (which are
392 different again from the previous and present studies) in Rochester, NY, USA, and obtained a typical
393 decline rate of -4.6% per year for total particles. These outcomes and our data as well seem to be
394 different from the results obtained by Saha et al. (2018) in the urban Pittsburgh, PA, USA by comparing
395 two intervals of 2001–2002 and 2016–2017. It should be mentioned that in the latter research, the
396 experimental setup for measuring particle number size distributions had a lower diameter limit of
397 detection at 11 nm, some methodological approaches (e.g. classification of events) were different from
398 ours and that the time trend was not derived by statistical modelling. The authors concluded that both
399 the frequency of NPF events and their dynamic properties were reduced by (40–50)% over the past 15
400 years, resulting in ca. 48% reduction of UF concentrations. The changes were attributed to dramatic
401 reductions in SO_2 emissions in the larger region.

402 **3.2 Diurnal time scale**

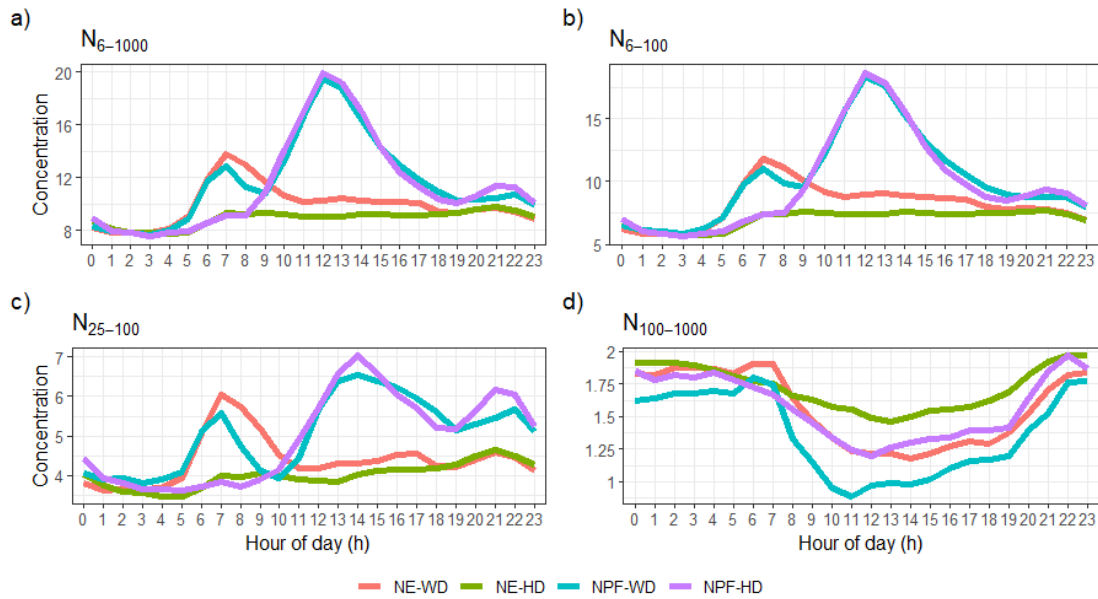
403 Diurnal statistical patterns of the particle number concentrations in different size fractions were
404 predicted by the GLMM considering the following variables: GRad, RH, concentrations of SO_2 , NO_2 ,
405 O_3 , and labels for workdays/holidays, for NPF event days/non-event days and for MCP codes. The initial
406 screening for possible prediction variables was done in earlier papers. Studies such as Hyvönen et al.
407 (2005), Mikkonen et al. (2006) and Nieminen et al. (2014) suggested that meteorological and trace gas
408 variables affect NPF. Furthermore, e.g. Mikkonen et al. (2011a), Guo et al. (2012) and Zaidan et al.
409 (2018) studied the factors which influence the growth of freshly formed particles as well as the
410 concentrations of particles in larger size fractions and specified the possible predictors. All variables
411 found in these screenings and measured at our site were tested one-by-one in the GLMM model in a
412 stepwise manner. In each step, the significance of the added or removed variable was investigated by a
413 likelihood ratio test (e.g. Pinheiro and Bates, 2000) until the final model shown in Eq. 4 was formed.
414 The effect of the H_2SO_4 proxy was also tested, and the results for the daytime concentrations were
415 similar to those obtained with the selection of variables above. The modelling results for night-time
416 were, however, biased since the proxy is defined for $\text{GRad} > 10 \text{ W m}^{-2}$, and, therefore, we decided not to
417 include the proxy into the final model.

418 **3.2.1 Diurnal statistical patterns**

419 Modelled diurnal pattern of particle number concentrations for event days on workdays, event days on
420 holidays, non-event days on workdays and non-event days on holidays separately for different size

421 fractions are shown in Fig. 3. The curves on Fig. 3a–c resemble tendentious variations, which can be
422 associated with typical diurnal activity–time pattern of inhabitants in cities, particularly with road traffic.
423 They are also perfectly in line with the mean diurnal tendencies of experimentally determined
424 concentrations in central Budapest (Salma et al., 2014; 2017) and are consistent with the time variations
425 in many other European cities (Hussein et al., 2004; Aalto et al., 2005; Moore et al., 2007; Avino et al.,
426 2011; Dall’Osto et al., 2013).

427 In the statistical diurnal patterns of UF particles (Fig. 3b), there is a huge peak from late morning to late
428 afternoon on event days. This is unambiguously caused by NPF and growth process. The peaks on
429 workdays and holidays are rather similar to each other in the position, shape and magnitude (area), which
430 means that the dynamics and timing of NPF events in general are not substantially influenced by
431 anthropogenic activities, which are more intensive on workdays than on holidays. It is worth mentioning
432 that the overall contribution of the NPF to particle number concentrations is less than what is seemingly
433 indicated by the diurnal patterns alone since NPF events occur on approximately 20% of days (Table 2).
434 Emissions from vehicular road traffic is represented by a notable peak during the morning rush hours
435 (between 05:30 and 08:30) on workdays. It is noted that the boundary layer mixing height is usually
436 increased during this interval because of the increasing solar radiation intensity and mixing intensity.
437 Another peak occurred around 21:00, thus later than the afternoon rush, which usually happens between
438 16:30 and 18:30. Under strong anti-cyclonic conditions, the evolution of the boundary layer mixing
439 height and mixing intensity can decrease the concentration levels in the afternoons until sunset, and this
440 can compensate the increased intensity of emissions. This all means that the afternoon peak is realised
441 in a fuzzy manner since it is more influenced by local meteorology than by vehicular emissions. The
442 effect of residential heating and combustion activities at evenings can also play a role. It is worth noting
443 that the early-morning rush-hour peak on event days was smaller than on non-event days, which agrees
444 with our earlier observation derived directly from experimental data (Salma et al., 2017) and is in line
445 with the overall picture on urban NPF events (Zhang et al., 2015; Kulmala et al., 2017). On holidays,
446 the modelled diurnal variation for non-event days contained an increasing part in the morning to a
447 modest concentration level, which remains fairly constant over the daytime. This is explained by the
448 differences in daily activities of citizens on workdays and holidays as far as both their intensity and
449 timing are concerned.



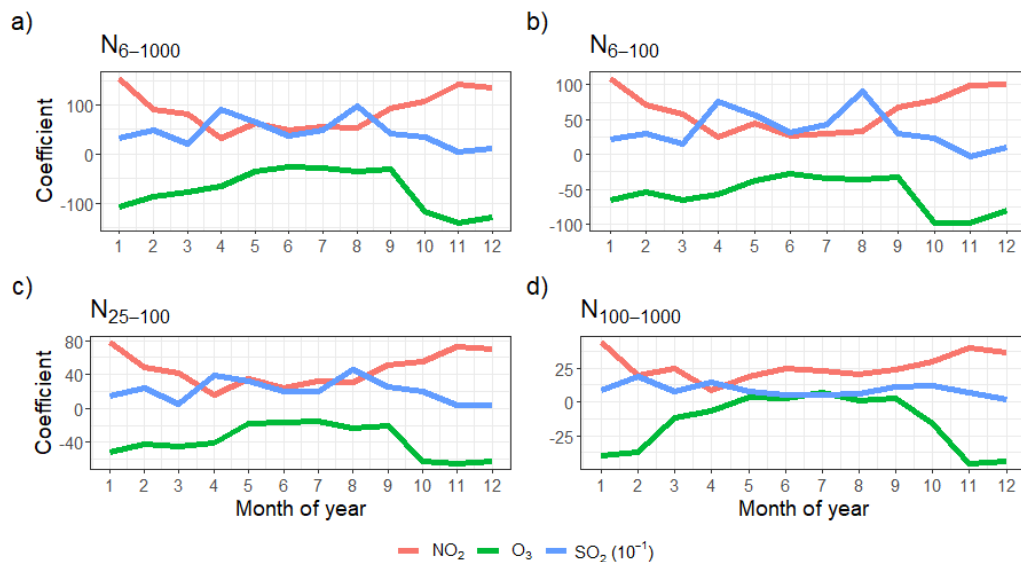
450
 451 **Figure 3.** Diurnal patterns of particle number concentrations in the diameter ranges from 6 to 1000 nm (N_{6-1000}),
 452 from 6 to 100 nm (N_{6-100}), from 25 to 100 nm (N_{25-100}) and from 100 to 1000 nm ($N_{100-1000}$) in units of 10^3 cm^{-3} .
 453 Red: non-event on workdays, green: non-event on holidays, cyan: event on workdays, purple: event on holidays.

454 The statistical diurnal patterns of N_{6-1000} trends (Fig. 3a) were very similar or analogous to those of the
 455 N_{6-100} . These two size fractions are strongly connected with each other as explained in Sect. 3.1. The
 456 diurnal curves for N_{25-100} (Fig. 3c) were also similar to the previous corresponding curves as far as the
 457 character and shape are concerned, while there were also evident differences between their relative
 458 structures. The peaks for the early morning and late afternoon rush hours were relatively larger than in
 459 the trends of 6–100- or 6–1000-nm size fractions due to the higher contribution of primary particles
 460 from high temperature sources in this size fraction. New particle formation generally occurs on days
 461 when N_{25-100} are smaller before the event onset (between 08:00 and 11:00). The maximum of the peaks
 462 associated with NPF events in Fig. 3a and b – which is between 12:00 and 13:00 – was also shifted to
 463 later, i.e. to ca. 14:00 in Fig. 3c. This can be explained by the time needed for freshly nucleated particles
 464 to reach the diameter range >25 nm.

465 The statistical diurnal patterns for $N_{100-1000}$ seem very different from the smaller size ranges. First, their
 466 time variations were rather small in comparison to the other size fractions. On workdays, they only
 467 showed a modest elevation from 06:00 to 08:00 (morning rush hours), which is mainly caused by
 468 resuspension of road/surface dust particles by moving vehicles or by emissions of coarse particles from
 469 material wear. This morning peak was even missing on holidays, but another small and broad elevation
 470 showed up from 21:00 to 22:00. This and the overall changes during the daylight time are primarily
 471 related to the daily cycling of local meteorological conditions, in particular of boundary layer mixing
 472 height under stable anti-cyclonic weather conditions, outlined above.

473 3.2.2 Effects of variables

474 Monthly mean coefficients (mean v_m slopes in Eq. 4) of NO₂, O₃ and SO₂ derived by GLMM, which
 475 express their partial effects on particle number concentrations are shown in Fig. 4 for different size
 476 fractions.



477
 478 **Figure 4.** Distribution of monthly mean coefficients (which are proportional to the partial effects) for NO₂, O₃ and
 479 SO₂ on particle number concentrations separately in the diameter ranges from 6 to 1000 nm (N_{6-1000}), from 6 to
 480 100 nm (N_{6-100}), from 25 to 100 nm (N_{25-100}) and from 100 to 1000 nm ($N_{100-1000}$).

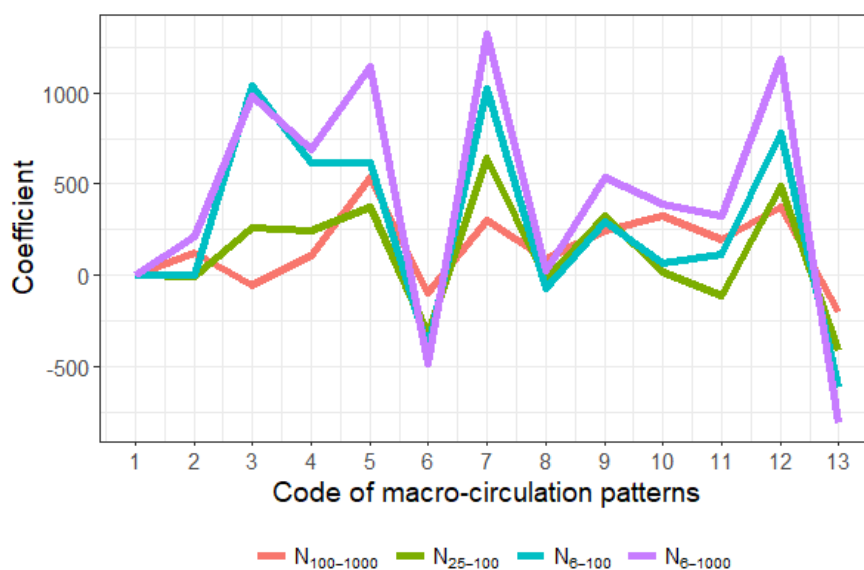
481 The coefficients of SO₂ and NO₂ are positive, while O₃ seems to have a decreasing effect on particle
 482 number concentrations. The coefficients all have seasonal patterns, which means that the magnitude of
 483 their effect on particle concentrations are of different magnitude in different months. This means for
 484 example that 1 $\mu\text{g m}^{-3}$ increase in NO₂ concentration increases N_{6-1000} concentration in January by 154
 485 m^{-3} but in June by 50 m^{-3} . This could, however, be partly caused by annual changes of boundary layer
 486 mixing height or some other variable affecting particle concentrations, and correlating with these, but
 487 not measured at the site. The boundary layer mixing height tends to be smaller in Budapest in winter
 488 than in the other seasons (Salma et al., 2011), which ordinarily results in higher atmospheric
 489 concentrations at steady-state absolute amounts of chemical species. The coefficients of NO₂ on N_{6-1000} ,
 490 N_{6-100} and N_{25-100} were higher in winter. This may indicate that large fractions of particles in these three
 491 size fractions originate from residential heating and NO₂ acts as an indicator for this source. Another
 492 major source of NO₂ and primary particles is the road traffic, but this does not show seasonal variation
 493 in Budapest. The seasonal effect of NO₂ on chemically aged, regional type particles ($N_{100-1000}$) may not
 494 be significant.

495 The partial effect of O₃ on N_{6-1000} , N_{6-100} and N_{25-100} was weaker in summer, late spring and early autumn.
 496 This interval coincides with relatively large O₃ concentrations in the area. Ozone has a strong seasonal
 497 variation (as shown in Fig. S1 in the Supplement). The negative correlation between O₃ concentration

498 and its effect on particle concentrations need further clarification since O_3 participates in a large variety
 499 of complex atmospheric processes and also serves as a marker for photochemical processes which
 500 influence secondary particle formation. The influence of O_3 on $N_{100-1000}$ was virtually negligible due
 501 likely to the regional character of these particles (which are usually chemically aged and often represent
 502 larger spatial scale due to their larger atmospheric residence time) similarly to NO_2 . In addition, O_3
 503 might act as an indicator of particulate pollution from traffic, power plants and other anthropogenic
 504 sources. Then more ozone would indicate higher number of larger particles and due to coagulation less
 505 smaller particles.

506 The partial effects of SO_2 on the particle number concentrations were the largest of the three gases
 507 considered. In the N_{6-1000} , N_{6-100} and N_{25-100} , two peaks appeared, one in spring and another one in late
 508 summer. This shape is in line with the average distribution of the monthly mean relative NPF occurrence
 509 frequency in Budapest (Salma and Németh, 2019). The latter distribution consists of an absolute and a
 510 local minimum in January (with a monthly mean occurrence frequency of 5.9%) and in August (17.0%),
 511 respectively, and an absolute and a local maximum in April (41%) and in September with (26%),
 512 respectively. The distribution of the SO_2 coefficient suggests and confirms that SO_2 , via NPF events
 513 contribute in a substantial extent to the particle number concentrations in cities. The influence of SO_2
 514 on $N_{100-1000}$ was virtually negligible due likely to the regional character of these particles similarly to the
 515 other two gases included into the model.

516 Figure 5 summarizes the effect of macro-circulation patterns on particle number concentrations in the
 517 different size fractions. It is seen that the larger regional-type particles are less affected by the MCPs
 518 than the smaller particles. The weather conditions favouring NPF events can be identified from the
 519 curves by looking at the largest coefficients for size fraction of 6–100 nm.

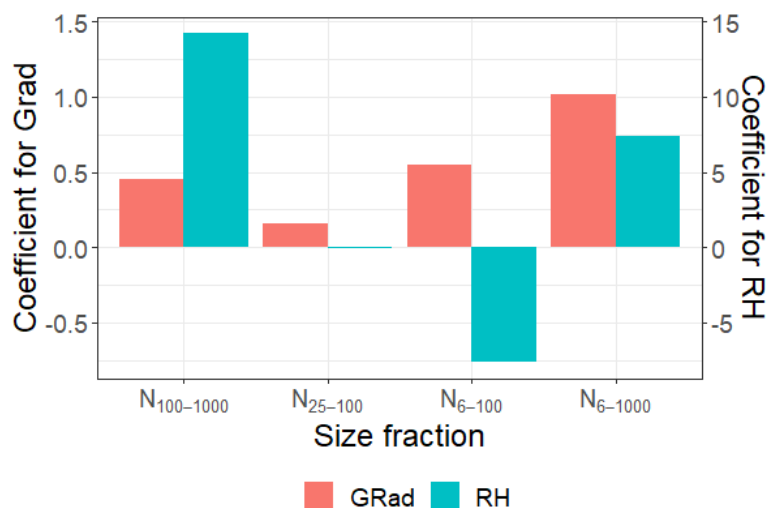


520

521 **Figure 5.** Distribution of monthly mean coefficients (which are proportional to the partial effects) for macro-
522 circulation patterns (Péczezy codes) on particle number concentrations separately in the diameter ranges from 100
523 to 1000 nm ($N_{100-1000}$), from 25 to 100 nm (N_{25-100}), from 6 to 100 nm (N_{6-100}) and from 6 to 1000 nm (N_{6-1000}).

524 It seems that the MCP no. 3 (Mediterranean cyclone with a cold front over S Europe, N wind), 7 (highly
525 developed cyclone over N Europe, W wind) and 12 (anticyclone over the Carpathian Basin, changing
526 wind direction) can represent favourable conditions for NPF events than the other MCPs. Under these
527 conditions, the weather in the area is typically windy, with average solar radiation (expect for MCP no.
528 3 in summer when it shows low daily values), with strong planetary bounding layer evolution and
529 consequently, iv) the pollutants concentrations are below the average (expect for the winter inversions
530 in MCP no. 12). The air pollution situations are better separated by MCP codes in summer than in winter.
531 The weather type classified as no. 6 (Mediterranean cyclone with a warm front over S Europe, S wind)
532 disfavour the events. Under these conditions, the weather is typically cloudy and rainy with lower than
533 average solar radiation. This situation is often associated with polluted air in Budapest. Proportions for
534 NPF days for different MCP codes, which are shown Table S1 in the Supplement, also confirm these
535 conclusions. In order to see if the decreasing concentrations are due to changes in meteorological
536 patterns, we investigated separately the occurrence of the MCP patterns during the measurement period.
537 We found no significant changes in the occurrence of the patterns and thus the decreasing particle
538 concentrations are due to something else than the meteorological patterns.

539 The coefficients for GRad and RH for different size fractions are shown in Fig. 6. It was found that these
540 variables do not have seasonal dependency, i.e. they contribute with equal strength to particle
541 concentrations throughout the year. Effect of GRad is positive for all size fractions, but it is weaker for
542 larger (regional-type or already chemically aged or processed) particles. The latter contribution could
543 be related to the bias in meteorological properties as well. The RH has negligible effect on size fraction
544 of 25–100 nm. It affects strongly and positively the largest particles, which means that the particles are
545 larger within higher humidity. This might be related to local meteorology, as higher RH probably means
546 more clouds and more clouds probably means less radiation and lower boundary layer and this could



547 cause higher particle concentration. In contrast, the effect of RH on the smallest particles was negative,
 548 which is probably caused by high RHs, which limit NPF (e.g. Hamed et al., 2011).

549 **Figure 6.** Distribution of monthly mean coefficients (which are proportional to the partial effects) for global
 550 radiation (GRad) and relative humidity (RH) separately in the diameter ranges from 100 to 1000 nm ($N_{100-1000}$),
 551 from 25 to 100 nm (N_{25-100}), from 6 to 100 nm (N_{6-100}) and from 6 to 1000 nm (N_{6-1000}).

552 3.2.3 Goodness-of-fit evaluation for GLMM

553 In order to estimate the uncertainty of the models for different size fractions, we calculated the mean
 554 absolute errors relative to the dependent variable mean, given by Willmot et al. (2009):

$$555 \text{Err} = (n^{-1} \sum_{i=1}^n |y_i - \hat{y}_i|) \cdot \bar{y}^{-1}, \quad (5)$$

556 where n is the number of observations, y_i are the observed particle number concentrations, \hat{y}_i are the
 557 predicted values given by the GLMM and \bar{y} is the mean of the observed values. In addition, we
 558 calculated Spearman's rank correlation coefficients between the observed and predicted values for all
 559 size fractions. Both goodness-of-fit estimates are shown in Table 4. As the relative errors for different
 560 size fractions are within a range of 0.30–0.34 and the correlations are higher than 0.70, it can be
 561 concluded that the model fitted the data with this size and measurement uncertainty well.

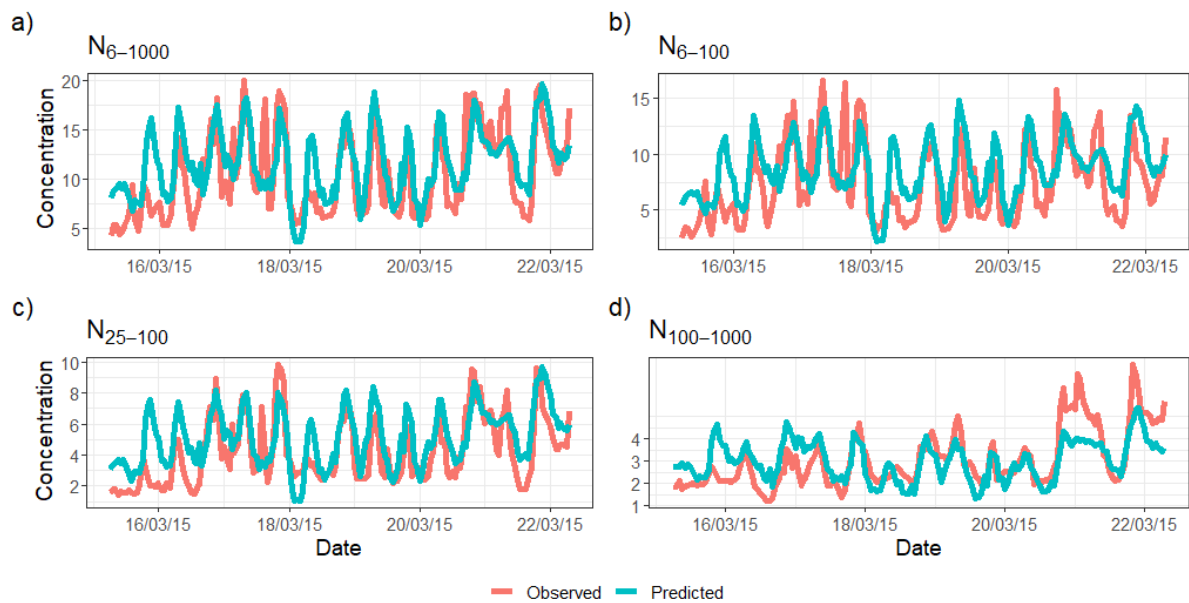
562

563 **Table 4.** Goodness-of-fit estimates for GLMM as expressed by the mean absolute error relative to the dependent
 564 variable mean and by Spearman's rank correlation coefficient separately in the size fractions of 6–1000, 6–100,
 565 25–100 and 100–1000 nm.

Size fraction	Error	Correlation
6–1000	0.30	0.73
6–100	0.32	0.72
25–100	0.34	0.71
100–1000	0.34	0.73

566

567 Figure 7 illustrates how well the GLMM model predicts the observations in all size fractions within a
 568 randomly selected period of one week in March 2015. The figure shows that the predicted values follow
 569 the observations fairly well in all size fractions. Overall, the statistical model finds the peaks of the
 570 concentration, but slightly underestimates the highest peaks and the fastest fluctuations and in some
 571 cases, overestimates the lowest concentrations.



572
 573 **Figure 7.** Observed (red line) and predicted (cyan line) time series for an illustrative example period separately in
 574 the size fractions of 6–1000, 6–100, 25–100 and 100–1000 nm.

575 4 Conclusions

576 In the present study, we determined decennial statistical time trends and diurnal statistical patterns of
 577 atmospheric particle number concentrations in various relevant size fractions in the city centre of
 578 Budapest in an interval of 2008–2018. The decennial statistical trends showed decreasing character
 579 ~~except for the size fraction representing the regional~~ in all applied size fractions of particle
 580 concentrations. The mean overall decrease rate was approximately –5% scaled for the 10-year
 581 measurement interval. One of the likely explanations of t ~~The decline can be interpreted as a consequence~~
 582 of is due to the decreased anthropogenic emissions in the city. The diurnal statistical patterns suggested
 583 that reduced traffic emissions were most likely an important factor in causing the observed changes. It
 584 is expected that traffic intensity changed in a modest manner in the city centre during the time interval
 585 of interest, so our results indicate that the reductions is most likely related to lower emission factors.
 586 This appears to follow some changes of sulfur content in fuels and control measures on emissions for
 587 on-road heavy-duty diesel vehicles. Introduction of better particle filters in diesel cars, cleaner fuel and
 588 more sophisticated diesel engines could also contribute. Modernised technologies in residential and
 589 household heating could also contribute. Our present interpretation ~~The magnitude of the reduced-traffic~~
 590 emission reductions cannot be completely conclusive in all aspects for the moment and further
 591 investigations are planned on the basis of the present results. The changes appear to have responded to
 592 both the policy on urban air quality and the influence of economic circumstances of inhabitants.
 593 Excitingly, the mean ages of passenger cars and busses in Hungary increased during the years under
 594 investigation. The exact explanation and confirmation of the decrease requires continuation of the

595 related measurements [with independent experimental systems](#) and further dedicated studies. The present
596 results can be also used for evaluating the effectiveness of present and prospective mitigation policies.

597 The diurnal statistical patterns can be also utilized in interpreting some properties of NPF events in urban
598 environments, and in explaining time evolution of particle number concentration. As a result of GLMM,
599 we could, for instance, give a parametrization for predicting particle concentrations in different size
600 fractions. Models similar to those developed in the present study could be used for other particle sizes or
601 locations as well. The same parameterization could be used at least in areas with similar concentration
602 levels of particles and pollutants, while the extrapolation of the results to cleaner or more polluted
603 environments needs to be confirmed before the use. Conjugate or linked parameterizations to be
604 developed for varying environments can be implemented as a part of atmospheric models to predict the
605 concentrations of climatically active particles in order to reduce their extensive computational times. In
606 addition, this could also contribute to solving some current uncertain issues in the theoretical description
607 of NPF and growth process, particularly when predicting cloud condensation nuclei concentrations.

608 **Data availability.** The observational data used in this paper are available on request from the corresponding author
609 Imre Salma.

610 **Author contributions.** IS and SM formulated the original concept; ZN, VV, TW and IS collected and processed
611 the experimental data; SM, VL and TY were responsible for the statistical data analyses and their physical basis;
612 SM and IS interpreted the results; IS and SM wrote the manuscript with contributions from all co-authors.

613 **Competing interest.** The authors declare that they have no conflict of interest.

614 **Financial support.** The research was supported by the National Research, Development and Innovation Office,
615 Hungary (contracts K116788, PD124283 and K132254), by the János Bolyai Research Scholarship of the
616 Hungarian Academy of Sciences (ZN) and by the European Regional Development Fund and the Hungarian
617 Government (GINOP-2.3.2-15-2016-00028), The Nessling Foundation, The Academy of Finland Centre of
618 Excellence (grant no. 307331) and The Academy of Finland Competitive funding to strengthen university research
619 profiles (PROFI) for the University of Eastern Finland (grant no. 325022) and Academy of Finland project (grant
620 no. 299544)

621 **References**

- 622 Aalto, P., Hämeri, K., Becker, E., Weber, R., Salm, J., Mäkelä, J., Hoell, C., O'Dowd, C., Karlsson, H., Väkevä,
623 M., Koponen, I. K., Buzorius, G., and Kulmala, M.: Physical characterization of aerosol particles during
624 nucleation events, *Tellus*, 53B, 344–358, 2001.
- 625 Aalto, P., Hämeri, K., Paatero, P., Kulmala, M., Bellander, T., Berglind, N., Bouso, L., Castaño-Vinyals, G.,
626 Sunyer, J., Cattani, G., Marconi, A., Cyrus, J., von Klot, S., Peters, A., Zetzsche, K., Lanki, T., Pekkanen, J.,
627 Nyberg, F., Sjövall, B., and Forastiere, F.: Aerosol particle number concentration measurements in five
628 European cities using TSI-3022 condensation particle counter over a three-year period during health effects of
629 air pollution on susceptible subpopulations, *J. Air Waste Manage. Assoc.*, 55, 1064–1076, 2005.

630 Asmi, A., Collaud Coen, M., Ogren, J. A., Andrews, E., Sheridan, P., Jefferson, A., Weingartner, E., Baltensperger,
631 U., Bukowiecki, N., Lihavainen, H., Kivekas, N., Asmi, E., Aalto, P. P., Kulmala, M., Wiedensohler, A.,
632 Birmili, W., Hamed, A., O'Dowd, C., Jennings, S. G., Weller, R., Flentje, H., Fjaeraa, A. M., Fiebig, M., Myhre,
633 C. L., Hallar, A. G., Swietlicki, E., Kristensson, A., and Laj, P.: Aerosol decadal trends - Part 2: In-situ aerosol
634 particle number concentrations at GAW and ACTRIS stations, *Atmos. Chem. Phys.*, 13, 895–916, 2013.

635 Avino, P., Casciardi, S., Fanizza, C., and Manigrasso, M.: Deep investigation of ultrafine particles in urban air,
636 *Aerosol Air Qual. Res.*, 11, 654–663, 2011.

637 Birmili, W., Wiedensohler, A., Heintzenberg, J., and Lehmann, K.: Atmospheric particle number size distribution
638 in central Europe: Statistical relations to air masses and meteorology, *J. Geophys. Res., Atmospheres*,
639 106(D23), 32005-18, 2001.

640 Braakhuis, H. M., Park, M. V., Gosens, I., De Jong, W. H., and Cassee, F. R.: Physicochemical characteristics of
641 nanomaterials that affect pulmonary inflammation, *Part. Fibre Toxicol.*, 11:18, doi: 10.1186/1743-8977-11-18,
642 2014.

643 Brines, M., Dall'Osto, M., Beddows, D. C. S., Harrison, R. M., Gómez-Moreno, F., Núñez, L., Artñano, B.,
644 Costabile, F., Gobbi, G. P., Salimi, F., Morawska, L., Sioutas, C., and Querol, X.: Traffic and nucleation events
645 as main sources of ultrafine particles in high-insolation developed world cities, *Atmos. Chem. Phys.* 15, 5929–
646 5945, 2015.

647 Cassee, F. R., Héroux, M.-E., Gerlofs-Nijland, M. E., and Kelly, F. J.: Particulate matter beyond mass: recent
648 health evidence on the role of fractions, chemical constituents and sources of emission, *Inhal. Toxicol.* 25,
649 802–812, 2013.

650 Carslaw, K. S., Lee, L. A., Reddington, C. L., Pringle, K. J., Rap, A., Forster, P. M., Mann, G. W., Spracklen, D.
651 V., Woodhouse, M. T., Regayre, L. A., and Pierce, J. R.: Large contribution of natural aerosols to uncertainty
652 in indirect forcing, *Nature*, 503, 67–71, 2013.

653 Dada, L., Ylivinkka, I., Baalbaki, R., Li, Ch., Guo, Y., Yan, Ch., Yao, L., Sarnela, N., Jokinen, T., Daellenbach,
654 K. D., Yin, R., Deng, Ch., Chu, B., Nieminen, T., Kontkanen, J., Stolzenburg, D., Sipilä, M., Hussein, T.,
655 Paasonen, P., Bianchi, F., Salma, I., Weidinger, T., Pikridas, M., Sciare, J., Jiang, J., Liu, Y., Petäjä, T.,
656 Kerminen, V.-M., and Kulmala, M.: Sources and sinks driving sulphuric acid concentrations in contrasting
657 environments: implications on proxy calculations, *Atmos. Chem. Phys. Discuss.*, under evaluation, 2020.

658 Dal Maso, M., Kulmala, M., Lehtinen, K. E. J., Mäkelä, J. M., Aalto, P. P., and O'Dowd, C.: Condensation and
659 coagulation sinks and formation of nucleation mode particles in coastal and boreal forest boundary layers, *J.*
660 *Geophys. Res.*, 107(19D), 8097, 10.1029/2001jd001053, 2002.

661 Dal Maso, M., Kulmala, M., Riipinen, I., Wagner, R., Hussein, T., Aalto, P. P., and Lehtinen, K. E. J.: Formation
662 and growth of fresh atmospheric aerosols: eight years of aerosol size distribution data from SMEAR II,
663 Hyytiälä, Finland, *Boreal Environ. Res.*, 10, 323–336, 2005.

664 Dall'Osto, M., Querol, X., Alastuey, A., O'Dowd, C., Harrison, R. M., Wenger, J., and Gómez-Moreno, F. J.: On
665 the spatial distribution and evolution of ultrafine particles in Barcelona, *Atmos. Chem. Phys.*, 13, 741–759,
666 2013.

667 Directive 2009/30/EC, Official Journal of the European Union, L 140, EN, 88–113, 5. 6. 2009.

668 Dunne, E. M., Gordon, H., Kürten, A., Almeida, J., Duplissy, J., Williamson, C., Ortega, I. K., Pringle, K. J.,
669 Adamov, A., Baltensperger, U., Barmet, P., Benduhn, F., Bianchi, F., Breitenlechner, M., Clarke, A., Curtius,
670 J., Dommen, J., Donahue, N. M., Ehrhart, S., Flagan, R. C., Franchin, A., Guida, R., Hakala, J., Hansel, A.,
671 Heinritzi, M., Jokinen, T., Kangasluoma, J., Kirkby, J., Kulmala, M., Kupc, A., Lawler, M. J., Lehtipalo, K.,
672 Makhmutov, V., Mann, G., Mathot, S., Merikanto, J., Miettinen, P., Nenes, A., Onnela, A., Rap, A.,
673 Reddington, C. L. S., Riccobono, F., Richards, N. A. D., Rissanen, M. P., Rondo, L., Sarnela, N.,
674 Schobesberger, S., Sengupta, K., Simon, M., Sipilä, M., Smith, J. N., Stozkhov, Y., Tomé, A., Tröstl, J.,
675 Wagner, P. E., Wimmer, D., Winkler, P. M., Worsnop, D. R., and Carslaw, K. S.: Global atmospheric particle
676 formation from CERN CLOUD measurements, *Science* 354, 1119–1124, 2016.

677 Durbin, J. and Koopman, S. J.: Time series analysis by state space methods, Oxford University Press, Oxford,
678 2012.

679 Giechaskiel, B., Lahde, T., Suarez-Bertoa, R., Clairotte, M., Grigoratos, T., Zardini, A., Perujo, A., and Martini,
680 G.: Particle number measurements in the European legislation and future JRC activities, *Combustion Engines*,
681 174, 3–16, 2018.

682 Gordon, H., Sengupta, K., Rap, A., Duplissy, J., Frege, C., Williamson, C., Heinritzi, M., Simon, M., Yan, C.,
683 Almeida, J., Tröstl, J., Nieminen, T., Ortega, I. K., Wagner, R., Dunne, E. M., Adamov, A., Amorim, A.,
684 Bernhammer, A. K., Bianchi, F., Breitenlechner, M., Brilke, S., Chen, X., Craven, J. S., Dias, A., Ehrhart, S.,
685 Fischer, L., Flagan, R. C., Franchin, A., Fuchs, C., Guida, R., Hakala, J., Hoyle, C. R., Jokinen, T., Junninen,
686 H., Kangasluoma, J., Kim, J., Kirkby, J., Krapf, M., Kürten, A., Laaksonen, A., Lehtipalo, K., Makhmutov, V.,
687 Mathot, S., Molteni, U., Monks, S. A., Onnela, A., Peräkylä, O., Piel, F., Petäjä, T., Praplan, A. P., Pringle, K.
688 J., Richards, N. A. D., Rissanen, M. P., Rondo, L., Sarnela, N., Schobesberger, S., Scott, C. E., Seinfeld, J. H.,
689 Sharma, S., Sipilä, M., Steiner, G., Stozhkov, Y., Stratmann, F., Tomé, A., Virtanen, A., Vogel, A. L., Wagner,
690 A. C., Wagner, P. E., Weingartner, E., Wimmer, D., Winkler, P. M., Ye, P., Zhang, X., Hansel, A., Dommen,
691 J., Donahue, N. M., Worsnop, D. R., Baltensperger, U., Kulmala, M., Curtius, J., and Carslaw, K. S.: Reduced
692 anthropogenic aerosol radiative forcing caused by biogenic new particle formation, *Proc. Natl. Acad. Sci.*
693 *U.S.A.*, 113, 12053–12058, 2016.

694 Guo, H., Wang, D. W., Cheung, K., Ling, Z. H., Chan, C. K., and Yao, X. H.: Observation of aerosol size
695 distribution and new particle formation at a mountain site in subtropical Hong Kong, *Atmos. Chem. Phys.*, 12,
696 9923–9939, <https://doi.org/10.5194/acp-12-9923-2012>, 2012.

697 Hamed, A., H. Korhonen, S.-L. Sihto, J. Joutsensaari, H. Järvinen, T. Petäjä, F. Arnold, T. Nieminen, M. Kulmala,
698 J. N. Smith, K. E. J. Lehtinen, A. Laaksonen: The role of relative humidity in continental new particle
699 formation, *J. Geophys. Res.*, 116, D03202, doi:10.1029/2010JD014186, 2011.

700 Hussein, T., Puustinen, A., Aalto, P. P., Mäkelä, J. M., Hämeri, K., and Kulmala, M.: Urban aerosol number size
701 distributions, *Atmos. Chem. Phys.*, 4, 391–411, 2004.

702 Hyvönen, S., Junninen, H., Laakso, L., Dal Maso, M., Grönholm, T., Bonn, B., Keronen, P., Aalto, P., Hiltunen,
703 V., Pohja, T., Launiainen, S., Hari, P., Mannila, H., and Kulmala, M.: A look at aerosol formation using data
704 mining techniques, *Atmos. Chem. Phys.*, 5, 3345–3356, 2005.

705 Károssy, Cs.: A Kárpát-medence Péczely-féle makroszinoptikus időjárás helyzeteinek katalógusa 1881–2015
706 (Catalogue of the Péczely macrosynoptic weather types for the Carpathian Basin 1881–2015, in Hungarian),
707 OSKAR Kiadó, Budapest, 2016.

708 Kerminen, V.-M., Paramonov, M., Anttila, T., Riipinen, I., Fountoukis, C., Korhonen, H., Asmi, E., Laakso, L.,
709 Lihavainen, H., Swietlicki, E., Svenningsson, B., Asmi, A., Pandis, S. N., Kulmala, M., and Petäjä, T.: Cloud
710 condensation nuclei production associated with atmospheric nucleation: a synthesis based on existing literature
711 and new results, *Atmos. Chem. Phys.*, 12, 12037–12059, 2012.

712 Kerminen, V.-M., Chen, X., Vakkari, V., Petäjä, T., Kulmala, M., and Bianchi, F.: Atmospheric new particle
713 formation and growth: review of field observations, *Environ. Res. Lett.*, 13 (2018) 103003, 2018.

714 KSH, National register of road vehicles (in Hungarian), Hungarian Central Statistical Office, Budapest, 2019.

715 Kulmala, M., Dal Maso, M., Mäkelä, J. M., Pirjola, L., Väkevä, M., Aalto, P., Miiikkulainen, P., Hämeri, K., and
716 O'Dowd, C. D.: On the formation, growth and composition of nucleation mode particles, *Tellus B*53, 479–490,
717 2001.

718 Kulmala, M., Petäjä, T., Nieminen, T., Sipilä, M., Manninen, H. E., Lehtipalo, K., Dal Maso, M., Aalto, P. P.,
719 Junninen, H., Paasonen, P., Riipinen, I., Lehtinen, K. E. J., Laaksonen, A., and Kerminen, V.-M.: Measurement
720 of the nucleation of atmospheric aerosol particles, *Nat. Protoc.*, 7, 1651–1667, doi:10.1038/nprot.2012.091,
721 2012.

722 Kulmala, M., Kontkanen, J., Junninen, H., Lehtipalo, K., Manninen, H. E., Nieminen, T., Petäjä, T., Sipilä, M.,
723 Schobesberger, S., Rantala, P., Franchin, A., Jokinen, T., Järvinen, E., Äijälä, M., Kangasluoma, J., Hakala, J.,
724 Aalto, P. P., Paasonen, P., Mikkilä, J., Vanhanen, J., Aalto, J., Hakola, H., Makkonen, U., Ruuskanen, T.,
725 Mauldin, R. L. III, Duplissy, J., Vehkamäki, H., Bäck, J., Kortelainen, A., Riipinen, I., Kurtén, T., Johnston,
726 M. V., Smith, J. N., Ehn, M., Mentel, T. F., Lehtinen, K. E. J., Laaksonen, A., Kerminen, V.-M., and Worsnop,
727 D. R.: Direct observations of atmospheric aerosol nucleation, *Science*, 339, 943–946, 2013.

728 Kulmala, M., Petäjä, T., Ehn, M., Thornton, J., Sipilä, M., Worsnop, D. R., and Kerminen, V.-M.: Chemistry of
729 atmospheric nucleation: On the recent advances on precursor characterization and atmospheric cluster
730 composition in connection with atmospheric new particle formation, *Annu. Rev. Phys. Chem.*, 65, 21–37,
731 2014.

732 Kulmala, M., Kerminen, V. M., Petäjä, T., Ding, A. J., and Wang, L.: Atmospheric gas-to-particle conversion:
733 why NPF events are observed in megacities, *Faraday Discuss.*, doi:10.1039/C6FD00257A, 2017.

734 Laine, M.: Introduction to Dynamic Linear Models for Time Series Analysis. In: Montillet, J. P., Bos, M. (eds),
735 Geodetic Time Series Analysis in Earth Sciences, Springer, pp. 139–156, 2020.

736 Maheras, P., Tolika, K., Tegoulis, I., Anagnostopoulou, Ch., Szpirosz, K. Károssy, Cs., and Makra, L.:
737 Comparison of an automated classification system with an empirical classification of circulation patterns over
738 the Pannonian basin, Central Europe, Meteorol. Atmos. Phys., <https://doi.org/10.1007/s00703-018-0601-x>,
739 2018.

740 Makkonen, R., Asmi, A., Korhonen, H., Kokkola, H., Järvenoja, S., Räisänen, P., Lehtinen, K. E. J., Laaksonen,
741 A., Kerminen, V.-M., Järvinen, H., Lohmann, U., Bennartz, R., Feichter, J., and Kulmala, M.: Sensitivity of
742 aerosol concentrations and cloud properties to nucleation and secondary organic distribution in ECHAM5-
743 HAM global circulation model, Atmos. Chem. Phys., 9, 1747–1766, 2009.

744 Masiol, M., Squizzato, S., Chalupa, D., Utell, M. J., Rich, D. Q., and Hopke, P. K.: Long-term trends in submicron
745 particle concentrations in a metropolitan area of the northeastern United States, Sci. Total Environ., 633, 59–
746 70, 2018.

747 McCulloch, C. E., Searle, S. R., and Neuhaus, J. M.: Generalized, linear, and mixed models, 2nd ed., Wiley, New
748 York, 2008.

749 McFiggans, G., Mentel, T. F., Wildt, J., Pullinen, I., Kang, S., Kleist, E., Schmitt, S., Springer, M., Tillmann, R.,
750 Wu, C., Zhao, D., Hallquist, M., Faxon, C., Le Breton, M., Hallquist, A. M., Simpson, D., Bergstroem, R.,
751 Jenkin, M. E., Ehn, M., Thornton, J. A., Alfarra, M. R., Bannan, T. J., Percival, C. J., Priestley, M., Topping,
752 D., and Kiendler-Scharr, A.: Secondary organic aerosol reduced by mixture of atmospheric vapours, Nature,
753 565, 587–593, 2019.

754 Merikanto, J., Spracklen, D. V., Mann, G. W., Pickering, S. J., and Carslaw, K. S.: Impact of nucleation on global
755 CCN, Atmos. Chem. Phys., 9, 8601–8616, 2009.

756 Mikkonen, S., Lehtinen, K. E. J., Hamed, A., Joutsensaari, J., Facchini, M. C., and Laaksonen, A.: Using
757 discriminant analysis as a nucleation event classification method, Atmos. Chem. Phys., 6, 5549–5557,
758 <https://doi.org/10.5194/acp-6-5549-2006>, 2006.

759 Mikkonen, S., Korhonen, H., Romakkaniemi, S., Smith, J. N., Joutsensaari, J., Lehtinen, K. E. J., Hamed, A.,
760 Breider, T. J., Birmili, W., Spindler, G., Plass-Duelmer, C., Facchini, M. C., and Laaksonen, A.:
761 Meteorological and trace gas factors affecting the number concentration of atmospheric Aitken ($D_p=50$ nm)
762 particles in the continental boundary layer: parameterization using a multivariate mixed effects model, Geosci.
763 Model Dev., 4, 1–13, <https://doi.org/10.5194/gmd-4-1-2011>, 2011a.

764 Mikkonen, S., Romakkaniemi, S., Smith, J. N., Korhonen, H., Petäjä, T., Plass-Duelmer, C., Boy, M., McMurry,
765 P. H., Lehtinen, K. E. J., Joutsensaari, J., Hamed, A., Mauldin III, R. L., Birmili, W., Spindler, G., Arnold, F.,
766 Kulmala, M., and Laaksonen, A.: A statistical proxy for sulphuric acid concentration, Atmos. Chem. Phys., 11
767 11319–11334, <https://doi.org/10.5194/acp-11-11319-2011>, 2011b.

768 Mikkonen, S., Laine, M., Mäkelä, H. M., Gregow, H., Tuomenvirta, H., Lahtinen, M., Laaksonen, A.: Trends in
769 the average temperature in Finland, 1847–2013, Stoch. Environ. Res. Risk Ass., 29, 1521–1529, 2015.

770 Moore, K. F., Ning, Z., Ntziachristos, L., Schauer, J. J., and Sioutas, C.: Daily variation in the properties of urban
771 ultrafine aerosol - Part I: Physical characterization and volatility, Atmos. Environ., 41, 8633–8646, 2007.

772 Moosmuller, H., Chakrabarty, R. K. and Arnott, W.: Aerosol light absorption and its measurement: A review, J.
773 Quant. Spectrosc. Radiat. Transf., 110, 844–878, 2009.

774 Németh, Z. and Salma, I.: Spatial extension of nucleating air masses in the Carpathian Basin, Atmos. Chem. Phys.,
775 14, 8841–8848, 2014.

776 Németh, Z., Rosati, B., Zíková, N., Salma, I., Bozó, L., Dameto de España, C., Schwarz, J., Ždímal, V., and
777 Wonašchütz, A.: Comparison of atmospheric new particle formation and growth events in three Central
778 European cities, Atmos. Environ., 178, 191–197, 2018.

779 Nieminen, T., Asmi, A., Dal Maso, M., P. Aalto, P., Keronen, P., Petäjä, T., Kulmala, M. & Kerminen, V.-M.:
780 Trends in atmospheric new-particle formation: 16 years of observations in a boreal-forest environment. Boreal
781 Env. Res. 19 (suppl. B): 191–214, 2014.

782 Nieminen, T., Kerminen, V.-M., Petäjä, T., Aalto, P. P., Arshinov, M., Asmi, E., Baltensperger, U., Beddows, D.
783 C. S., Beukes, J. P., Collins, D., Ding, A., Harrison, R. M., Henzing, B., Hooda, R., Hu, M., Hörrak, U.,
784 Kivekäs, N., Komsaare, K., Krejci, R., Kristensson, A., Laakso, L., Laaksonen, A., Leaitch, W. R., Lihavainen,
785 H., Mihalopoulos, N., Németh, Z., Nie, W., O'Dowd, C., Salma, I., Sellegri, K., Svenningsson, B., Swietlicki,
786 E., Tunved, P., Ulevicius, V., Vakkari, V., Vana, M., Wiedensohler, A., Wu, Z., Virtanen, A., and Kulmala,

787 M.: Global analysis of continental boundary layer new particle formation based on long-term measurements,
788 Atmos. Chem. Phys., 18, 14737–14756, 2018.

789 Oberdörster, G., Oberdörster, E., and Oberdörster, J.: Nanotoxicology: an emerging discipline evolving from
790 studies of ultrafine particles, Environ. Health Perspect., 113, 823–839, 2005.

791 Ohlwein, S., Kappeler, R., Joss, M. K., Künzli, N., and Hoffmann, B.: Health effects of ultrafine particles: a
792 systematic literature review update of epidemiological evidence, Int. J. Public Health, 685, 547–559, 2019.

793 Ostro, B., Hu, J., Goldberg, D., Reynolds, P., Hertz, A., Bernstein, L., and Kleeman, M. J.: Associations of
794 mortality with long-term exposures to fine and ultrafine particles, species and sources: results from the
795 California teachers study cohort, Environ. Health Perspect., 123, 549–556, 2015.

796 Paasonen, P., Kupiainen, K., Klimont, Z., Visschedijk, A., Denier van der Gon, H. A. C., and Amann, M.:
797 Continental anthropogenic primary particle number emissions, Atmos. Chem. Phys., 16, 6823–6840, 2016.

798 Péczely, Gy.: Grosswetterlagen in Ungarn (Large-scale weather situations in Hungary, in German), Publication of
799 the Hungarian Meteorological Institute, 30, pp. 86, Budapest, 1957.

800 Petäjä, T., Mauldin, III, R. L., Kosciuch, E., McGrath, J., Nieminen, T., Paasonen, P., Boy, M., Adamov, A.,
801 Kotiaho, T., and Kulmala, M.: Sulfuric acid and OH concentrations in a boreal forest site, Atmos. Chem. Phys.,
802 9, 7435–7448, 2009.

803 Petris, G., Petrone, S., and Campagnoli, P.: Dynamic linear models, Springer, New York, 2009.

804 Pinheiro, J.C., and Bates, D.M.: Mixed-Effects Models in S and S-PLUS, Springer, 2000.

805 Platt, S. M., El Haddad, I., Pieber, S. M., Zardini, A. A., Suarez-Bertoa, R., Clairotte, M., Daellenbach, K. R.,
806 Huang, R.-J., Slowik, J. G., Hellebust, S., Temime-Roussel, B., Marchand, N., de Gouw, J., Jimenez, J. L.,
807 Hayes, P. L., Robinson, A. L., Baltensperger, U., Astorga, C., and Prévôt, A. S. H.: Gasoline cars produce
808 more carbonaceous particulate matter than modern filter-equipped diesel cars, Sci. Rep., 7, 4926, 2017,
809 <https://doi.org/10.1038/s41598-017-03714-9>.

810 Pöschl, U., Rudich, Y., and Ammann, M.: Kinetic model framework for aerosol and cloud surface chemistry and
811 gas-particle interactions – Part 1: General equations, parameters, and terminology, Atmos. Chem. Phys., 7,
812 5989–6023, 2007.

813 Raes, F., Van Dingenen, R., Vignati, E., Wilson, J., Putaud, J. P., Seinfeld, J. H., and Adams, P.: Formation and
814 cycling of aerosol in the global troposphere, Atmos. Environ., 34, 4215–4240, 2000.

815 Rich, D. Q., Zareba, W., Beckett, W., Hopke, P. K., Oakes, D., Frampton, M. W., Bisognano, J., Chalupa, D.,
816 Bausch, J., O’Shea, K., Wang, Y., and Utell, M. J.: Are ambient ultrafine, accumulation mode, and fine particles
817 associated with adverse cardiac responses in patients undergoing cardiac rehabilitation?, Environ. Health
818 Perspect., 120, 1162–1169, 2012.

819 Saha, P. K., Robinson, E. S., Shah, R. U., Zimmerman, N., Apte, J. S., Robinson, A. L., and Presto, A. A.: Reduced
820 ultrafine particle concentration in urban air: changes in nucleation and anthropogenic emissions, Environ. Sci.
821 Technol., 52, 6798–6806, 2018.

822 Salma, I., Borsós, T., Weidinger, T., Aalto, P., Hussein, T., Dal Maso, M., and Kulmala, M.: Production, growth
823 and properties of ultrafine atmospheric aerosol particles in an urban environment, Atmos. Chem. Phys., 11,
824 1339–1353, 2011.

825 Salma, I., Borsós, T., Németh, Z., Weidinger, T., Aalto, T., and Kulmala, M.: Comparative study of ultrafine
826 atmospheric aerosol within a city, Atmos. Environ., 92, 154–161, 2014.

827 Salma, I., Németh, Z., Weidinger, T., Kovács, B., and Kristóf, G.: Measurement, growth types and shrinkage of
828 newly formed aerosol particles at an urban research platform, Atmos. Chem. Phys., 16, 7837–7851, 2016a.

829 Salma, I., Németh, Z., Kerminen, V. M., Aalto, P., Nieminen, T., Weidinger, T., Molnár, Á., Imre, K., and
830 Kulmala, M.: Regional effect on urban atmospheric nucleation, Atmos. Chem. Phys., 16, 8715–8728, 2016b.

831 Salma, I., Varga, V., and Németh, Z.: Quantification of an atmospheric nucleation and growth process as a single
832 source of aerosol particles in a city, Atmos. Chem. Phys., 17, 15007–15017, 2017.

833 Salma, I. and Németh, Z.: Dynamic and timing properties of new aerosol particle formation and consecutive
834 growth events, Atmos. Chem. Phys., 19, 5835–5852, 2019.

835 Salvo, A., Brito, J., Artaxo, P., and Geiger, F. M.: Reduced ultrafine particle levels in São Paulo’s atmosphere
836 during shifts from gasoline to ethanol use, Nat. Commun., 8, 77, DOI: 10.1038/s41467-017-00041-5, 2017.

837 Schmid, O. and Stoeger, T.: Surface area is the biologically most effective dose metric for acute nanoparticle
838 toxicity in the lung, J. Aerosol Sci., 99, 133–143, 2016.

839 Sihto, S.-L., Mikkilä, J., Vanhanen, J., Ehn, M., Liao, L., Lehtipalo, K., Aalto, P. P., Duplissy, J., Petäjä, T.,
840 Kerminen, V.-M., Boy, M., and Kulmala, M.: Seasonal variation of CCN concentrations and aerosol activation
841 properties in boreal forest, *Atmos. Chem. Phys.*, 11, 13269–13285, 2011.

842 Sipilä, M., Berndt, T., Petäjä, T., Brus, D., Vanhanen, J., Stratmann, F., Patokoski, J., Mauldin, R. L. 3rd,
843 Hyvärinen, A. P., Lihavainen, H., and Kulmala, M.: The role of sulfuric acid in atmospheric nucleation,
844 *Science*, 327(5970), 1243–6. doi: 10.1126/science.1180315, 2010.

845 Spracklen, D. V., Carslaw, K. S., Merikanto, J., Mann, G. W., Reddington, C. L., Pickering, S., Ogren, J. A.,
846 Andrews, E., Baltensperger, U., Weingartner, E., Boy, M., Kulmala, M., Laakso, L., Lihavainen, H., Kivekäs,
847 N., Komppula, M., Mihalopoulos, N., Kouvarakis, G., Jennings, S. G., O'Dowd, C., Birmili, W., Wiedensohler,
848 A., Weller, R., Gras, J., Laj, P., Sellegri, K., Bonn, B., Krejčí, R., Laaksonen, A., Hamed, A., Minikin, A.,
849 Harrison, R. M., Talbot, R., and Sun, J.: The contribution of boundary layer nucleation events to total particle
850 concentrations on regional and global scales, *Atmos. Chem. Phys.*, 6, 5631–5648, 2006.

851 Sun, J., Birmili, W., Hermann, M., Tuch, T., Weinhold, K., Merkel, M., Rasch, F., Müller, T., Schladitz, A.,
852 Bastian, S., Löschau, G., Cyrus, J., Gu, J., Flentje, H., Briel, B., Asbach, C., Kaminski, H., Ries, L., Sohmer,
853 R., Gerwig, H., Wirtz, K., Meinhardt, F., Schwerin, A., Bath, O., Ma, N., and Wiedensohler, A.: Decreasing
854 trends of particle number and black carbon mass concentrations at 16 observational sites in Germany from
855 2009 to 2018, [Atmos. Chem. Phys.](https://doi.org/10.5194/acp-20-7049-2020), 20, 7049–7068, doi:10.5194/acp-20-7049-2020, 2020. [Atmos.
856 Chem. Phys. Discuss.](https://doi.org/10.5194/acp-2019-754), doi:10.5194/acp-2019-754, 2019.

857 Wehner, B. and Wiedensohler, A.: Long term measurements of submicrometer urban aerosols: statistical analysis
858 for correlations with meteorological conditions and trace gases, *Atmos. Chem. Phys.*, 3, 867–879, 2003

859 [Wiheraari, H., Pirjola, L., Karjalainen, P., Saukko, E., Kuuluvainen, H., Kulmala, K., Keskinen, J. and Rönkkö,
860 T.: Particulate emissions of a modern diesel passenger car under laboratory and real-world transient driving
861 conditions, *Environ. Pollut.*, 265, 114948, doi:10.1016/j.envpol.2020.114948, 2020.](https://doi.org/10.1016/j.envpol.2020.114948)

862 Wiedensohler, A., Cheng, Y. F., Nowak, A., Wehner, B., Achtert, P., Berghof, M., Birmili, W., Wu, Z. J., Hu, M.,
863 Zhu, T., Takegawa, N., Kita, K., Kondo, Y., Lou, S. R., Hofzumahaus, A., Holland, F., Wahner, A., Gunthe,
864 S. S., Rose, D., Su, H., and Pöschl, U.: Mobility particle size spectrometers: harmonization of technical
865 standards and data structure to facilitate high quality long-term observations of atmospheric particle number
866 size distributions, *Atmos. Meas. Tech.*, 5, 657–685, 2012.

867 Willmott, C. J., Matsuura, K., and Robeson, S. M.: Ambiguities inherent in sums-of-squares-based error statistics,
868 *Atmos. Environ.*, 43, 749–752, doi:10.1016/j.atmosenv.2008.10.005, 2009.

869 Yu, F., Luo, G., Bates, T. S., Anderson, B., Clarke, A., Kapustin, V., Yantosca, R. M., Wang, Y., and Wu, S.:
870 Spatial distributions of particle number concentrations in the global troposphere: simulations, observations,
871 and implications for nucleation mechanisms, *J. Geophys. Res.*, 115, D17205, doi:10.1029/2009JD013473,
872 2010.

873 Zaidan, M. A., Haapasilta, V., Relan, R., Paasonen, P., Kerminen, V.-M., Junninen, H., Kulmala, M., and Foster,
874 A. S.: Exploring non-linear associations between atmospheric new-particle formation and ambient variables: a
875 mutual information approach, *Atmos. Chem. Phys.*, 18, 12699–12714, 2018.

876 Zhang, R., Wang, G., Guo, S., Zamora, M. L., Ying, Q., Lin, Y., Wang, W., Hu, M., and Wang, Y.: Formation of
877 urban fine particulate matter, *Chem. Rev.*, 115, 3803–3855, 2015.